Application of the TRIUMF Dual Arm Spectrometer System to the Study of the $^{12}C(p, d\pi^+)^{11}B$ Reaction

BY

MONA JOAN BENJAMINTZ

A Thesis
Submitted to the Faculty of Graduate Studies
in Partial Fulfillment of the Requirements
for the Degree of

MASTER OF SCIENCE

Department of Physics
University of Manitoba
Winnipeg, Manitoba

April, 1996

ISBN 0-612-12979-9

Name Mona Joan Benjamintz

Dissertation Abstracts International and *Masters Abstracts International* are arranged by broad, general subject categories. Please select the one subject which most nearly describes the content of your dissertation or thesis. Enter the corresponding four-digit code in the spaces provided.

Nuclear Physics

SUBJECT TERM

0	6	1	0

SUBJECT CODE

UMI

Subject Categories

THE HUMANITIES AND SOCIAL SCIENCES

COMMUNICATIONS AND THE ARTS
- Architecture 0729
- Art History 0377
- Cinema 0900
- Dance 0378
- Fine Arts 0357
- Information Science 0723
- Journalism 0391
- Library Science 0399
- Mass Communications 0708
- Music 0413
- Speech Communication 0459
- Theater 0465

EDUCATION
- General 0515
- Administration 0514
- Adult and Continuing 0516
- Agricultural 0517
- Art 0273
- Bilingual and Multicultural 0282
- Business 0688
- Community College 0275
- Curriculum and Instruction 0727
- Early Childhood 0518
- Elementary 0524
- Finance 0277
- Guidance and Counseling 0519
- Health 0680
- Higher 0745
- History of 0520
- Home Economics 0278
- Industrial 0521
- Language and Literature 0279
- Mathematics 0280
- Music 0522
- Philosophy of 0998
- Physical 0523
- Psychology 0525
- Reading 0535
- Religious 0527
- Sciences 0714
- Secondary 0533
- Social Sciences 0534
- Sociology of 0340
- Special 0529
- Teacher Training 0530
- Technology 0710
- Tests and Measurements 0288
- Vocational 0747

LANGUAGE, LITERATURE AND LINGUISTICS
- Language
  - General 0679
  - Ancient 0289
  - Linguistics 0290
  - Modern 0291
- Literature
  - General 0401
  - Classical 0294
  - Comparative 0295
  - Medieval 0297
  - Modern 0298
  - African 0316
  - American 0591
  - Asian 0305
  - Canadian (English) 0352
  - Canadian (French) 0355
  - English 0593
  - Germanic 0311
  - Latin American 0312
  - Middle Eastern 0315
  - Romance 0313
  - Slavic and East European 0314

PHILOSOPHY, RELIGION AND THEOLOGY
- Philosophy 0422
- Religion
  - General 0318
  - Biblical Studies 0321
  - Clergy 0319
  - History of 0320
  - Philosophy of 0322
- Theology 0469

SOCIAL SCIENCES
- American Studies 0323
- Anthropology
  - Archaeology 0324
  - Cultural 0326
  - Physical 0327
- Business Administration
  - General 0310
  - Accounting 0272
  - Banking 0770
  - Management 0454
  - Marketing 0338
- Canadian Studies 0385
- Economics
  - General 0501
  - Agricultural 0503
  - Commerce-Business 0505
  - Finance 0508
  - History 0509
  - Labor 0510
  - Theory 0511
- Folklore 0358
- Geography 0366
- Gerontology 0351
- History
  - General 0578
  - Ancient 0579
  - Medieval 0581
  - Modern 0582
  - Black 0328
  - African 0331
  - Asia, Australia and Oceania 0332
  - Canadian 0334
  - European 0335
  - Latin American 0336
  - Middle Eastern 0333
  - United States 0337
- History of Science 0585
- Law 0398
- Political Science
  - General 0615
  - International Law and Relations 0616
  - Public Administration 0617
- Recreation 0814
- Social Work 0452
- Sociology
  - General 0626
  - Criminology and Penology 0627
  - Demography 0938
  - Ethnic and Racial Studies 0631
  - Individual and Family Studies 0628
  - Industrial and Labor Relations 0629
  - Public and Social Welfare 0630
  - Social Structure and Development 0700
  - Theory and Methods 0344
- Transportation 0709
- Urban and Regional Planning 0999
- Women's Studies 0453

THE SCIENCES AND ENGINEERING

BIOLOGICAL SCIENCES
- Agriculture
  - General 0473
  - Agronomy 0285
  - Animal Culture and Nutrition 0475
  - Animal Pathology 0476
  - Food Science and Technology 0359
  - Forestry and Wildlife 0478
  - Plant Culture 0479
  - Plant Pathology 0480
  - Plant Physiology 0817
  - Range Management 0777
  - Wood Technology 0746
- Biology
  - General 0306
  - Anatomy 0287
  - Biostatistics 0308
  - Botany 0309
  - Cell 0379
  - Ecology 0329
  - Entomology 0353
  - Genetics 0369
  - Limnology 0793
  - Microbiology 0410
  - Molecular 0307
  - Neuroscience 0317
  - Oceanography 0416
  - Physiology 0433
  - Radiation 0821
  - Veterinary Science 0778
  - Zoology 0472
- Biophysics
  - General 0786
  - Medical 0760

EARTH SCIENCES
- Biogeochemistry 0425
- Geochemistry 0996
- Geodesy 0370
- Geology 0372
- Geophysics 0373
- Hydrology 0388
- Mineralogy 0411
- Paleobotany 0345
- Paleoecology 0426
- Paleontology 0418
- Paleozoology 0985
- Palynology 0427
- Physical Geography 0368
- Physical Oceanography 0415

HEALTH AND ENVIRONMENTAL SCIENCES
- Environmental Sciences 0768
- Health Sciences
  - General 0566
  - Audiology 0300
  - Chemotherapy 0992
  - Dentistry 0567
  - Education 0350
  - Hospital Management 0769
  - Human Development 0758
  - Immunology 0982
  - Medicine and Surgery 0564
  - Mental Health 0347
  - Nursing 0569
  - Nutrition 0570
  - Obstetrics and Gynecology 0380
  - Occupational Health and Therapy 0354
  - Ophthalmology 0381
  - Pathology 0571
  - Pharmacology 0419
  - Pharmacy 0572
  - Physical Therapy 0382
  - Public Health 0573
  - Radiology 0574
  - Recreation 0575
  - Speech Pathology 0460
  - Toxicology 0383
- Home Economics 0386

PHYSICAL SCIENCES

Pure Sciences
- Chemistry
  - General 0485
  - Agricultural 0749
  - Analytical 0486
  - Biochemistry 0487
  - Inorganic 0488
  - Nuclear 0738
  - Organic 0490
  - Pharmaceutical 0491
  - Physical 0494
  - Polymer 0495
  - Radiation 0754
- Mathematics 0405
- Physics
  - General 0605
  - Acoustics 0986
  - Astronomy and Astrophysics 0606
  - Atmospheric Science 0608
  - Atomic 0748
  - Electronics and Electricity 0607
  - Elementary Particles and High Energy 0798
  - Fluid and Plasma 0759
  - Molecular 0609
  - Nuclear 0610
  - Optics 0752
  - Radiation 0756
  - Solid State 0611
- Statistics 0463

Applied Sciences
- Applied Mechanics 0346
- Computer Science 0984
- Engineering
  - General 0537
  - Aerospace 0538
  - Agricultural 0539
  - Automotive 0540
  - Biomedical 0541
  - Chemical 0542
  - Civil 0543
  - Electronics and Electrical 0544
  - Heat and Thermodynamics 0348
  - Hydraulic 0545
  - Industrial 0546
  - Marine 0547
  - Materials Science 0794
  - Mechanical 0548
  - Metallurgy 0743
  - Mining 0551
  - Nuclear 0552
  - Packaging 0549
  - Petroleum 0765
  - Sanitary and Municipal 0554
  - System Science 0790
- Geotechnology 0428
- Operations Research 0796
- Plastics Technology 0795
- Textile Technology 0994

PSYCHOLOGY
- General 0621
- Behavioral 0384
- Clinical 0622
- Developmental 0620
- Experimental 0623
- Industrial 0624
- Personality 0625
- Physiological 0989
- Psychobiology 0349
- Psychometrics 0632
- Social 0451

Application of the TRIUMF Dual Arm Spectrometer System to the Study of the $^{12}C(p, d\pi^+)^{11}B$ Reaction

BY

MONA JOAN BENJAMINTZ

A Thesis/Practicum submitted to the Faculty of Graduate Studies of The University of Manitoba in partial fulfillment of the requirements for the degree of

MASTER OF SCIENCE

To Araz and Robert

Abstract

TRIUMF's **S**econd **A**rm **Sp**ectrometer (**SASP**) system is a quadrupole-quadrupole-dipole system with multiwire drift chambers and scintillator paddle detectors. The **M**edium **R**esolution **S**pectrometer (**MRS**) at TRIUMF is a quadrupole-dipole system also with drift chambers and scintillator paddles. Together, these two spectrometers form a **D**ual **A**rm **S**pectrometer **S**ystem (**DASS**) and were used to collect data from the ^{12}C$(\vec{p}, d\pi^+)^{11}$B and ^{2}H$(\vec{p}, d\pi^+)$n reactions at proton bombarding energies of 370 and 500 MeV. The SASP detected pions while the MRS detected deuterons. Using the two spectrometers in coincidence mode permitted a full kinematic reconstruction of the three-body reactions explored. Thus the energies, momenta and masses of the residual target ground and excited states were readily determined. The standard Transport coordinate system was used for all kinematics calculations. Differential cross sections and analyzing powers were measured at high and low momentum transfers. The results exhibit many features of the free $pp \rightarrow d\pi^+$ reaction.

Leaf left blank to correct page numbering

Acknowledgements

I would like to extend my appreciation and gratitude to my supervisor, Dr. Willie Falk; his guidance made this thesis and the work it represents possible. I am grateful also to the other committee members, Dr. Jim Birchall and Dr. Stan Yen, for their attentive reviewing of my thesis.

The knowledge imparted to me by Drs. Dave Hutcheon, Alan Ling, Andy Miller, Pat Walden and Stan Yen also proved invaluable in the course of my research. I acknowledge Donald Arseneau, Jacques Chakhalyan, Joe Chuma, Luis Fernandes, Peter Green, Ken Hicks, Fred Jones, Russell King, Elie Korkmaz, Allena Opper, Grant Orielly, Munasinghe Punasena for various bits of know-how, Steve Chan, Joe Huser, Salma Jivan and Chris Stevens for providing facilities and equipment for oxygen target assembly and testing, and Jim Fleetwood, Zoa Hartry and Munasinghe Punasena for providing me with figures 2.1, 2.2 and 2.3 (Jim), 2.5 (Zoa) and 3.4 (Munasinghe). Drs. Paul Knowles and Mark Welsh also provided me with extensive Latex and moral support.

I'd also like to thank the University of Manitoba 'lunch club' members. I was very fortunate to work amongst such an amiable and helpful group of people. Specifically, I'd like to extend bushels of thanks and appreciation to friends and colleagues Araz Hamian and Robert Pleydon, who helped me maintain some semblance of sanity and made my master's degree a truly memorable experience. Oh, and thanks to Mr. Squirrel for eating all my apple cores.

Leaf left blank to correct page numbering

Contents

Abstract ix

Acknowledgements xi

Contents xiii

List of Tables xvi

List of Figures xvii

1 INTRODUCTION 1
- 1.1 The Pion . . . 1
- 1.2 The $pp \rightarrow d\pi^+$ and Nuclear $(p, d\pi^+)$ Reactions . . . 1
- 1.3 The E634 Experiment . . . 2

2 The DUAL ARM SPECTROMETER SYSTEM 6
- 2.1 SASP . . . 6
- 2.2 MRS . . . 6
- 2.3 DASS System . . . 6
- 2.4 Particle Detection . . . 9
  - 2.4.1 Front End Chamber . . . 9
  - 2.4.2 Vertical Drift Chambers . . . 9
  - 2.4.3 Scintillator Paddle Arrays . . . 11
  - 2.4.4 Focal Plane Paddle Scintillators . . . 11
- 2.5 Run Plan . . . 11
  - 2.5.1 Reactions Studied . . . 11
  - 2.5.2 Targets Used . . . 11
  - 2.5.3 Experimental Parameters . . . 12
- 2.6 The NOVA Analysis Program . . . 14
- 2.7 DASS Event Trigger . . . 14
  - 2.7.1 Setting Trigger Conditions Within NOVA . . . 15
  - 2.7.2 SASP Trigger . . . 15
  - 2.7.3 MRS Trigger . . . 17
- 2.8 Data Acquisition . . . 17
- 2.9 TWOTRAN, Data Stream . . . 17
- 2.10 Dispersion . . . 23
- 2.11 Transfer Matrix Elements . . . 24

3 E634 ANALYSIS **27**
3.1 Definitions of NOVA Variables Used for Particle Trajectories 27
3.2 The Transport Coordinate System 33
3.3 SASP Focal Plane 35
3.4 MRS Focal Plane 41
3.5 Conversion of Measured Quantities to Transport Units 42
3.5.1 SASP Variables 43
3.5.2 MRS Variables 46
3.6 Missing Mass Calculations 47
3.6.1 Formulation 47
3.6.2 Calculation 49
3.6.3 Kinematic Description of Beam Dispersion 51
3.6.4 Momentum P_π and P_d 53
3.7 Event Reconstruction 53
3.7.1 Event Coordinates 53
3.7.2 Empirical Resolution Corrections 55
3.8 Calibrations 57
3.8.1 Beam Energy Calibration 57
3.8.2 SASP Calibrations 57
3.8.3 MRS Calibrations 59
3.8.4 SASP and MRS Solid Angles 62
3.8.5 Beam Flux and SEM and Polarimeter Calibration 68
3.8.6 Spin Off Correction 71
3.8.7 Background Subtraction 71
3.9 Efficiencies 76
3.9.1 Wire Chamber Efficiencies 76
3.9.2 NOVA Cuts on VDC and FEC Data 77
3.9.3 Computer Live Time 78
3.10 Cross Section Calculation 78
3.11 Analyzing Power Calculation 80

4 RESULTS AND DISCUSSION **82**
4.1 NOVA Plots Generated From Analysis 82
4.2 Cross Sections and Analyzing Powers 91

5 THEORY **96**
5.1 DWIA Model 96
5.2 Comparison of Theory with Experimental Results 97

6 RECOMMENDATIONS and CONCLUSION **99**
6.1 Recommendations 99
6.2 Conclusion 100

Bibliography **101**

A Calculation of Unit Vectors for Particle Trajectories Through the SASP and MRS **103**

B MRS Momentum Calibration 106

C SASP Effective Pion Length 112

D The E634_ANAL.FOR Program 117

E DASS.TWO program 134

F USRQ Subroutine 145

G E634 NOVA OPSEQ 148

List of Tables

2.1 This table lists the reactions studied in experiment E634. 12
2.2 This table provides a summary of the E634 runs. 13

3.1 This table lists the centers of FECs, VDCs and focal planes; these were the values used for E634 (may be subject to change for other experiments). . . 33
3.2 This table lists the known and unknown variables in the E634 DASS three-body reaction. 49
3.3 The coordinates calculated for E634 event reconstruction are listed in this table. 54
3.4 The In-Beam Polarimeter (IBP) and Secondary Emission Monitor (SEM) calibration constants are listed here. 69
3.5 This table lists the histograms incremented upon satisfaction of the LTMRS_P and LTMRS_R conditions given in the NOVA operation sequence. LTMRS_P corresponds to peak events of the LTMRS histogram, representing valid coincidence events. The LTMRS_R condition corresponds to random events (background). For a description of the histograms, see table 3.6. 74
3.6 This table briefly describes the histograms listed in table 3.5. Unless otherwise specified, the incrementation of each histogram is by units of one. . . . 75

B.1 These measurements were used to determine absolute beam energy calibration. 107
B.2 These quantities were used to determine the kinematically corrected P_p/P_π ratio. The columns titled 'corrected' show quantities corrected for energy losses incurred at the target and at the FEC, as specified in equation (B.2). 107
B.3 A comparison between old and new expressions for the P/B ratio is shown here. 111

C.1 This table lists the coefficients for path lengths at various SDEL values. . . 113
C.2 Geometrical parameters used in program PI_DECAY_MC.FOR are listed in this table. 113
C.3 Shifts used to align the centers of the scintillation detectors with the central particle trajectory are given here. 114
C.4 The parameters of the fifth order fit to the SASP effective pion length are listed above. 114
C.5 The parameters of the third order fit to the coefficients of the fit for the SASP effective pion length are given in the above table. 115
C.6 This table lists test output of parameterization of coefficients given in table C.4. 116

List of Figures

1.1 A model of the quasifree $(p, d\pi^+)$ reaction in nuclei is depicted here. (A) depicts time prior to the collision between the incident proton (p_i) and the target nucleus containing the target proton (p_t); (B) shows the situation after collision where the 'spectator' nucleus recoils while a pion and deuteron head off in other directions. 2

1.2 These are kinematics plots for the $^{12}C(\vec{p}, d\pi^+)^{11}B$ reaction at four angle combinations and 500 MeV beam energy. The momentum locus (in MeV/c) for the pion and deuteron (for ^{11}B ground state) is shown in each plot. Pion momentum is plotted on the horizontal axes (in MeV/c). The vertical axis is used to read values of the deuteron momentum (in MeV/c), transfer momentum (p_{Recoil}, in MeV/c), deuteron time of flight (TOF(d), in ns), pp-scattering equivalent kinetic energy ($T_{pp}Lab$, in MeV) and pion angle ($\theta_{\pi'}$, in degrees) in the $pp \rightarrow d\pi^+$ frame. Theoretical curves for the analyzing power and cross section are also shown. 3

1.3 These are kinematics plots for the $^{12}C(\vec{p}, d\pi^+)^{11}B$ reaction at four angle combinations and 370 MeV beam energy. Other details are as given in figure 1.2. 4

2.1 The Second Arm SPectrometer (SASP) layout is shown here. The curved line directly under VDC1 is a theoretical representation of the SASP focal plane. The target resides in the scattering chamber. 7

2.2 The Medium Resolution Spectrometer (MRS) layout is depicted here. The target resides in the scattering chamber. 8

2.3 The SASP and MRS are shown here in DASS mode. 10

2.4 A schematic of the SASP event-defining trigger is shown here. 16

2.5 This figure shows a schematic of the MRS event-defining trigger. 18

2.6 This figure illustrates data acquisition operations. 19

2.7 This figure depicts a schematic representation of data stream movement between the STARBURST and the VAX. 20

2.8 The TWOTRAN data stream for a DASS experiment is shown here. 21

3.1 This figure shows the Transport coordinate system at the target. Angles θ_{TR} and ϕ_{TR} are named STH_TGT_TR and SPH_TGT_TR in the NOVA analysis program. Note that in this figure, θ_{TR} is negative. 30

3.2 Shown here are the Transport and DASS coordinate systems. Transport coordinates are indicated by the 'TR' subscript; unsubscripted coordinates use the DASS convention. 34

3.3 This is a schematic representation of the SASP focal surface and VDCs. $\vec{R}_0$ and $\vec{R}_1$ are the position vectors, relative to the origin 0_1, of the points where the central and arbitrary trajectories intersect the focal surface. 36
3.4 A fourth order polynomial fit to the empirically determined SASP focal surface, in the X-Z coordinate system is shown here. 37
3.5 A schematic representation of a vertical drift chamber (VDC) showing the orientation of X and U wire planes, as viewed from above is shown here. X_c , U_c indicate the center wires in each plane. The directions of increasing momentum and X, U position indicated are specific to the SASP VDC orientation. 39
3.6 An arbitrary particle trajectory is shown here intersecting the SASP VDC planes at points ($X1_{TR}$,$Y1_{TR}$,$Z1_{TR}$) and ($X2_{TR}$,$Y2_{TR}$,$Z2_{TR}$). The trajectory is in the positive X_{TR}-Y_{TR}-Z_{TR} octant. θ is in the X-Z plane and ϕ is in the Y-Z plane. 40
3.7 The MRS focal surface and VDCs are shown here, as per experiment E634. 41
3.8 This figure shows a particle trajectory passing through SASP VDCs. 45
3.9 This is a missing mass spectrum for $^{12}C(\vec{p}, d\pi^+)^{11}B$, showing the four excited states and the $1s$ continuum state of ^{11}B. The recoil particle ground state rest mass is subtracted from the DRMASS definition so that in the missing mass spectrum the ground state will be at zero MeV. 48
3.10 Madison and Transport coordinate systems for particle trajectories traversing the SASP and MRS are depicted here. The unit vectors $\hat{n}_{MRS}$ and $\hat{n}_{SASP}$ are oriented in the direction of an arbitrary particle trajectory. . . . 50
3.11 The momentum-X displacement relation illustrating beam dispersion is illustrated here. 52
3.12 These plots demonstrate the effects of empirical corrections applied to θ at the target for SASP (STH_TGT_TR) and the SASP focal plane position (SDEL). Plots (a) and (b) show these plots before corrections are applied, plots (c) and (d) show the resulting plots after corrections are applied. . . . 56
3.13 Shown is a fit to data for SASP experimental acceptance yields from $pp \rightarrow d\pi^+$ data corrected for pion decay. The data is normalized to unity at the peak of the curve. 58
3.14 These plots show the variation of different SDEL values versus SDEL9 (SDEL calculated using the USR9 subroutine): (a), (b) show the difference between empirically corrected SDEL, $SDEL_{NEW}$, and SDEL9, at beam energies 370 MeV and 500 MeV, respectively; (c) shows the difference between calibrated SDEL value and SDEL9, at 280 MeV beam energy. 60
3.15 The SASP effective pion length versus SDEL is plotted in this figure for various central pion momenta. 61
3.16 This figure shows the MRS acceptance for proper FPP cage orientation. . . 63
3.17 This figure shows the MRS acceptance for improper FPP cage orientation. . 63
3.18 The MRS momentum calibration from November 1994 data is shown here. . 64
3.19 Plots of solid angle tests for the SASP for three runs are shown here: (a) has cuts on θ only, (b) has cuts on ϕ only and (c) has cuts on θ and ϕ combined. The horizontal scale in (c) is expressed relative to the maximum solid angle defined by the largest cuts on θ and ϕ. 65

3.20 Plots of solid angle tests for the MRS for three E634 runs are shown here: (a) has cuts on X0 only, (b) has cuts on Y0 only and (c) has cuts on X0 and Y0 combined. The horizontal scale in (c) is expressed relative to the maximum solid angle defined by the largest cuts on X and Y. 67

3.21 These plots show polarimeter and SEM counts in various forms: (a) polarimeter spin up/down ratio, (b) SEM spin up/down ratio, (c) spin up (circles) and down (crosses) polarization as determined by the polarimeter and (d) polarimeter/SEM ratio; the X-axis range on all plots covers the duration of the E634 experiment. 70

3.22 Spin off polarization versus run time for the duration of the E634 experiment is plotted here. The circles represent spin up, the crosses, spin down data. This apparent polarization is due to the IBP instrumental asymmetry. . . . 72

3.23 The HLTMRS spectrum showing the relative timing between the SASP and MRS is given above. The small peaks represent accidental deuteron-pion coincidences with pions and deuterons coming from other beam bursts. The large peak represents valid coincidence plus accidental events. Each proton beam burst is separated in time by 43 ns. 73

4.1 These spectra show the detected particles in (a) the MRS and (b) the SASP. The identified particles are: 1: deuterons, 2: accidental protons from other beam bursts, 3: scattered protons, 4: pions (π^+) and 5: accidental protons from other beam bursts. The Y-axis variable is the scintillator paddle sum for the MRS (MAPDSUM) and SASP (LAPDSUM); each is the sum of the digitized ADC counts for the charge in the signals in the individual paddles (comprising the paddle array), integrated over the time that the ADC gate signal is present. Thus, the vertical scales for the two plots give an indication of the amount of ionization that occurred in the scintillator array. 83

4.2 The above histogram represents a 'top view' of the missing mass spectrum; it is a plot of pion momentum versus deuteron momentum. The loci shown are identified as the following states of ^{11}B: 1, ground state; 2, first excited state, 2.12 MeV; 3, second excited state, 4.45 MeV; 4, third excited state, 5.02 MeV. 84

4.3 These four plots show the relation between ϕ and θ at the target and the missing mass, after empirical aberration corrections have been applied. The top two plots show this relation for the MRS, the bottom two for the SASP. 85

4.4 This figure contains plots of SASP focal plane position, SDEL, versus missing mass, DRMASS, showing (a) both true and random events (total events) and (b) only random events. 86

4.5 These are plots of SASP focal plane position, SDEL, versus missing mass, DRMASS. (a), (c) and (e) in the left column represent net events after subtraction of random events. (a) contains events for both spin up and down, (c) shows spin up events only and (e) contains spin down events only. Plots (b), (d) and (f) in the right column are the corresponding efficiency spectra incremented/decremented by all/random events. 87

4.6 Plots of SASP focal plane position, SDEL, versus missing mass, DRMASS are given here. The details of this figure are the same as that for figure 4.5 except that here the missing mass scale is extended to include the continuum states. 88

4.7 (a) shows the missing mass spectra incremented for events satisfying the LTMRS_P condition (a peak in the HLTMRS plot - see figure 3.23). (c) and (d) show the same but for spin up and down events respectively. (b) shows the missing mass spectra gated only on random events (satisfying the LTMRS_R condition) and (d) and (f) show random spin up and random spin down respectively. 89

4.8 The above three spectra are incremented according to one of three efficiency factors: (a) MRS acceptance, (b) SASP acceptance and (c) the SASP pion survival fraction. The horizontal axes show the range of the SASP focal plane in terms of percent momentum deviation from central momentum. SDEL = 0% corresponds to the central momentum focal plane position. . . 90

4.9 These plots show the cross section and analyzing power results for 500 MeV carbon target runs with the following MRS and SASP angle combinations: (a) MRS=15.5°, SASP=30.0°, (b) MRS=15.6°, SASP=55.0°, (c) MRS=24.9°, SASP=30.0°, (d) MRS=25.0°, SASP=55.0°. The short dashed curve in the analyzing power graphs represents the free $pp \rightarrow d\pi^+$ analyzing power. P_{recoil} represents the momentum of the recoil target nucleus; its value is read off the vertical scale in MeV/c, by multiplying by the reduction factor as specified in the plots (ie, 100, 200). 93

4.10 The above plots illustrate cross section and analyzing power results for 370 MeV carbon target runs with the following MRS and SASP angle combinations: (a) MRS=15.5°, SASP=30.3°, (b) MRS=15.6°, SASP=55.1°, (c) MRS=25.0°, SASP=30.2°, (d) MRS=25.0°, SASP=55.1°. Other details are the same as for figure 4.9. 94

4.11 These plots show cross section and analyzing power results for deuterium target runs with the following beam energies and MRS and SASP angle combinations: (a) 370 MeV, MRS=15.5°, SASP=30.3°, (b) 370 MeV, MRS=15.6°, SASP=55.1°, (c) 500 MeV, MRS=15.5°, SASP=30.4°, (d) 500 MeV, MRS=15.6°, SASP=55.0°. Other details are the same as for figure 4.9. 95

Chapter 1

INTRODUCTION

1.1 The Pion

In 1934, Yukawa introduced the idea of meson exchange to describe nucleon-nucleon interaction [1]. The pion was observed in 1947 to have mass $\simeq$140 MeV/c^2, spin 0, and strong interactions with nuclei, and was designated as the nuclear force quantum [2]. The virtual pion can become a physical particle in collisions between nucleons in which sufficient energy is available to supply the rest-mass energy of the pion (139.6 MeV for $\pi^{\pm}$, 135.0 MeV for π^o) These pions play a significant role in enhancing the deposition of energy in the nucleus, as their short mean free paths correspond to large cross sections for interactions with nucleons [3].

1.2 The $pp \rightarrow d\pi^+$ and Nuclear $(p, d\pi^+)$ Reactions

Over the last decade, nuclear pion production from such facilities as Indiana University Cyclotron Facility (IUCF), TRI-University Meson Facility (TRIUMF) and Los Alamos Meson Physics Facility (LAMPF) have consistently revealed that the most important $NN \rightarrow NN\pi^+$ reaction at 200-500 MeV laboratory energies is the $pp \rightarrow d\pi^+$ reaction. The analyzing powers of the nuclear $(\vec{p}, \pi^+)$ reaction have a character very similar to those of the $pp \rightarrow d\pi^+$ reaction. Thus, the two-nucleon $pp \rightarrow d\pi^+$ mechanism has become a basis for the qualitative interpretation of data on pion production on ^{12,13}C [4].

A further step in observing the role of this process in pion production would be to study the $(p, d\pi^+)$ reaction on nuclei. In the quasifree region, the incident proton interacts with one of the target protons while the residual nucleus behaves like a spectator during the interaction, as depicted in figure 1.1 [5]. This concept was examined in TRIUMF experiment E634, which is the main topic of this thesis. In the quasifree region, the momentum transfer is lower and thus larger cross sections are expected. This can be seen in figures 1.2 and 1.3 where kinematics of the ^{12}C$(\vec{p}, d\pi^+)^{11}$B reaction are displayed as a function of pion momentum. The pion-deuteron momentum locus for ^{11}B in the ground state is shown as the solid line in each plot (p_d). Measurements were made utilizing several

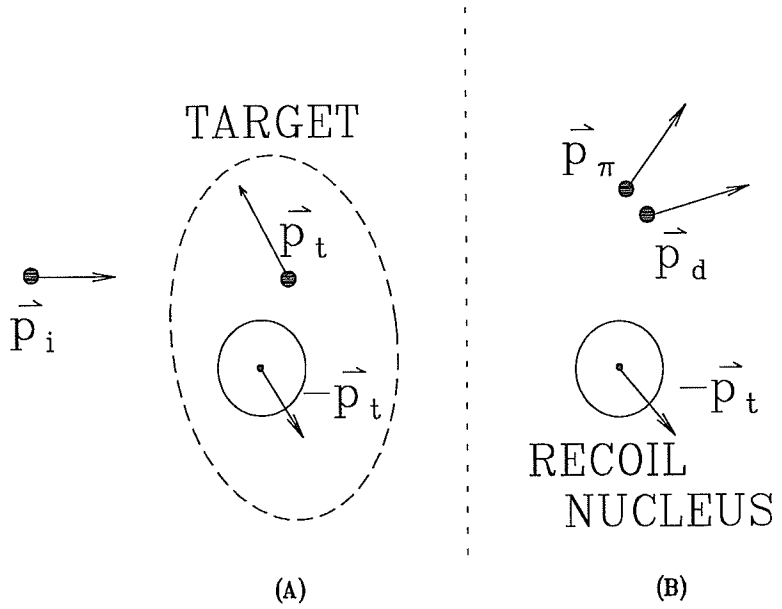

Figure 1.1: A model of the quasifree $(p, d\pi^+)$ reaction in nuclei is depicted here. (A) depicts time prior to the collision between the incident proton (p_i) and the target nucleus containing the target proton (p_t); (B) shows the situation after collision where the 'spectator' nucleus recoils while a pion and deuteron head off in other directions.

magnet settings for both spectrometers and beam energies of 500 MeV and 370 MeV at each of four spectrometer angle combinations. The MRS deuteron detection angles used were $\theta_d = 15°$, 25° and the SASP pion detection angles used were $\theta_\pi = 30°$, 55°. The $\theta_{\pi'}$ curve gives the center of mass pion angle of the equivalent $pp \rightarrow d\pi^+$ process. This is reconstructed from the kinematics of the outgoing pion and deuteron momenta (given by the solid line). The p_{recoil} curve indicates the recoil momentum of the ^{11}B nucleus. Note the relation between the p_{recoil} curve and the cross section curve (indicated by 'XS'); the cross section is greatest when the recoil momentum of the ^{11}B nucleus is the least. The cross section curve has been calculated using a simple model as discussed in §5.2. The T_{pp} curve represents the effective proton laboratory kinetic energy incident on a stationary target proton yielding a $pp \rightarrow d\pi^+$ center of mass energy which is equal to the center of mass energy observed for the deuteron and pion system in the ^{12}C$(\vec{p}, d\pi^+)^{11}$B reaction. The numbered boxes represent momentum 'bites'; each momentum bite is determined by different magnetic field settings for both spectrometers. More details of the plots in figures 1.2 and 1.3 will be discussed in §2.5.

1.3 The E634 Experiment

The purpose of TRIUMF experiment E634 was to investigate the degree to which reactions of type A$(\vec{p}, d\pi^+)$B proceed via the quasifree $pp \rightarrow d\pi^+$ process, and how this process is

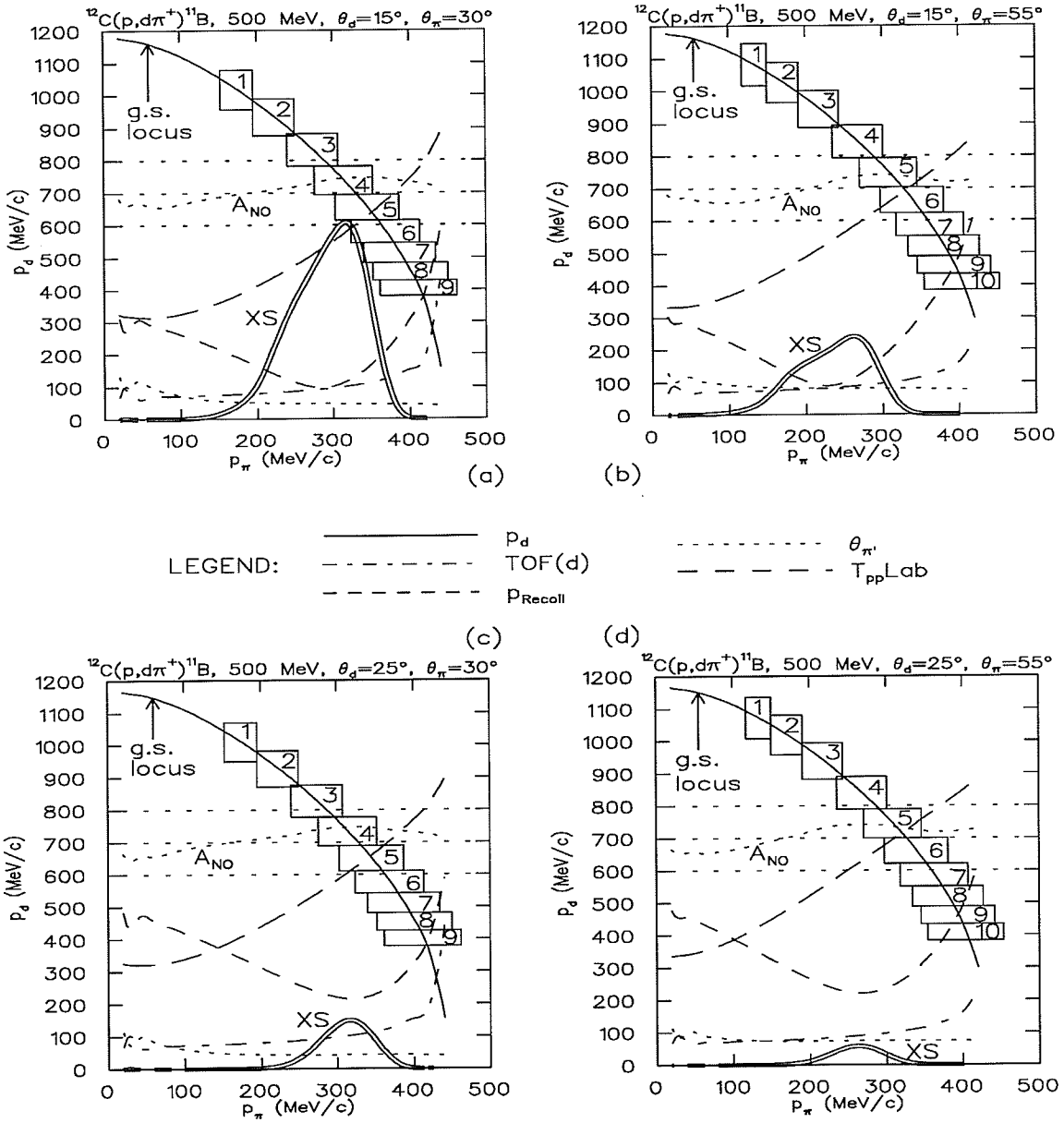

Figure 1.2: These are kinematics plots for the $^{12}\mathrm{C}(\vec{p}, d\pi^+)^{11}\mathrm{B}$ reaction at four angle combinations and 500 MeV beam energy. The momentum locus (in MeV/c) for the pion and deuteron (for ^{11}B ground state) is shown in each plot. Pion momentum is plotted on the horizontal axes (in MeV/c). The vertical axis is used to read values of the deuteron momentum (in MeV/c), transfer momentum (p_{Recoil}, in MeV/c), deuteron time of flight (TOF(d), in ns), pp-scattering equivalent kinetic energy ($\mathrm{T}_{pp}Lab$, in MeV) and pion angle ($\theta_{\pi'}$, in degrees) in the $pp \rightarrow d\pi^+$ frame. Theoretical curves for the analyzing power and cross section are also shown.

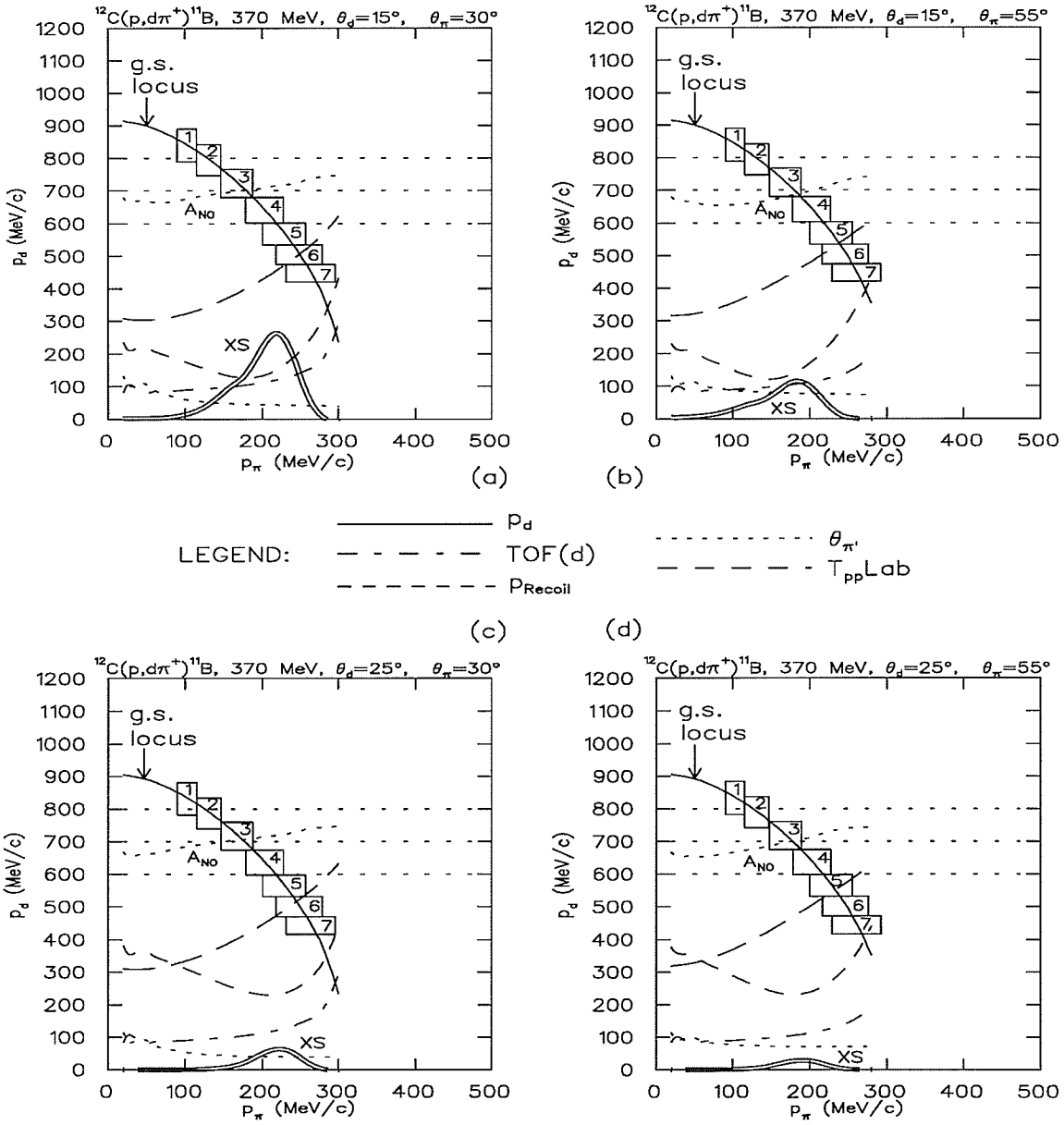

Figure 1.3: These are kinematics plots for the $^{12}\mathrm{C}(\vec{p}, d\pi^+)^{11}\mathrm{B}$ reaction at four angle combinations and 370 MeV beam energy. Other details are as given in figure 1.2.

modified by the nuclear medium. To this end, cross sections and analyzing powers for the $(\vec{p}, d\pi^+)$ reaction on ^{12}C, ^{16}O and CD_2 in the quasifree region at the two incident proton energies of 370 and 500 MeV were measured [6]. These two incident proton energies correspond to long (1-5 fm) and short ($\leq$1 fm) mean free paths of pions, respectively. A polarized proton beam was used so that analyzing powers could be extracted [5].

TRIUMF's MRS and SASP spectrometers, located in the 4B experimental hall, were used for the measurement of these reactions. The SASP and MRS are discussed in §2.1 and §2.2, respectively. The two spectrometers were operated together in DASS (Dual Arm Spectrometer System) mode, with the MRS detecting the deuterons and the SASP detecting the pions. By measuring the momenta of the deuteron and the pion, the kinematics of the three-body final state were fully determined; that is, the energy and momentum of the undetected particle, the ^{11}B residual nucleus, can be calculated. This experiment was one of the first to incorporate the SASP together with the MRS in DASS mode, which helped to further characterize the features and abilities of the SASP, first commissioned in August 1993.

Chapter 2

The DUAL ARM SPECTROMETER SYSTEM

2.1 SASP

The Second **A**rm **SP**ectrometer at TRIUMF is a quadrupole-quadrupole-dipole spectrometer with a design central momentum of 660 MeV/c. The dipole magnet is clamshell shaped and thus this spectrometer is referred to as a 'Q-Q-Clamshell' second arm spectrometer [7]. Its general layout together with detectors composed of drift chambers and scintillators is illustrated in figure 2.1. The SASP is a large solid angle device (maximum 13.5 msr) and the term 'second arm' refers to its usage as a second spectrometer in conjunction with the MRS for DASS (Dual Arm Spectrometer System) mode experiments, as in experiment E634. [7]. During this experiment, the SASP detected pions at scattering angles of -30° and -55°. The sign of these angles is in keeping with the Madison coordinate system convention. The SASP detectors are described in §2.4. For more information on the SASP, please see reference [7].

2.2 MRS

TRIUMF's **M**edium **R**esolution **S**pectrometer is a quadrupole-dipole system with multiwire drift chambers and scintillator paddle detectors as shown in figure 2.2. Its solid angle detection capabilities depend on the mode of running, but is approximately 2.5 msr. The momentum acceptance is about ±7% for particle momenta up to 1.5 GeV/c [8]. During the E634 experiment, the MRS was used to detect deuterons at scattering angles of +15° and +25°. The main MRS particle detecting components are discussed in §2.4. For more details on the MRS, please see reference [8].

2.3 DASS System

For the three-body final state E634 experiment, the SASP and MRS are used together as a **D**ual **A**rm **S**pectrometer **S**ystem. Figure 2.3 depicts the two spectrometers in the DASS

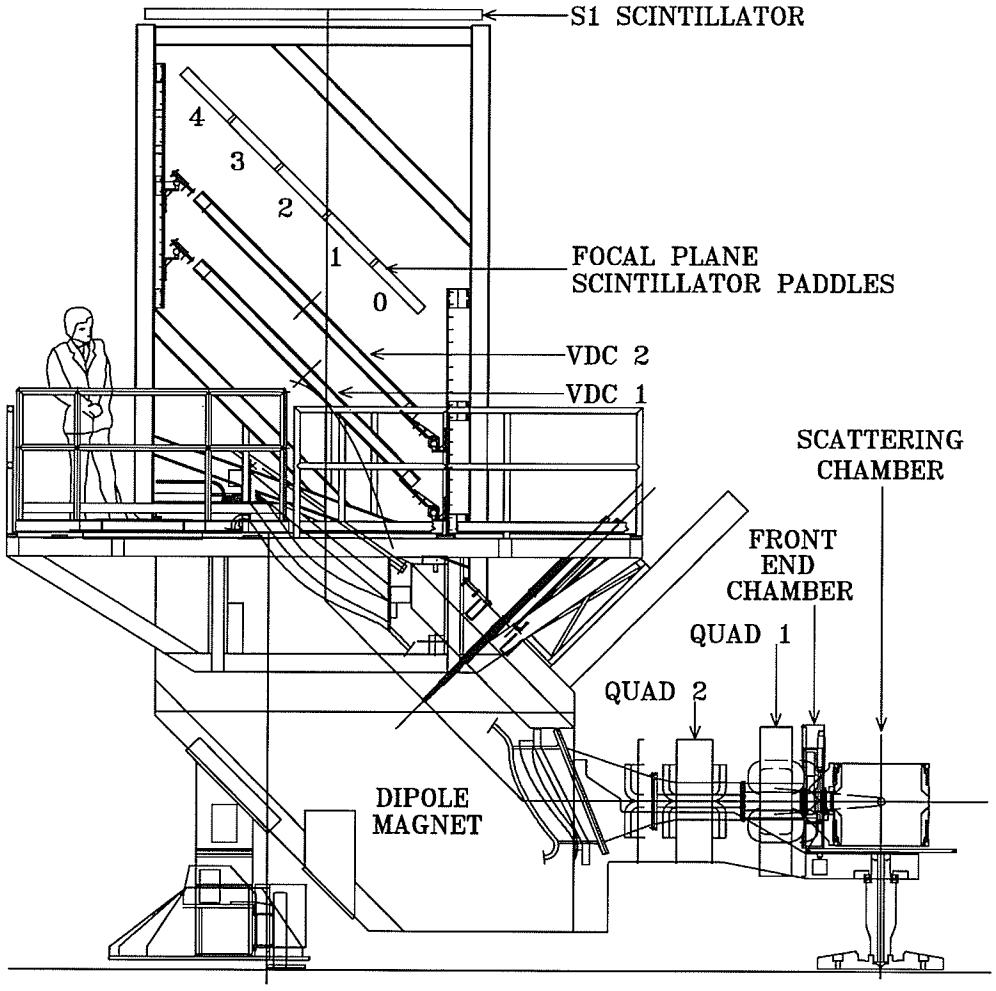

Figure 2.1: The Second Arm SPectrometer (SASP) layout is shown here. The curved line directly under VDC1 is a theoretical representation of the SASP focal plane. The target resides in the scattering chamber.

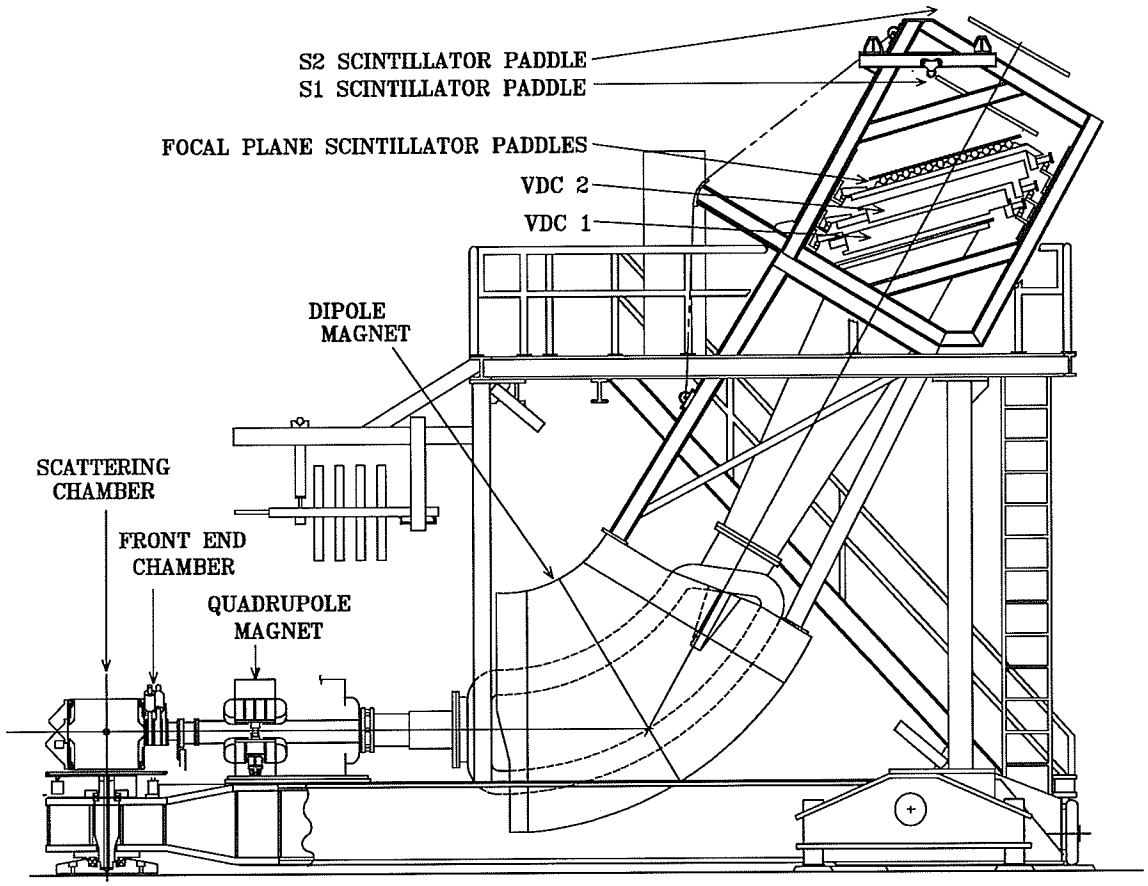

Figure 2.2: The Medium Resolution Spectrometer (MRS) layout is depicted here. The target resides in the scattering chamber.

setup. Both the MRS and SASP spectrometers utilize similar particle detection devices, and these are described in the following sections.

2.4 Particle Detection

The locations of the detectors for each spectrometer are indicated in figure 2.1 for the SASP and figure 2.2 for the MRS. In the E634 experiment, the MRS particle detection setup included a **f**ront **e**nd wire **c**hamber (FEC) near the target and two **v**ertical **d**rift **c**hambers (VDC) at the top end of the spectrometer. A scintillator detection array consisting of ten paddle scintillators and a large scintillator, S1, was located near the focal plane (just above the VDCs).

The SASP detector arrangement for E634 was composed of two VDCs, a scintillator detector array of five paddle scintillators and a large scintillator, S1. No front end chamber was used as the resulting background events occurring close to the FEC were found to be too numerous to be practically managed.

The various detectors utilized by the SASP and MRS are described in the following sections. Most of the detectors used by both spectrometers are very similar in design and are discussed in parallel.

2.4.1 Front End Chamber

As shown in figure 2.2, the MRS front end chamber is the first detector encountered by the particles leaving the target area. The purpose of the FEC is to allow particle trajectory traceback to the target in order to set software gates (to define the spectrometer solid angle, for example) and to correct for aberrations in the MRS [8].

The wire spacing for both the SASP and MRS FECs is 5 mm, and the MRS FEC measures 8 cm $\times$ 8 cm. The SASP FEC measures 8 cm $\times$ 16 cm [9]. The FEC consists of four wire planes, two in each of the X and Y directions. The X direction corresponds to the vertical (bend) plane and the Y direction corresponds to the horizontal (non-bend) plane of the spectrometer. The four FEC planes are known as $X0, X0', Y0$ and $Y0'$. Each MRS FEC plane contains 16 pairs of alternating anode and cathode wires. Each SASP FEC X plane contains 32 pairs of wires and each Y plane contains 16 pairs of wires.

The primed planes are offset from the unprimed planes by one half of the anode spacing in order to determine whether the incoming particle has passed to the right or left of a struck wire, and to allow interpolation using drift times. For more information on the MRS FEC features, please see reference [8].

2.4.2 Vertical Drift Chambers

The vertical drift chambers (VDCs) in the SASP and the MRS utilize the same design concept except that the SASP VDCs are larger because the SASP has a larger solid an-

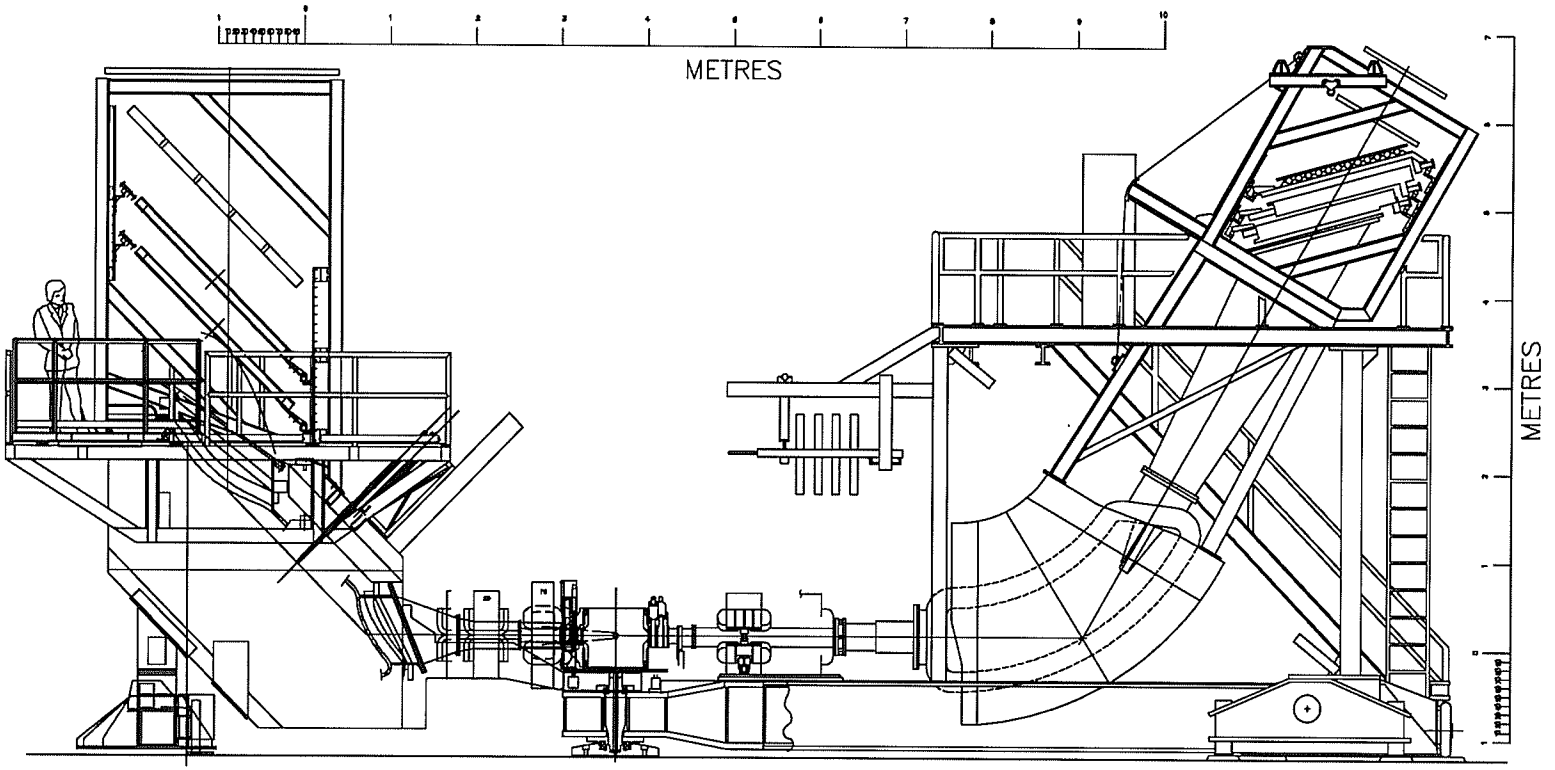

Figure 2.3: The SASP and MRS are shown here in DASS mode.

gle acceptance and a larger momentum bite. The SASP VDCs have an active area of 35 cm × 182.4 cm [10]. In both spectrometers, the two VDCs are positioned just above the focal plane at an angle of 45° to the central trajectory.

The total number of X plane cathode wires in the SASP VDC is 304 and the wire spacing is 6 mm [10]. Each VDC plane (for both the SASP and MRS) consists of two wire planes - an X plane (bend plane) and a U plane; the U plane is oriented at 30° with respect to the X plane. The planes are labelled X1, U1, X2 and U2. The Y position (non-bend plane) was then determined from the trigonometric relation of the X and U planes; see equations (3.16) through (3.20) in §3.3. For more details regarding the VDCs, please see reference [8].

2.4.3 Scintillator Paddle Arrays

The MRS has an array of ten scintillator paddles located just above the VDCs. These paddles are numbered '0' through '9' and their function is to provide the trigger (timing and energy loss information) for an event. In addition, they can be used to limit the focal plane span which is considered in the trigger. This reduces the uninteresting data on tape and computer dead-time [8].

The SASP has an array of five scintillator paddles, numbered '0' through '4'. These are wider than the MRS scintillator paddles but their function is the same.

2.4.4 Focal Plane Paddle Scintillators

Above the scintillator paddle arrays of the MRS are the **f**ocal **p**lane **p**olarimeter (FPP) scintillators, S1 and S2. These two large area scintillators are often included in the valid event trigger to provide cleaner events. The S1 paddle covers most of the active area of the focal plane whereas S2 does not and for that reason should be used with caution. The SASP has a large single scintillator called S1, situated beyond the paddle array, which serves a similar purpose as S1 and S2 of the MRS.

2.5 Run Plan

2.5.1 Reactions Studied

Two spectrometers allow for a full kinematic description of all bodies involved in three-body final state reactions. Three reactions were studied; their targets are described in table 2.1.

2.5.2 Targets Used

The ^{16}O target that was originally intended for use comprised approximately 3 cc of water contained within stainless steel foil walls. The foil walls were 0.0005" (1/2 mil $\simeq$ 0.0127 mm) thick, and had a density of $\sim$ 7.75 g/cm^3. The foil was attached to the aluminum frame

REACTION	TARGET
$^{12}C(\vec{p}, d\pi^+)^{11}B$	natural carbon, 50.2 mg/cm^2
$^{2}H(\vec{p}, d\pi^+)n$	CD_2, 200 mg/cm^2
$^{16}O(\vec{p}, d\pi^+)^{15}N$	Mylar ($C^{10}H^8O^4$), 89 mg/cm^2

Table 2.1: This table lists the reactions studied in experiment E634.

using epoxy. This target experienced a leak in the evacuated target chamber despite initial success under similar test conditions. Finally, a small piece of 89 mg/cm^2 Mylar foil ($C_{10}H_8O_4$) was used as the ^{16}O target. However, interaction between the incident proton and the carbon in the Mylar had to be accounted for in the off-line analysis. Subsequently, only a very small number of ^{16}O runs were successfully performed and written to tape.

The protons comprising ^{16}O nominally fill both the $p_{1/2}$ and $p_{3/2}$ shells in the doubly magic ^{16}O nucleus. The purpose of using the ^{16}O target was to examine the relative effective polarizations of the $p_{1/2}$ and $p_{3/2}$ protons. Please see reference [11] for more details on this effective polarization.

The CD_2 target, also known as *deuterated polyethylene*, provided a simple case of the $A(\vec{p}, d\pi^+)B$ reaction and was primarily used to check the validity of the experimental setup. For this target the quasifree reaction observed was $^{2}H(\vec{p}, d\pi^+)n$ where the neutron behaves as the spectator particle during the reaction, as it is only loosely bound within the deuterium nucleus.

The majority of the beam time for the experiment was devoted to using the carbon target to observe the $^{12}C(\vec{p}, d\pi^+)^{11}B$ reaction. The incident proton interacts with a proton in the $p_{3/2}$ shell of the ^{12}C nucleus, producing and emitting a deuteron and a pion, and leaves the residual ^{11}B nucleus in the ground state or an excited state.

2.5.3 Experimental Parameters

The beam current used for the 500 MeV runs was in the 6-20 nA range, while a range of 20-50 nA, on average, was used for the 370 MeV runs. The current for each run was determined by a combination of the desired statistics and MRS FEC limitations.

Table 2.2 lists the beam energy and spectrometer angle settings for the runs of this experiment. The convention used for analysis was such that the MRS angle was positive for scattering to the left of the incident beam (in the direction of incidence) into the MRS and the SASP angle was positive for scattering to the right of the incident beam into the SASP. Note that this does not follow the Madison convention (which would require that the SASP angles be negative). For each angle-energy combination, several dipole and quadrupole magnet settings for both spectrometers were used to measure the pion-deuteron

E634 RUN SUMMARY				
Beam Energy (MeV)	MRS Angle (°)	SASP Angle (°)	Target Used	Run Number(s)
- carbon target -				
500	15.51	30.40	^{12}C	7-28
500	15.60	54.98	^{12}C	33-42
500	24.94	30.01	^{12}C	46-57
500	25.01	55.02	^{12}C	59-67
370	15.53	30.29	^{12}C	69-89
370	15.56	55.09	^{12}C	97-109
370	25.01	30.21	^{12}C	125-131
370	25.02	55.09	^{12}C	113-121
- deuterium target -				
500	15.51	30.40	CD_2	29-31
500	15.60	54.98	CD_2	43-44
370	15.53	30.29	CD_2	94-96
370	15.56	55.07	CD_2	111
- oxygen target -				
370	15.47	30.21	^{16}O	123-124

Table 2.2: This table provides a summary of the E634 runs.

momentum locus for the ^{11}B ground state. Figure 1.2(a) on page 3 shows a plot of this locus for the $^{12}C(\vec{p}, d\pi^+)^{11}B$ reaction at beam energy 500 MeV with MRS angle (θ_d) at 15° and SASP angle (θ_π) at 30°. The theoretical analyzing power and cross section are also shown; these will be discussed in §4.2. The cross section shown is based on a very simple plane wave model, details of which appear in chapter five. Numbered boxes along the ground state locus indicate momentum bites investigated during the experiment. The momentum bites situated above the peak of the cross section curve provide the greatest statistics for that energy-angle combination.

2.6 The NOVA Analysis Program

Peter Green's NOVA analysis program was used for analysis of the acquired data, both on- and off-line. On-line, NOVA-created histograms were examined to assess the quality of the incoming data, so that adjustments to experimental parameters could be made if necessary. In the DASS mode, MRS and SASP variables were distinguished by the following nomenclature: 'M' or 'R' for the MRS and 'S' or 'L' for SASP ('L' for *large* acceptance).

NOVA manipulates raw data input according to user-specified declarations, conditions and calculations. After a list of variable declarations and conditions is specified in the NOVA 'sub-process', an OPeration SEQuence (OPSEQ) follows; this is a program executed for each input event, the main feature of which is the creation of histograms of the input and output data [12]. The NOVA OPSEQ used for E634 is given in appendix G.

2.7 DASS Event Trigger

A particle traversing a spectrometer activates various detectors along its path. A valid event in DASS mode is usually determined by a two-level event trigger. An event trigger for each spectrometer is defined by a logical combination of signals from various detectors and sets a latch which prevents subsequent signals from mixing with the latched signal. When the first level trigger is activated, this indicates that an event may be of interest and digitizing of the detector signals commences. Meanwhile, a signal from another detector or detector array comprises the second level trigger, also called the *auxiliary trigger*. While the digitizing of the first level trigger signals has already started, the second level trigger decides if the event is valid. If the auxiliary trigger indicates a valid event, digitizing of all signals proceeds to completion and a LAM ('Look-At-Me') module is activated which is then read by the STARBURST (or J-11) module, which is a *front end processor*. The STARBURST plays a major role in building the event data stream which is written onto tape (this is discussed in more detail in §2.9). On the other hand, if the auxiliary trigger indicates an invalid event, a fast clear is issued.

In DASS operation, the SASP and MRS run asynchronously and the MRS is a 'slave' to the SASP 'master'. This is demonstrated by the fact that the SASP has a LAM but

the MRS does not, so the SASP must send the LAM signal to the STARBURST module which will clear the LAM, meanwhile inhibiting the MRS so that the MRS does not start processing another signal until the SASP is ready to do so as well. After a first level trigger occurs, if there is no corresponding valid second level trigger, the first level triggered event is fast-cleared to enable the triggering of new events. Any clear (computer clear or fast clear) from the SASP clears both spectrometers; for a DASS experiment, the MRS only has the ability to clear itself.

2.7.1 Setting Trigger Conditions Within NOVA

The ECL (Emitter-Coupled Logic) programmable trigger electronics enable the user to alter the trigger conditions 'on-the-fly' during an experiment. To facilitate this process, the trigger conditions are identified with special variable names within NOVA, allowing the various ECL parameters to be addressed in terms of physical quantities. Changing the settings on one module may affect others and NOVA will also handle the module inter-dependence automatically. When the trigger system is programmed by a special NOVA command based on the values of the special trigger variables and the logical expressions relating them, trigger settings can be verified by using the 'LOOKTRIG' NOVA command. This can produce results such as

```
LFETRIG       I*4 Var    0
  ((BIT0|BIT1)|BIT7)*(LFTX0|LFTY0)
LEVENT        I*4 Var    -160
  (BIT5|BIT7)*((LEPADL&LES1)&LEX1)
LSLOWAUX      I*4 Var    -134
  ((BIT1|BIT7)|BIT2)*LMRS .
```

For example, when LFETRIG appears in the expression for LSLOWAUX (the SASP auxiliary trigger), this means that the SASP FEC is in the trigger. For experiment E634, no SASP FEC was used so LFEGATE (see figure 2.4) was not included in the inputs to LSLOWAUX. The SASP FEC X and Y position variables LFTX0 and LFTY0 are zero and consequently LFETRIG is zero. The above LOOKTRIG output shows trigger conditions for the SASP only; at the time of experiment E634, a NOVA display of MRS trigger conditions was not yet available. For more details on ECL trigger electronics, please see reference [13].

2.7.2 SASP Trigger

For E634, the first level trigger signified a valid SASP event, namely, a valid hit in one of the scintillator paddles (paddles 0 through 4), the S1 scintillator, and a hit in VDC plane X1. This opened a gate for the ADCs, and issued a start pulse to all TDCs. The corresponding electronic schematic for this trigger is illustrated in figure 2.4. The SASP

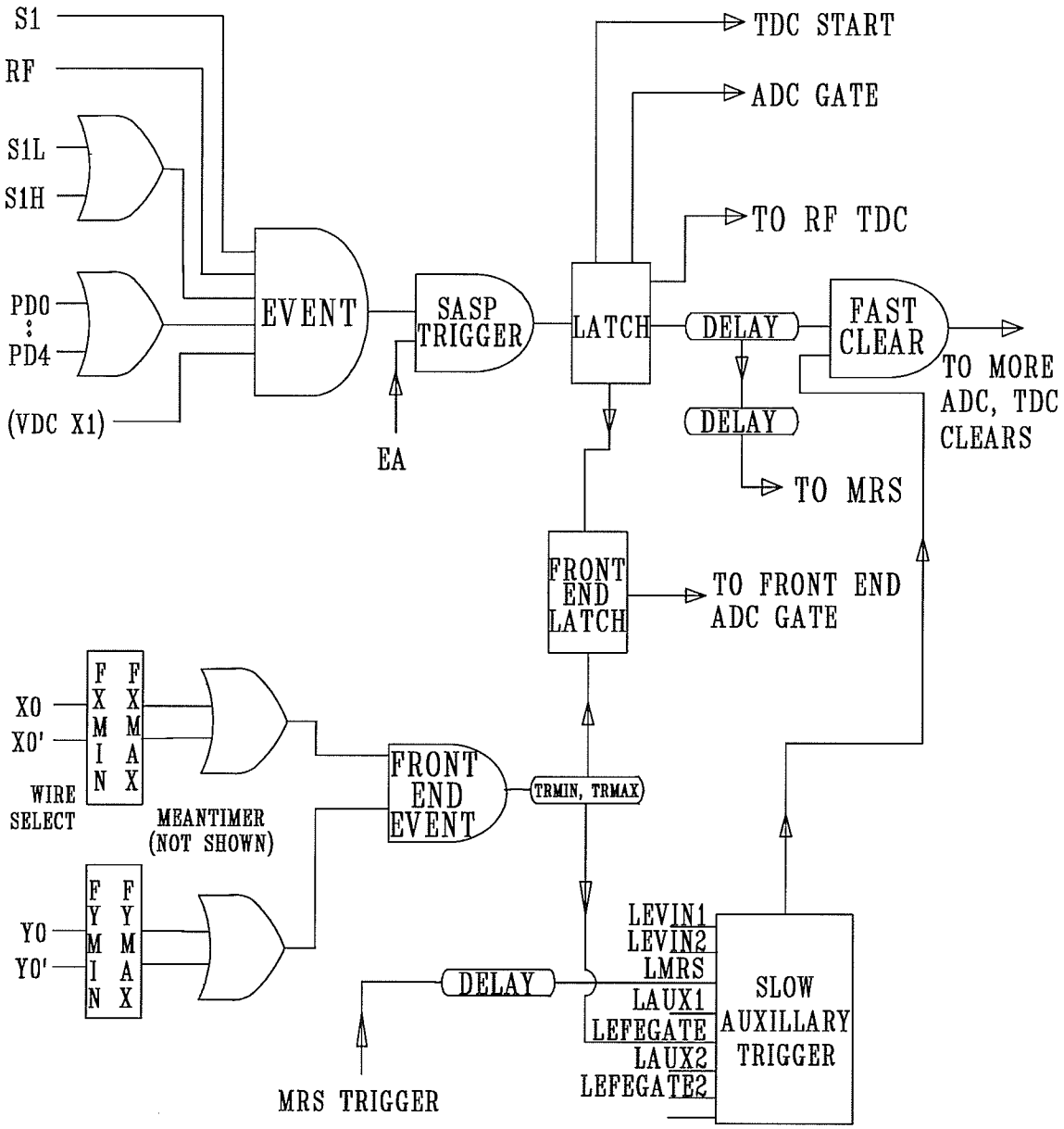

Figure 2.4: A schematic of the SASP event-defining trigger is shown here.

first level trigger is defined in terms of NOVA variables as

```
LEVENT=(BIT5|BIT7)*((LEPADL&LES1)&LEX1)
```

where all the terms represent bit patterns. These bit patterns correspond to the bits used as input or output from logic modules in the electronics used to collect the incoming data. LEPADL, LES1 and LEX1 represent SASP scintillator paddle hits, S1 paddle hits and VDC X1 plane hits, respectively. If there is a simultaneous hit in the VDC X1 plane, a signal in paddle S1 and a signal in one of the paddles 0 through 4, a first level trigger would occur.

2.7.3 MRS Trigger

A valid trigger in the MRS was defined by a hit in one of the FEC planes, the VDC X1 plane, one of the ten scintillator paddles and the S1 scintillator paddle. These signals in coincidence formed a master trigger which specified whether or not a particle had travelled through the MRS. This trigger is shown schematically in figure 2.5 [8]. For details on MRS trigger operation, please see reference [8]. The activation of an MRS event starts the digitizing of the MRS detectors, sets the latch and the SASP auxiliary trigger (LSLOWAUX) in NOVA. In terms of NOVA variables, LSLOWAUX was defined as

```
LSLOWAUX=((BIT1|BIT7)|BIT2)*LMRS.
```

2.8 Data Acquisition

For SASP, MRS and DASS experiments, a data acquisition system called "VDACS" (**V**ax **D**ata **AC**quisition **S**ystem) is used to perform functions such as responding to the LAMs, reading data from CAMAC modules and writing data to tape. VDACS runs under the VMS operating system. VDACS consists of a front end processor called a CES 2180 STARBURST module (J-11) , several VMS commands which allow the user to manage such things as tape drives and data, and a computer program written in the high-level language TWOTRAN. The TWOTRAN code instructs the STARBURST to build the event data stream which is subsequently read by VDACS and written onto tape for future analysis by the NOVA analysis program. This data may also be analyzed online simultaneously [14], [10], [9].

The flow of data and communication during the data acquisition process is depicted in figure 2.6.

2.9 TWOTRAN, Data Stream

The TWOTRAN program contains several modules. One configures the CAMAC hardware before acquisition starts, setting up the digitizers appropriate to the mode of operation.

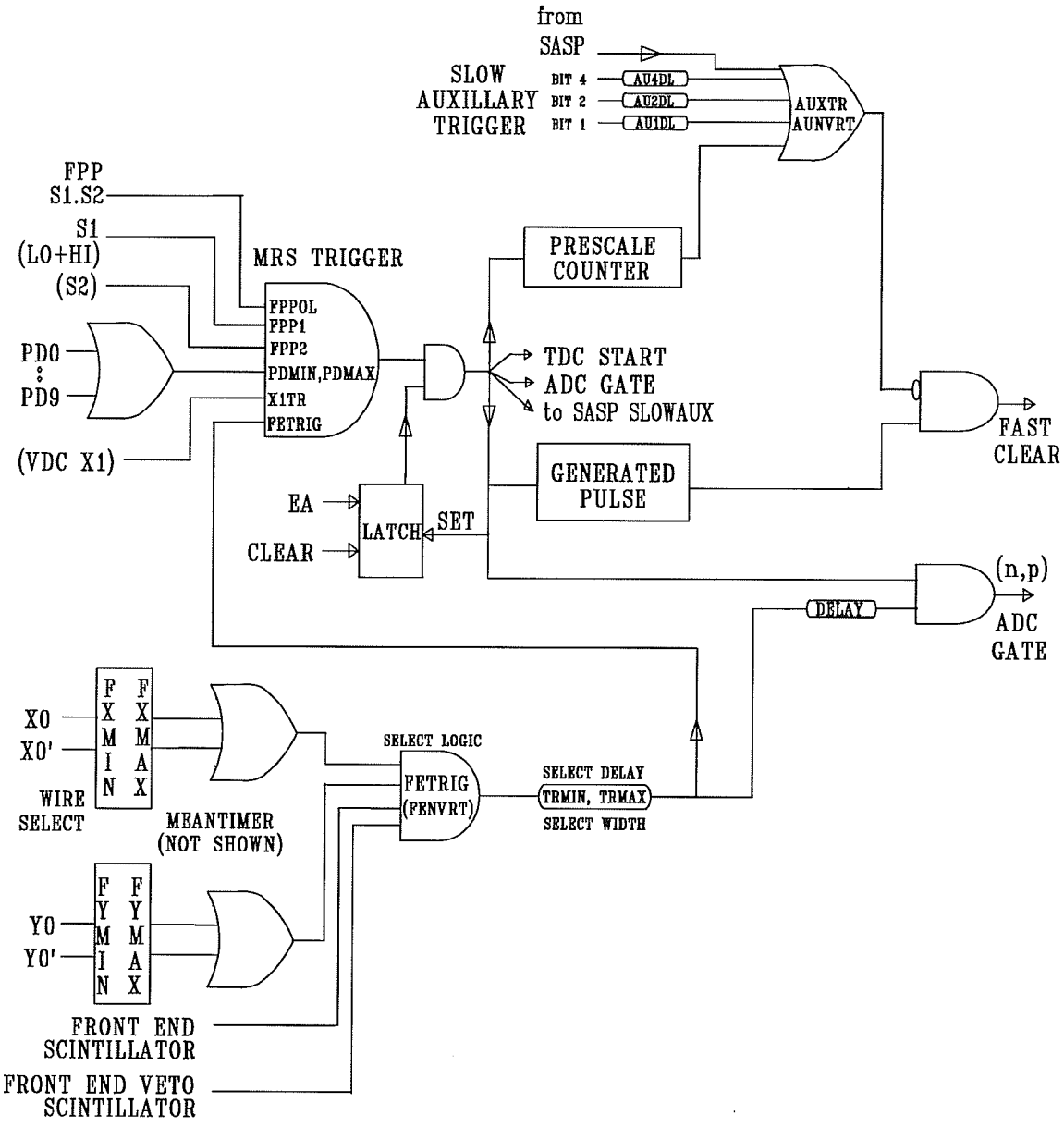

Figure 2.5: This figure shows a schematic of the MRS event-defining trigger.

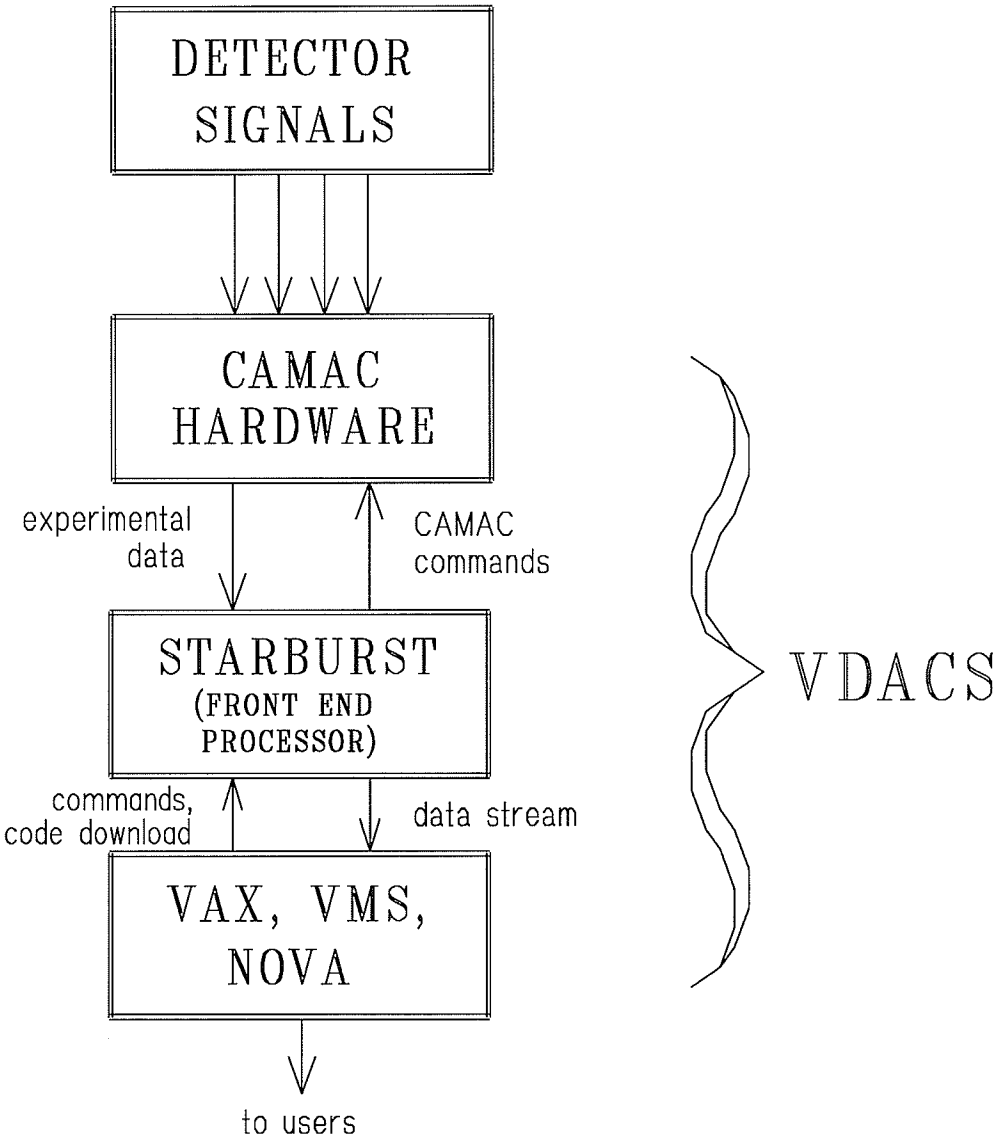

Figure 2.6: This figure illustrates data acquisition operations.

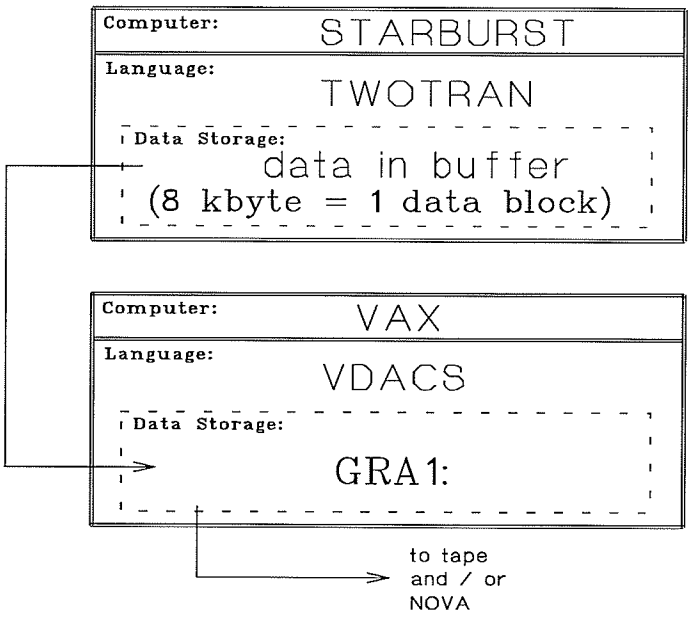

Figure 2.7: This figure depicts a schematic representation of data stream movement between the STARBURST and the VAX.

Another responds to LAM interrupts by building events as it reads data from the CAMAC digitizers. In this way the TWOTRAN program organizes the data into a data stream. The data stream is stored in a buffer in the STARBURST until it is shipped in 8 kilobyte blocks to a virtual device called 'GRA1:', which is part of the VAX memory. From GRA1:, samples of data can be analyzed on-line by NOVA in order to monitor the nature and quality of the incoming data. Meanwhile, the data stream is sent to the VAX and subsequently written to tape. Figure 2.7 illustrates this movement of data between the STARBURST module and the VAX.

In NOVA, variables known as 'pointers' are associated with most data words (the pointers themselves are two byte words, I*2). For clarity, these pointer names, rather than the data word addresses themselves, are given in figure 2.8, which shows the format of the DASS data stream. The data stream will now be described in terms of these NOVA pointers.

The header of the data stream consists of five words that describe the event type (ie, whether the event is a scaler read or a normal event trigger, what the event length is, etc.). NOVA pointers refer to the words following these header words. Thus, in describing the data stream, the enumeration of data words usually commences after these first five header words. Bearing that in mind, the zeroth word in the data stream tells NOVA what the mode of spectrometer operation is for the given experiment; the three possibilities are: MRS only, SASP only or a DASS configuration. The MRS part of the data stream follows the zeroth word, as indicated by the first word being MSTART; NOVA attributes to it the

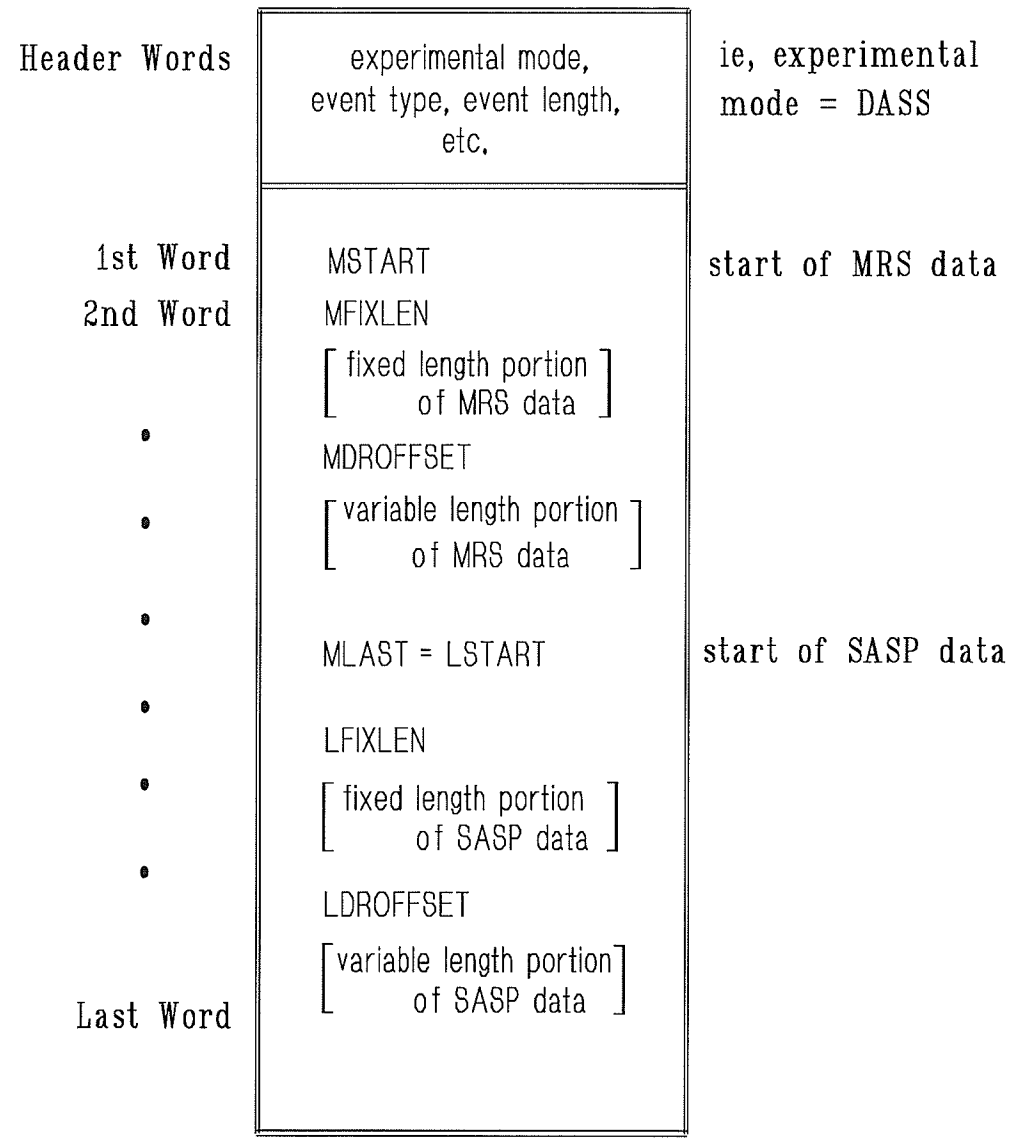

Figure 2.8: The TWOTRAN data stream for a DASS experiment is shown here.

value of '1'. After MSTART, the data word MFIXLEN follows, and this word indicates that a fixed number of data words is about to follow. That is, the number of data words following MFIXLEN is the same for every incoming event. The value of MFIXLEN is the number of data words in this fixed length portion of the data. For experiment E634, MFIXLEN = 32. Therefore the fixed length data is 32 words long.

The data which falls into the 'fixed length' category is DCR output (digital coincidence register, used to accept polarization state information, for example), ADC information (scintillator paddles pulse area, for example) and TDC output (which supplies timing information of the various detectors with respect to the trigger time).

The next data word is pointed to by MDROFFSET. This word describes the length of the variable length part of the data stream. The 'offset' part of the name MDROFFSET is understandable when considering the definition of MDROFFSET,

```
MDROFFSET=MSTART+MFIXLEN = 1 + 32 = 33
```

Thus, the start of the variable length data is 'offset' by 33 data words. Data which satisfies this description is drift chamber and front end chamber data. This data is of variable length depending on the particular event because different events may hit a different number of wires.

The SASP data now follows in the data stream, and this is indicated by the next word being MLAST, which is also equivalent to LSTART, the start of the SASP data. MLAST is defined as

```
MLAST=MDROFFSET+$RAW(MDROFFSET)/2.
```

Without dividing $RAW(MDROFFSET) by two, we would have the length of the variable length data in bytes. Dividing the MDROFFSET byte count by two converts its dimensions to a measure in words. Thus, the start of the SASP data is offset by the sum of MSTART, MFIXLEN and the number of data words occupied by the variable length data. In analogy to the MRS data part of the data stream, LFIXLEN follows the LSTART. LFIXLEN has a value of 45. Thus, the fixed length portion of the SASP data is composed of 45 data words. Following the fixed length data in the data stream is the word LDROFFSET, where

```
LDROFFSET=LSTART+LFIXLEN.
```

LDROFFSET points to the location in the data stream where the wire chamber data begins. After this data, the data for the next event follows, in the same data stream format as described above.

As previously mentioned, the TWOTRAN program contains instructions which handle raw data and allow the STARBURST module to organize this raw data into the data stream format described above. TWOTRAN programs have been written for all three modes of spectrometer operation, and the TWOTRAN code used for this DASS experiment is

essentially a combination of the code in the TWOTRAN programs for MRS and SASP single spectrometer operation. The TWOTRAN program used for this DASS experiment is given in appendix E. For more details of TWOTRAN code, please see reference [15].

2.10 Dispersion

The beam transport system that delivers the protons to the target position in the scattering chamber usually provides an achromatic beam where particles of all momenta are focused to a nearly point-like spot. However, the beam transport system can also be set to disperse the beam according to the incident particle momentum. A typical diameter of this beam spot is 2 mm. This implies that the beam 'spot' may not necessarily be a 'spot', but rather an elongated area. Along the height of this area, the energy of the incident protons varies somewhat, typically a variation of 1 MeV about the central momentum. For example, a beam dispersion of -6 cm/% implies that changing the particle momentum by 1% of the incident particle central momentum would result in a change of particle position (measured at the target) of 6 cm [16]. A typical value of the deviation from central momentum for the incident particles coming from the cyclotron is 0.2% [17]. Using this value, a -6 cm/% dispersion implies that the dispersion of the beam 'spot' on the target would be 1.2 cm. The negative sign in the value of the dispersion is due to beam transport labelling conventions (discussed in §3.2). This corresponds to the particle with the larger momentum having the larger values of the Transport coordinate X_{TR}, as shown in figure 3.11 on page 52.

A dispersed beam thus provides a one-to-one correspondence between position on target and momentum of an incident proton. This can be used in the following way: if the outgoing particle trajectory from a reaction event can be reconstructed from the spectrometer information to yield the target interaction position, the incident proton momentum can be determined to within an uncertainty much smaller than the original beam spread of $\sim 0.2\%$. Consequently, the reaction kinematics are better determined and the energy resolution greatly improved. However, achieving a high quality dispersed beam tune is more technically challenging than achieving an achromatic beam tune, so there is a compromise involved.

A spectrometer also has its own inherent dispersion. This is characterized by the transfer matrix element $R_{16} = dX/d\delta$, where dX is the change in focal plane position for the percentage change in particle momentum $d\delta$. To achieve 'dispersion matching' between the beam and the spectrometers is to have the particles from a reaction's specific final state all fall at the same position in the focal plane. This of course leads to a better energy resolution at the focal plane since the energy resolution is then not adversely affected by variations in incident beam energy. Dispersion matching when using two spectrometers is more complex and technically challenging than the case described above for only one spectrometer. Fortunately, off-line analysis can correct for the condition where full dispersion matching is not achieved.

The value of interest for the spectrometers is the D/M value, where D is the dispersion of the spectrometer, characterized by transfer matrix element R_{16}, and M is the spectrometer magnification, characterized by transfer matrix element R_{11}. For more details on transfer matrix elements see §2.11; the derivation of the D/M relation is given in equation (2.5) of §2.11.

Ideally, the first order transfer matrix elements R_{11} and R_{16} are independent of focal plane position. However, the SASP has such a large acceptance (-10% to +15% of central momentum) that there is a correlation between magnification and dispersion and the focal plane position; thus the values of R_{11} and R_{16} are calculated as a function of focal plane position in the NOVA user routine 'USRE'.

The smaller MRS acceptance is approximately -7% to +7% of central momentum. For the MRS, no user routine is presently utilized to calculate the transfer matrix elements. Instead, it has proved adequate to use constant values for R_{11} and R_{16} for the MRS, inputted into NOVA as parameters.

For the 500 MeV runs in E634, technical difficulties made the use of a fully dispersion-matched beam impossible to achieve. Ideal dispersion matching is achieved by matching dispersion between the beam and *both* spectrometers. This involves different beam tunes for each angle and magnet setting combination and this was not feasible due to time constraints. The dispersion that was achieved proved adequate for the purposes of the experiment since deuteron energy loss through the target played the most significant role in determining the energy resolution. Another factor affecting energy resolution is multiple scattering occurring between VDC1 and VDC2 in both spectrometers, but this was not as significant as the deuteron energy loss.

A dispersed beam of -6 cm/% was used for the 500 MeV runs which provided a beam spot approximately 2 mm wide and 1 cm high. For the 370 MeV runs, an achromatic beam tune was used because a dispersed beam tune for this energy was not available at the time of the experiment. For a kinematic description of beam dispersion and to see how it was incorporated into an expression for beam energy, see §3.6.3.

2.11 Transfer Matrix Elements

The physical meaning of the *transfer matrix elements* is discussed in this section. These matrix elements will be referred to in §3.5 where conversion between coordinate systems is discussed.

The transport of particles from the target up to the focal surface of a spectrometer is described to first order by the matrix equation

$$\begin{array}{ccc} \textit{outgoing} & & \textit{incoming} \\ \textit{particle} & \textit{transfer matrix} & \textit{particle} \end{array}$$

$$\begin{pmatrix} x_f \\ \theta_f \\ y_f \\ \phi_f \\ l_f \\ \delta_f \end{pmatrix} = \begin{pmatrix} R_{11} & R_{12} & 0 & 0 & 0 & R_{16} \\ R_{21} & R_{22} & 0 & 0 & 0 & R_{26} \\ 0 & 0 & R_{33} & R_{34} & 0 & 0 \\ 0 & 0 & R_{43} & R_{44} & 0 & 0 \\ R_{51} & R_{52} & 0 & 0 & R_{55} & R_{56} \\ 0 & 0 & 0 & 0 & 0 & R_{66} \end{pmatrix} \begin{pmatrix} x_i \\ \theta_i \\ y_i \\ \phi_i \\ l_i \\ \delta_i \end{pmatrix} \tag{2.1}$$

where the subscript i denotes the initial or target coordinates and the subscript f denotes the final or focal surface coordinates. The transfer matrix parameterizes the beam optical transport properties of the spectrometer [18].The definitions of the target and focal surface coordinates are given in §3.1.

Equation (2.2) provides examples of some typical matrix element values; the values shown are those used for the MRS during E634 analysis.

$$\begin{pmatrix} x_f \\ \theta_f \\ y_f \\ \phi_f \\ l_f \\ \delta_f \end{pmatrix} = \begin{pmatrix} -0.3766 & 0.0 & 0 & 0 & 0 & 3.6965 \\ -11.671 & -2.6565 & 0 & 0 & 0 & 6.3408 \\ 0 & 0 & -7.1917 & -0.1530 & 0 & 0 \\ 0 & 0 & -11.4160 & -0.304 & 0 & 0 \\ R_{51} & R_{52} & 0 & 0 & R_{55} & R_{56} \\ 0 & 0 & 0 & 0 & 0 & 1 \end{pmatrix} \begin{pmatrix} x_i \\ \theta_i \\ y_i \\ \phi_i \\ l_i \\ \delta_i \end{pmatrix} \tag{2.2}$$

To a first order approximation, the final position and the associated angle (x_f, θ_f) in the bend plane depend only upon initial position and angle (x_i, θ_i) in that same plane and on the momentum deviation δ. Similarly, the non-bend plane coordinates are decoupled in first order from the bend plane coordinates, and hence some of the transfer matrix elements are zero. δ_i and δ_f are equivalent because the static magnetic field of the spectrometer does not change the magnitude of the particle's momentum [18]. Hence, the R_{66} element is taken to be unity. For brevity, future references to δ_i or δ_f will be replaced simply by δ.

δ is the momentum deviation of a given particle ray with respect to the central momentum p_o and is defined by

$$\delta = \left(\frac{p - p_o}{p_o}\right) \times 100\% = \frac{\Delta p}{p_o} \times 100\% \tag{2.3}$$

where p is the momentum of an arbitrary ray [18]. Note that 'central' momentum p_o is not actually central, as the nominal momentum acceptance of the SASP is $0.9p_o$ to $1.15p_o$, for a total momentum bite of 25% of p_o. Specifically, p_o is that momentum for which a ray entering the spectrometer along the incident optic axis will be bent through 90°, to exit along the outgoing optical axis [18].

A point-to-point focus in X implies that R_{12} is zero. Among the remaining elements, R_{11}, R_{16}, R_{21}, R_{22} and R_{26} are associated with parameters in the bend plane whereas R_{33},

R_{34}, R_{43}, and R_{44} are associated with parameters in the non-bend plane. The elements R_{51}, R_{52}, R_{55}, and R_{56} are related to path length through the spectrometer.

Using the transfer matrix elements and equation (2.1), we can derive the D/M expression discussed in §2.10. The following relationship is extracted from the matrix equation given in equation (2.1):

$$x_f = R_{11}x_i + R_{16}\delta_i \tag{2.4}$$

Since we want all rays to focus at the same location in the focal plane, we want Δx_f=0. Thus,

$$\begin{aligned} \Delta x_f &= R_{11}\Delta x_i + R_{16}\Delta\delta = 0, \\ \text{or, } \frac{-R_{16}}{R_{11}} &= \frac{\Delta x_i(cm)}{\Delta\delta(\%)} \\ \text{and } \frac{-R_{16}}{R_{11}} &= D/M. \end{aligned} \tag{2.5}$$

The transfer matrix elements can be determined experimentally. For details on how this is done, please see reference [18].

For the MRS, the transfer matrix elements are inputted directly into the NOVA program as constants, independent of particle momenta. For the SASP, the transfer matrix elements cannot be approximated as constants and are computed as a function of particle momentum, δ, in a NOVA user routine called 'USRE'. Typical values for the SASP at δ =0 are shown in equation (2.6) [18],

$$\begin{pmatrix} x_f \\ \theta_f \\ y_f \\ \phi_f \\ l_f \\ \delta_f \end{pmatrix} = \begin{pmatrix} 0.8153 & 0.0 & 0 & 0 & 0 & 2.6823 \\ 2.6988 & -1.7751 & 0 & 0 & 0 & 5.4054 \\ 0 & 0 & -3.9777 & -0.1764 & 0 & 0 \\ 0 & 0 & -12.280 & -0.7900 & 0 & 0 \\ R_{51} & R_{52} & 0 & 0 & R_{55} & R_{56} \\ 0 & 0 & 0 & 0 & 0 & 1 \end{pmatrix} \begin{pmatrix} x_i \\ \theta_i \\ y_i \\ \phi_i \\ l_i \\ \delta_i \end{pmatrix} . \tag{2.6}$$

Chapter 3

E634 ANALYSIS

3.1 Definitions of NOVA Variables Used for Particle Trajectories

NOVA is the program used for analysis, so the reader must understand the meanings of the NOVA variables which refer to kinematic quantities in order to follow the kinematics calculations discussed in §3.7. The spectrometer coordinates and related variables will be referred to by their NOVA names. A list of physical meanings associated with these names follows.

SASP Target Positions:

SXI_TR position of particle on target, measured along X-axis of target, in Transport units (cm). The corresponding transfer matrix element is x_i; see equation (2.1).

SYI_TR position of particle on target, measured along Y-axis of target, in Transport units (cm). The corresponding transfer matrix element is y_i; see equation (2.1).

STH_TGT_TR = θ_{TR}, SASP angle θ between particle trajectory and Z_{TR} axis, measured at the target, in the X_{TR}-Z_{TR} plane, in units of mrad. See figure 3.1. The corresponding transfer matrix element is θ_i; see equation (2.1).

SPH_TGT_TR = ϕ_{TR}, SASP angle ϕ between particle trajectory and Z_{TR} axis, measured at the target, in the Y_{TR}-Z_{TR} plane, in units of mrad. See figure 3.1. The corresponding transfer matrix element is ϕ_i; see equation (2.1).

SASP Front End Chamber Positions:

LX0_POS position of particle in SASP FEC, measured along X-axis of chamber, in 50 μm units.

LY0_POS position of particle in SASP FEC, measured along Y-axis of chamber, in 50 μm units.

SX0_CENT X-axis center of SASP FEC, in 50 μm units.

SY0_CENT Y-axis center of SASP FEC, in 50 μm units.

SX0_TR position of particle in SASP FEC, measured along X-axis of chamber, in Transport units (cm).

SY0_TR position of particle in SASP FEC, measured along Y-axis of chamber, in Transport units (cm).

SFECDIST_TR Distance, in meters, between the target and the MRS FEC. A typical value is 0.5485 m.

SASP Vertical Drift Chamber Positions:

LX1POS position of particle in SASP VDC1, measured along X-axis of chamber, in 50 μm units.

LX2POS position of particle in SASP VDC2, measured along X-axis of chamber, in 50 μm units.

LU1POS position of particle in SASP VDC1, measured along U-axis of chamber, in 50 μm units.

LU2POS position of particle in SASP VDC2, measured along U-axis of chamber, in 50 μm units.

SY1 Extracted VDC1 Y-axis particle position, in 50 μm units.

SY2 Extracted VDC2 Y-axis particle position, in 50 μm units.

SDY12 = SY2-SY1.

SX1_CENT X-axis center of SASP VDC1, in 50 μm units.

SX2_CENT X-axis center of SASP VDC2, in 50 μm units.

SY1_CENT Y-axis center of SASP VDC1, in 50 μm units.

SY2_CENT Y-axis center of SASP VDC2, in 50 μm units.

SX1_TR Intersection between the particle trajectory and SASP VDC1 measured perpendicular to the Z_{TR} axis and along the X_{TR} axis, in Transport units (cm). See figure 3.8 on page 45.

SX2_TR Intersection between the particle trajectory and SASP VDC2 measured perpendicular to the Z_{TR} axis and along the X_{TR} axis, in Transport units (cm). See figure 3.8 on page 45.

SDX12_TR = SX2_TR - SX1_TR. See figure 3.8 on page 45.

SY1_TR Intersection between the particle trajectory and SASP VDC1 measured perpendicular to the Z_{TR} axis and along the Y_{TR} axis, in Transport units (cm).

SY2_TR Intersection between the particle trajectory and SASP VDC2 measured perpendicular to the Z_{TR} axis and along the Y_{TR} axis, in Transport units (cm).

STH_VDC_TR SASP θ between particle trajectory and Z_{TR} axis,measured at the VDC, in the X_{TR}-Z_{TR} plane, in units of mrad; shown as θ in figure 3.8. The corresponding transfer matrix element is θ_f; see equation (2.1).

SPH_VDC_TR SASP ϕ between particle trajectory and Z_{TR} axis, measured at the VDC, in the Y_{TR}-Z_{TR} plane, in units of mrad. The corresponding transfer matrix element is ϕ_f; see equation (2.1).

SVDCDIST Distance between the two SASP VDCs, in 50 μm units, as shown in figure 3.3 on page 36. The value used for experiment E634 analysis was 7880.0 (50 μm units).

SVDCDIST_TR Distance between the two SASP VDCs, in meters. See figure 3.8 on page 45. The value used for experiment E634 analysis was 0.3940 m.

SDZ_TR Distance between the intersections of the particle trajectory with the VDC planes 1 and 2, measured along Transport Z-axis, in meters. See figure 3.8 and equation (3.46) on page 45.

SASP Focal Plane:

SDELTA_TR $= \delta = \left(\frac{p-p_o}{p_o}\right) \times 100\%$. For more details see equation (2.3) on page 25.

SDEL This gives the focal plane position, like SDELTA_TR, but differs in that SDEL is defined in terms of a polynomial fit of δ to focal plane position SXF_TR (see description below) from experimental data for different momentum deviations [18].

SXF The X position of a particle on the SASP focal plane, measured in 50 μm units. The corresponding transfer matrix element is x_f; see equation (2.1). It is at the focal plane that the particle trajectories are point-to-point focused by the spectrometer magnets. The zero X-position on the focal plane corresponds to central momentum, p_0.

SXF_CENT The location of the physical center of the SASP focal plane, in 50 μm units along the X-axis.

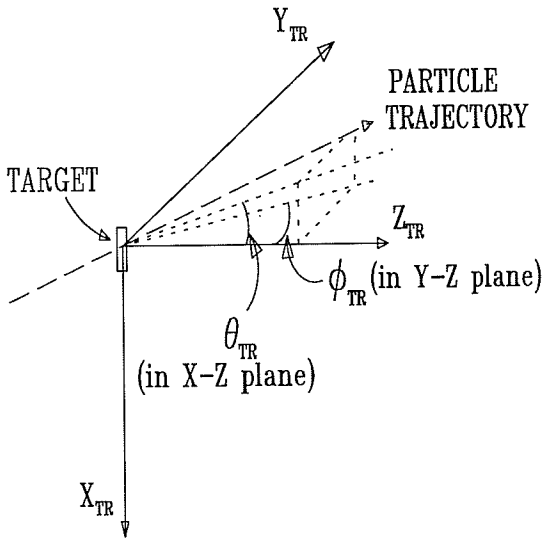

Figure 3.1: This figure shows the Transport coordinate system at the target. Angles θ_{TR} and ϕ_{TR} are named STH_TGT_TR and SPH_TGT_TR in the NOVA analysis program. Note that in this figure, θ_{TR} is negative.

SXF_TR The X position of a particle on the SASP focal plane, measured perpendicular to Z_{TR}, in Transport units of centimeters. For a more detailed explanation of focal plane, see **SXF** above.

Similarly, for the MRS we have the following NOVA definitions:

MRS Target Positions:

RXI_TR position of particle on target, measured along X-axis of chamber, in Transport units (cm). The corresponding transfer matrix element is x_i; see equation (2.1).

RYI_TR position of particle on target, measured along Y-axis of chamber, in Transport units (cm). The corresponding transfer matrix element is y_i; see equation (2.1).

RTH_TGT_TR $= \theta_{TR}$, MRS angle θ between the particle trajectory and Z_{TR} axis, measured at the target, in the X_{TR}-Z_{TR} plane, in units of mrad. See figure 3.1. The corresponding transfer matrix element is θ_i; see equation (2.1).

RPH_TGT_TR $= \phi_{TR}$, MRS angle ϕ between the particle trajectory and Z_{TR} axis, measured at the target, in the Y_{TR}-Z_{TR} plane, in units of mrad. See figure 3.1. The corresponding transfer matrix element is ϕ_i; see equation (2.1).

MRS Front End Chamber Positions:

MX0_POS position of particle in MRS FEC, measured along X-axis of chamber, in 50 μm units.

MY0_POS position of particle in MRS FEC, measured along Y-axis of chamber, in 50 μm units.

RX0_CENT X-axis center of MRS FEC, in 50 μm units.

RY0_CENT Y-axis center of MRS FEC, in 50 μm units.

RX0_TR position of particle in MRS FEC, measured along X-axis of chamber, in Transport units (cm).

RY0_TR position of particle in MRS FEC, measured along Y-axis of chamber, in Transport units (cm).

RFECDIST_TR Distance, in meters, between the target and the MRS FEC. For experiment E634, this distance was 0.63 m.

MRS Vertical Drift Chamber Positions:

MX1POS position of particle along in MRS VDC1, measured along X-axis of chamber, in 50 μm units.

MX2POS position of particle along in MRS VDC2, measured along along X-axis of chamber, in 50 μm units.

MU1POS position of particle along in MRS VDC1, measured along U-axis of chamber, in 50 μm units.

MU2POS position of particle along in MRS VDC2, measured along U-axis of chamber, in 50 μm units.

RY1 Extracted VDC1 Y-axis particle position, in 50 μm units.

RY2 Extracted VDC2 Y-axis particle position, in 50 μm units.

RX1_CENT X-axis center of MRS VDC1, in 50 μm units.

RX2_CENT X-axis center of MRS VDC2, in 50 μm units.

RY1_CENT Y-axis center of MRS VDC1, in 50 μm units.

RY2_CENT Y-axis center of MRS VDC2, in 50 μm units.

RX1_TR Intersection between particle trajectory and MRS VDC1 measured perpendicular to the Z_{TR} axis and along the X_{TR} axis, in Transport units (cm).

RX2_TR Intersection between particle trajectory and MRS VDC2 measured perpendicular to the Z_{TR} axis, and along the X_{TR} axis, in Transport units (cm).

RDX12_TR = RX2_TR - RX1_TR. See figure 3.8 on page 45 for the SASP analogy (SDX12_TR).

RY1_TR Intersection between particle trajectory and MRS VDC1 measured perpendicular to the Z_{TR} axis, and along the Y_{TR} axis, in Transport units (cm).

RY2_TR Intersection between particle trajectory and MRS VDC2 measured perpendicular to the Z_{TR} axis, and along the Y_{TR} axis, in Transport units (cm).

RTH_VDC_TR MRS angle θ between the particle trajectory and Z_{TR} axis, measured at the VDC, in the X_{TR}-Z_{TR} plane, in units of mrad. The equivalent θ for the SASP is shown in figure 3.8 on page 45. The corresponding transfer matrix element is θ_f; see equation (2.1).

RPH_VDC_TR MRS angle ϕ between the particle trajectory and Z_{TR} axis, measured at the VDC, in the Y_{TR}-Z_{TR} plane, in units of mrad. The corresponding transfer matrix element is ϕ_f; see equation (2.1).

RDY12 = RY2-RY1.

RVDCDIST Distance between the two MRS VDCs, in 50 μm units, as shown in figure 3.7. The value used for experiment E634 analysis was 5472.0 (50 μm units).

RVDCDIST_TR Distance between the two MRS VDCs, in meters. The value used for experiment E634 analysis was 0.2736 m.

RDZ_TR Distance between the intersections of the particle trajectory with the VDC planes 1 and 2, as measured along Transport Z-axis, in meters. See figure 3.8 on page 45 for the SASP analogy (SDZ_TR).

MRS Focal Plane:

RDELTA_TR = $\delta = \left(\frac{p-p_o}{p_o}\right) \times 100\%$. This is the same definition as for SDELTA_TR; for more details on SDELTA_TR, see equation (2.3) on page 25.

RXF The X position of a particle on the MRS focal plane, measured in 50 μm units. The corresponding transfer matrix element is x_f; see equation (2.1).

RXF_CENT The X position of the center of the MRS focal plane, in 50 μm units.

RXF_TR The X position of a particle on the MRS focal plane, measured perpendicular to Z_{TR}, in Transport units of centimeters.

The values for the centers of wire chambers and focal planes which were used for experiment E634 are given in table 3.1. Recall that no FEC was used in the SASP.

SASP	MRS
(all values are measured in 50 μm units)	
SX0_CENT (n/a)	RX0_CENT=800
SY0_CENT (n/a)	RY0_CENT=800
SX1_CENT=13154	RX1_CENT=10560
SX2_CENT=13185	RX2_CENT=10560
SY1_CENT=-3862	RY1_CENT=-1633
SY2_CENT=-3905	RY2_CENT=-1623
SXF_CENT=2409	RXF_CENT=18000

Table 3.1: This table lists the centers of FECs, VDCs and focal planes; these were the values used for E634 (may be subject to change for other experiments).

3.2 The Transport Coordinate System

The standard coordinate system used in beam transport calculations for beam lines and spectrometers is known as the Transport coordinate system. All kinematics calculations are performed with the variables in Transport units. The standard Transport conventions are as follows:

- Z is in the direction of the outgoing central particle ray, and is measured in meters,
- X and Y are measured in centimeters, with positive X in the direction of increasing particle momentum – in the *bend plane*, and positive Y in the *non-bend plane*, in the direction appropriate to a right-handed coordinate system,
- angles θ and ϕ of the ray measured at the target and at the VDCs are measured in milliradians. θ is the angle in the bend plane (X-Z plane) and ϕ is the angle in the non-bend plane (Y-Z plane).

The measured values of wire chamber position are peculiar to their construction, orientation and electronic read-out. The dimensions of these measured values are different from the Transport dimensions. In the course of the analysis, these measured values are translated into Transport units for use in kinematic calculations.

The DASS coordinate conventions and the Transport conventions are illustrated in figure 3.2. Transport coordinates are indicated by the subscript "TR". The DASS coordinate convention used for the X, Y-axes within the wire chambers places the origin at one corner of the chamber. In the DASS coordinates, only positive integer values – referred to as channel numbers – are allowed. The dimensions of these values are 50 μm units. The Transport conventions place the origin at the center of the wire chamber (intersecting the central particle trajectory), allowing for both positive and negative values; the units of these X and Y positions are in centimeters. A very important feature to note is that the VDC planes are positioned at 45° relative to the Transport Z-axis.

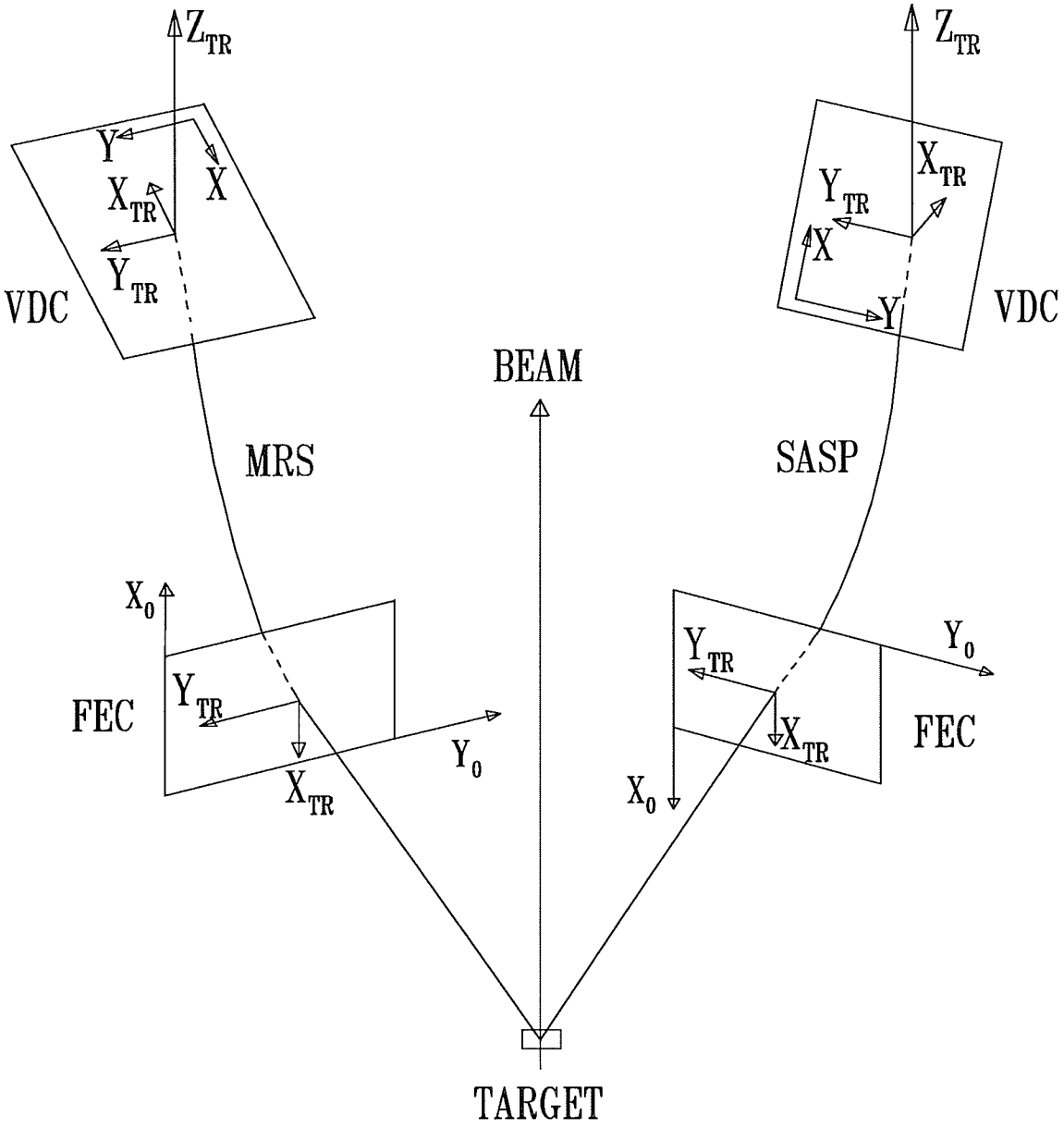

Figure 3.2: Shown here are the Transport and DASS coordinate systems. Transport coordinates are indicated by the 'TR' subscript; unsubscripted coordinates use the DASS convention.

3.3 SASP Focal Plane

In this section the SASP focal surface is parameterized in terms of Transport coordinates. A schematic diagram of the focal surface and its location in the SASP is shown in figure 3.3 [17]. Note that the VDC2 plane is offset by a distance LX1C0 with respect to the low momentum end of VDC1 plane, where LX1C0 = SVDCDIST. Let us define a coordinate system, (X_1,Z_1), with the origin, 0_1, at the left end of VDC1 plane. As shown in figure 3.3, an arbitrary particle trajectory intersects the focal surface at X_1 = SXF and Z_1 = SFOCALF. The shape of the focal surface was determined experimentally as described in reference [18].

In the X_1 coordinate system depicted in figure 3.3, the shape of the focal surface is given by (SXF,SFOCALF)=(X,Z). Figure 3.4 shows a plot of SXF versus SFOCALF. For a description on how the data were obtained, see reference [18]. The focal surface can be parameterized by the fourth-order polynomial,

$$SFOCALF = a_0 + a_1 SXF + a_2 SXF^2 + a_3 SXF^3 + a_4 SXF^4, \tag{3.1}$$

where the coefficients a_0 through a_4 are given in figure 3.4. The equation of an arbitrary particle ray can be determined from its position of intersection with each of the vertical drift chambers. The focal position of an arbitrary ray is then obtained by its point of intersection with the polynomial of the focal surface.

The particle trajectory shown in figure 3.3 is described by

$$Z_1 = mX_1 + b, \quad \text{where } m = \frac{SVDCDIST}{SX2 - SX1}, \tag{3.2}$$

where SX1 and SX2 are the points of intersection between the trajectory and VDC planes VDC1 and VDC2, respectively, as measured in the X_1 coordinate system. Since

$$0 = mSX1 + b, \tag{3.3}$$

then

$$b = -mSX1 \text{ and } Z_1 = -mSX1 + mX_1. \tag{3.4}$$

Therefore,

$$Z_1 = \left(\frac{SVDCDIST}{SX2 - SX1}\right)(X_1 - SX1). \tag{3.5}$$

For an arbitrary ray we define the X_1-Z_1 position by coordinates (x_1, z_1) and the X_{TR}-Z_{TR} position by coordinates (x_{TR}, z_{TR}). The particle ray intersects the focal surface at x_1, a position given by the simultaneous solution of equations (3.1) (with SXF = x_1 and SFOCALF = z_1) and (3.2) as follows

$$\begin{aligned} mx_1 + b &= a_0 + a_1 x_1 + a_2 x_1^2 + a_3 x_1^3 + a_4 x_1^4 \\ 0 &= (a_0 - b) + (a_1 - m)x_1 + a_2 x_1^2 + a_3 x_1^3 + a_4 x_1^4. \end{aligned} \tag{3.6}$$

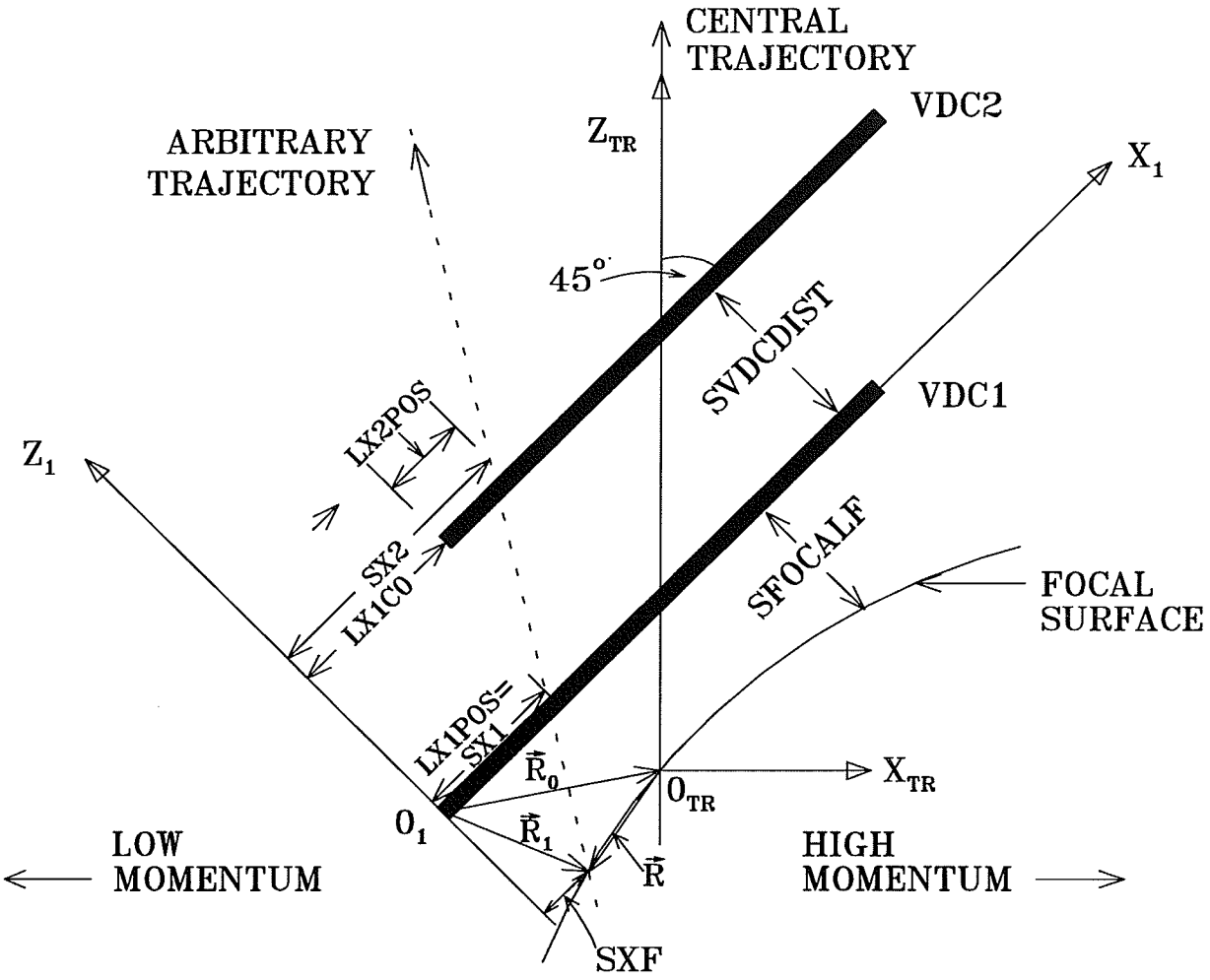

Figure 3.3: This is a schematic representation of the SASP focal surface and VDCs. $\vec{R}_0$ and $\vec{R}_1$ are the position vectors, relative to the origin 0_1, of the points where the central and arbitrary trajectories intersect the focal surface.

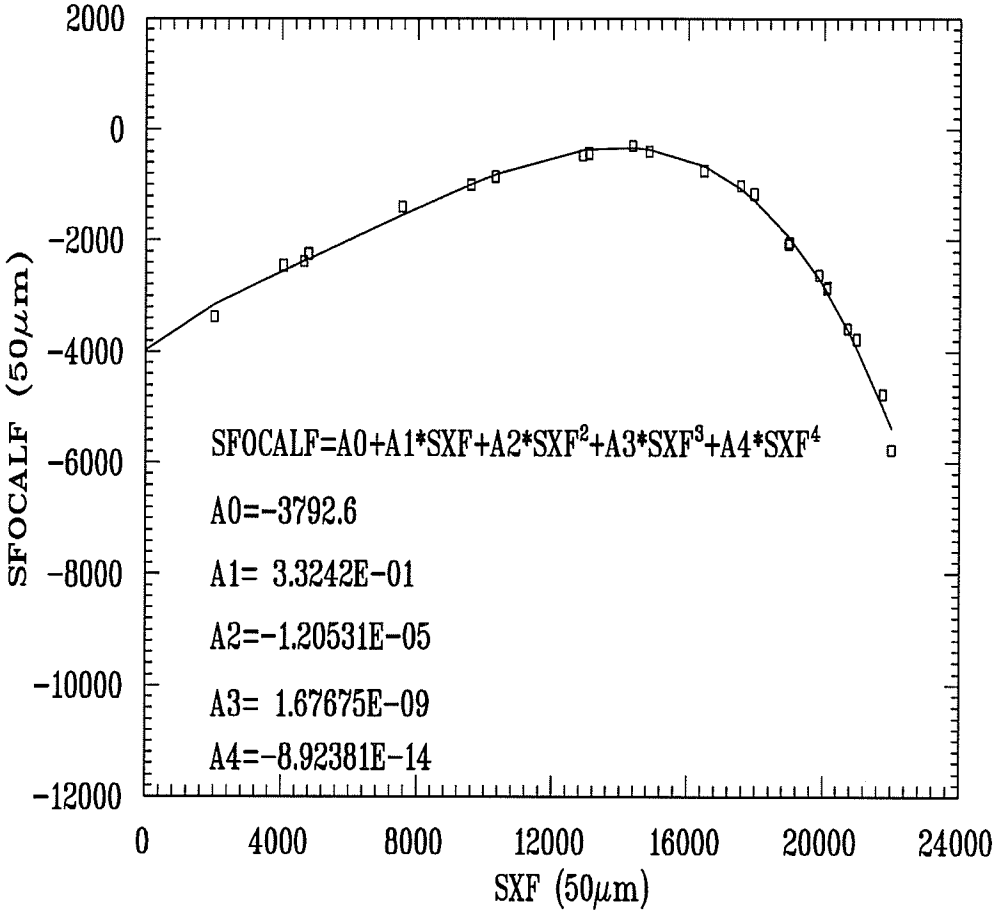

Figure 3.4: A fourth order polynomial fit to the empirically determined SASP focal surface, in the X-Z coordinate system is shown here.

This allows the focal position to be calculated by solving a fourth-order polynomial. Reference [18] illustrates the Newton-Raphson iterative numerical method utilized to solve equation (3.6).

To convert the X_1-Z_1 coordinate system depicted in figure 3.3 to the Transport coordinate system, X_{TR}-Z_{TR}, we note the following relationships between them, evident from figure 3.3,

$$\hat{i}_1 = \frac{1}{\sqrt{2}}(\hat{i}_{TR} + \hat{k}_{TR}) \text{ and } \hat{k}_1 = \frac{1}{\sqrt{2}}(-\hat{i}_{TR} + \hat{k}_{TR}), \tag{3.7}$$

where $\hat{i}_1, \hat{k}_1$ and $\hat{i}_{TR}, \hat{k}_{TR}$ are the unit vectors for the X_1-Z_1 and Transport systems, respectively. We define the coordinates of a central ray in the Transport coordinate system as (xc_{TR}, zc_{TR}). The vector $\vec{R}_0$ gives the location of Transport origin, 0_{TR}, with respect to the X_1-Z_1 origin, given by

$$\vec{R}_0 = xc_{TR}\hat{i}_1 + zc_{TR}\hat{k}_1. \tag{3.8}$$

From the figure we see that

$$\begin{aligned}
\vec{R} &= \vec{R}_1 - \vec{R}_0 \\
&= (x_1\hat{i}_1 + z_1\hat{k}_1) - (xc_{TR}\hat{i}_1 + zc_{TR}\hat{k}_1) \\
&= (x_1 - xc_{TR})\hat{i}_1 + (z_1 - zc_{TR})\hat{k}_1 \\
&= (x_1 - xc_{TR})\frac{1}{\sqrt{2}}(\hat{i}_{TR} + \hat{k}_{TR}) + (z_1 - zc_{TR})\frac{1}{\sqrt{2}}(-\hat{i}_{TR} + \hat{k}_{TR}) \\
&= \left(\frac{1}{\sqrt{2}}(x_1 - z_1) - \frac{1}{\sqrt{2}}(xc_{TR} - zc_{TR})\right)\hat{i}_{TR} \\
&\quad + \left(\frac{1}{\sqrt{2}}(x_1 + z_1) - \frac{1}{\sqrt{2}}(xc_{TR} + zc_{TR})\right)\hat{k}_{TR},
\end{aligned} \tag{3.9}$$

where all the x, z quantities are in 50 μm units. To convert these to the Transport dimensions of centimeters, we multiply by (0.005 cm)/(50 μm). The data set used in reference [18], based on scattering off a ^{208}Pb target at 200 MeV, contains the following values of SFOCALF and SXF for a central ray

$$SFOCALF = -463.399_{[50\ \mu m]} = zc_{TR} \tag{3.10}$$

$$SXF = 12877.95_{[50\ \mu m]} = xc_{TR}. \tag{3.11}$$

Using these values, we have

$$\frac{1}{\sqrt{2}}(xc_{TR} - zc_{TR}) \times 0.005_{[0.005\ cm/(50\ \mu m)]} =$$

$$\frac{1}{\sqrt{2}}(12877.95 + 463.399)_{[50\ \mu m]} \times 0.005_{[0.005\ cm/(50\ \mu m)]} = 47.1688 \text{ cm} \tag{3.12}$$

$$\frac{1}{\sqrt{2}}(xc_{TR} + zc_{TR}) \times 0.005_{[0.005\ cm/(50\ \mu m)]} =$$

$$\frac{1}{\sqrt{2}}(12877.95 - 463.399)_{[50\ \mu m]} \times 0.005_{[0.005\ cm/(50\ \mu m)]} = 43.8921 \text{ cm}. \tag{3.13}$$

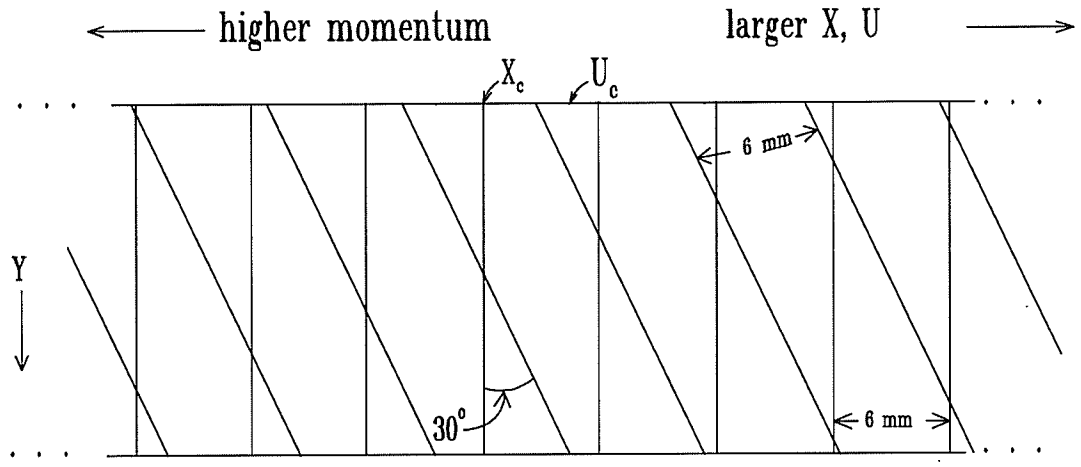

Figure 3.5: A schematic representation of a vertical drift chamber (VDC) showing the orientation of X and U wire planes, as viewed from above is shown here. X_c , U_c indicate the center wires in each plane. The directions of increasing momentum and X, U position indicated are specific to the SASP VDC orientation.

Hence with (x_{TR}, z_{TR}) as the Transport coordinates of $\vec{R}$,

$$\begin{aligned} \vec{R} &= x_{TR}\hat{i}_{TR} + z_{TR}\hat{k}_{TR}, \\ x_{TR[cm]} &= \frac{1}{\sqrt{2}}(x_1 - z_1) \times 0.005_{[0.005\ cm/(50\ \mu m)]} - 47.1688 \text{ cm, and} \qquad (3.14) \\ z_{TR[cm]} &= \frac{1}{\sqrt{2}}(x_1 + z_1) \times 0.005_{[0.005\ cm/(50\ \mu m)]} - 43.8921 \text{ cm.} \qquad (3.15) \end{aligned}$$

To extract Y_{TR} positions in the VDC planes, note that the VDCs are comprised of two planes, an X plane and a U plane. The wires in the U plane are strung at an angle of 30° with respect to the X plane wires, as shown in figure 3.5. Note that for the SASP VDCs, Y_{TR} and Y increase in opposite directions, as shown in figure 3.2. From figure 3.5, we see that

$$\tan(30°) = \frac{1}{\sqrt{3}} = \frac{-Y}{X} \quad \Rightarrow Y = \frac{-X}{\sqrt{3}} \qquad (3.16)$$

and

$$\sin(30°) = \frac{1}{2} \quad = \frac{-Y}{U} \quad \Rightarrow Y = \frac{-U}{2}. \qquad (3.17)$$

Now

$$4 \times (3.17) \quad \rightarrow \quad -2U = 4Y \qquad (3.18)$$

and

$$-3 \times (3.16) \quad \rightarrow \quad \sqrt{3}\,X = -3Y. \qquad (3.19)$$

Adding (3.18) and (3.19) produce

$$Y = \sqrt{3}\,X - 2U. \qquad (3.20)$$

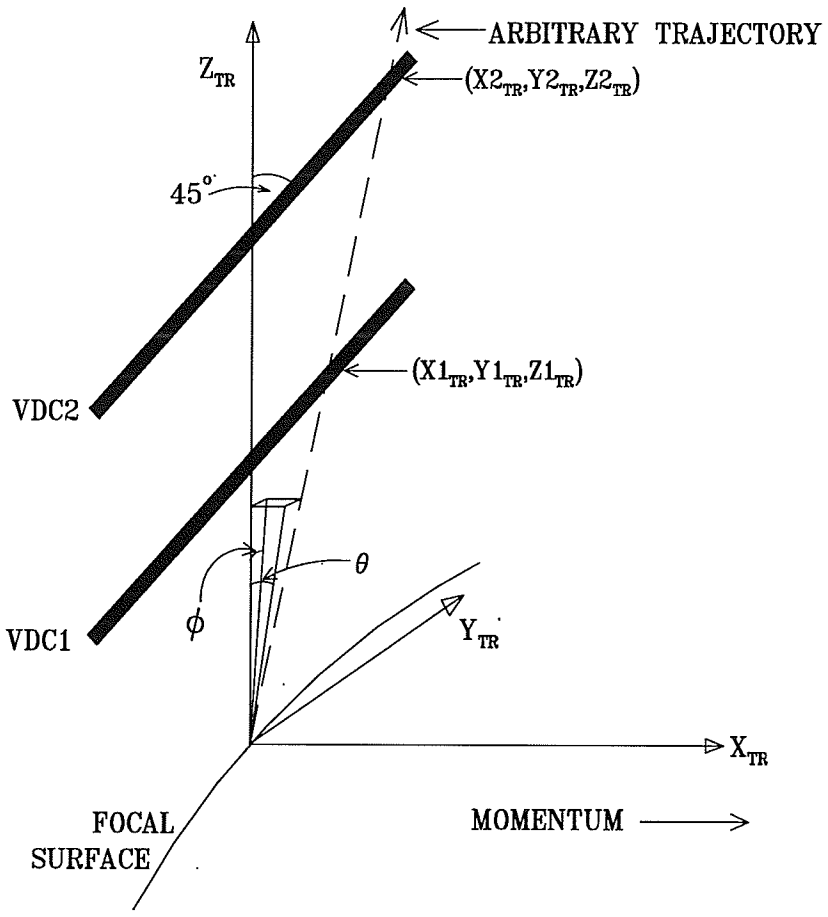

Figure 3.6: An arbitrary particle trajectory is shown here intersecting the SASP VDC planes at points ($X1_{TR}$,$Y1_{TR}$,$Z1_{TR}$) and ($X2_{TR}$,$Y2_{TR}$,$Z2_{TR}$). The trajectory is in the positive X_{TR}-Y_{TR}-Z_{TR} octant. θ is in the X-Z plane and ϕ is in the Y-Z plane.

To place this in the proper Transport coordinate system, in which the origin is located at the center of the VDC, we must subtract the VDC center offset (in channel number coordinates); the Y1 and Y2 centers are given in table 3.1 on page 33. Also, all dimensions of 50 μm must be converted to centimeters. Thus, the Y_{TR} Transport coordinates of $\vec{R}$ for the SASP VDC1 and VDC2 are

$$y1_{TR[cm]} = -(\sqrt{3}\,SX1 - 2U1 - SY1\_CENT)_{[50\mu m]} \times 0.005_{[cm/50\mu m]} \quad (3.21)$$

$$y2_{TR[cm]} = -(\sqrt{3}\,SX2 - 2U2 - SY2\_CENT)_{[50\mu m]} \times 0.005_{[cm/50\mu m]}. \quad (3.22)$$

From figure 3.6, we see that the angles θ and ϕ made by the particle trajectory in the X-Z and Y-Z planes, respectively, are

$$\theta_{TR[mrad]} = tan^{-1}\left(\frac{X2_{TR} - X1_{TR}}{Z2_{TR} - Z1_{TR}}\right) \times 1000_{[mrad/rad]}, \quad (3.23)$$

$$\phi_{TR[mrad]} = tan^{-1}\left(\frac{Y2_{TR} - Y1_{TR}}{Z2_{TR} - Z1_{TR}}\right) \times 1000_{[mrad/rad]}. \quad (3.24)$$

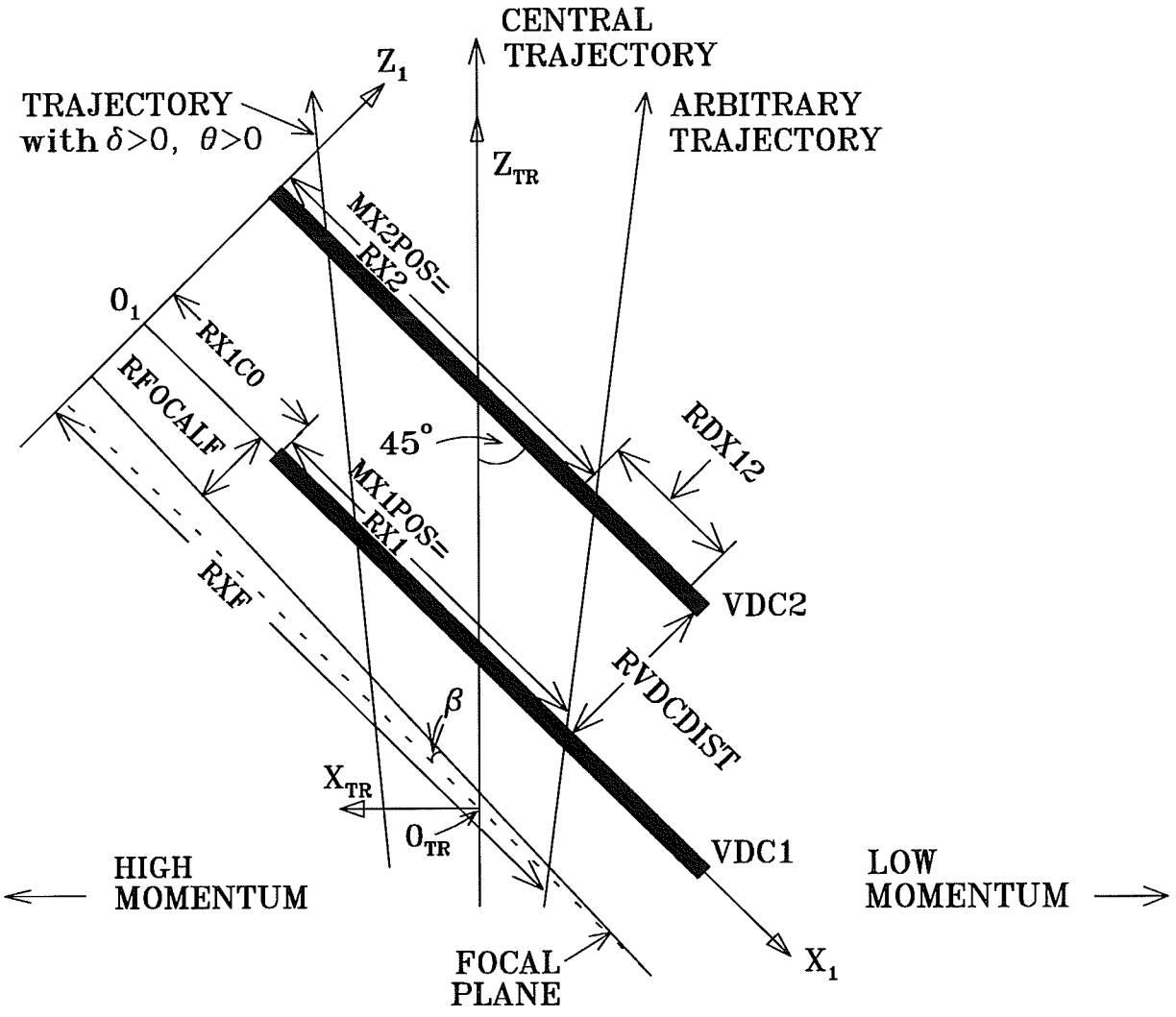

Figure 3.7: The MRS focal surface and VDCs are shown here, as per experiment E634.

For experiment E634, the NOVA subroutine "USR9" was used to calculate the focal plane coordinates (X_{TR},Y_{TR},Z_{TR}) and the angles θ and ϕ according to the above calculations.

3.4 MRS Focal Plane

The MRS focal surface, which spans a smaller momentum acceptance than does the SASP focal plane, is modelled as a simpler, flat focal surface. A diagram of the MRS focal surface and its location with respect to the MRS VDCs is shown in figure 3.7 [17]. In this section the MRS focal plane is specified in terms of Transport coordinates. The process is similar to that for the SASP, except that the flat focal plane of the MRS simplifies the situation considerably. The MRS VDC X1 plane is a distance of RX1C0 from the Z1 axis, where the

magnitudes of RX1C0 and RVDCDIST are the same. The focal plane is located a distance RFOCALF below the VDC X1 plane, at an angle β to it; typically, $\beta = 0$ and the focal plane is parallel to the VDCs. The following parameterization will be done for the general case, where β may not be zero.

In the X_1-Z_1 coordinate system depicted in figure 3.7, the equation describing the focal plane is

$$Z_{fp} = RFOCALF - X_{fp} \tan\beta \tag{3.25}$$

where we note that X_{fp} is the same as RXF in the figure. Also, take RDX12 = (RX1C0+RX1)-RX2. Noting that

$$0 = -\frac{RVDCDIST}{RDX12}(RX1C0 + RX1) + b \tag{3.26}$$

where b is the Z_1 intercept of the particle trajectory. Then the equation of the trajectory is

$$Z_{traj} = \frac{RVDCDIST(RX1C0 + RX1)}{RDX12} - \frac{RVDCDIST}{RDX12} X_{traj}. \tag{3.27}$$

Solving for the intersection of the trajectory with the focal plane, equating $Z_{traj} = Z_{fp}$ and setting $X_{traj} = X_{fp}$, we have

$$\begin{aligned} RFOCALF - X_{fp}\tan\beta &= \frac{RVDCDIST(RX1C0 + RX1)}{RDX12} - \frac{RVDCDIST}{RDX12} X_{fp} \\ X_{fp}\left(\frac{RVDCDIST}{RDX12} - \tan\beta\right) &= \frac{RVDCDIST(RX1C0 + RX1)}{RDX12} - RFOCALF \end{aligned}$$

and

$$X_{fp} = \frac{RVDCDIST(RX1C0 + RX1) - RFOCALF \times RDX12}{RVDCDIST - RDX12\tan\beta} \tag{3.28}$$

X_{fp} and Z_{fp} are the coordinates of the particle trajectory at the MRS focal surface. With $\tan\beta = 0$ and X_{fp}=RXF,

$$RXF = \frac{RVDCDIST \times RX1C - RFOCALF \times RDX12}{RVDCDIST}, \tag{3.29}$$

which is the NOVA expression used for experiment E634. RX1C = MX1POS + RX1C0 and MX1POS = RX1 as shown in figure 3.7.

The expressions for θ and ϕ at the MRS VDCs are derived in §3.5.2 and are given in equations (3.54) and (3.57) .

3.5 Conversion of Measured Quantities to Transport Units

In this section, SASP and MRS measured quantities will be converted to Transport units as was carried out for analysis of E634 data.

3.5.1 SASP Variables

Although the SASP front end chamber was not employed for experiment E634, conversion of SASP FEC-related quantities will be discussed here for completeness.

SX0_TR, SY0_TR, SX1_TR, SX2_TR, SY1_TR, SY2_TR:

Considering the SASP FEC measured quantities, note that the X_{TR} and X_0 axes increase in the same direction for the SASP, as shown in figure 3.2 on page 34. The position along the X_{TR} axis in the SASP FEC, in Transport units, is

$$SX0\_TR_{[cm]} = (LX0POS_{[50\ \mu m]} - SX0\_CENT_{[50\ \mu m]}) \times 0.005_{[cm/50\ \mu m]}. \quad (3.30)$$

The position along the Y_{TR} axis in the SASP FEC, in Transport units, is

$$SY0\_TR_{[cm]} = -(LY0POS_{[50\ \mu m]} - SY0\_CENT_{[50\mu m]}) \times 0.005_{[cm/50\mu m]}, \quad (3.31)$$

noting that Y_{TR} and Y_0 increase in opposite directions. To obtain the VDC X and Y coordinates in Transport units, the fact that the VDC planes are positioned at 45° relative to the Transport Z-axis must be considered. For the VDC1 plane, the X_{TR} position is given by

$$SX1\_TR_{[cm]} = ((LX1POS_{[50\mu m]} - SX1\_CENT_{[50\mu m]})/\sqrt{2}) \times 0.005_{[cm/50\mu m]}, \quad (3.32)$$

and for the VDC2 plane,

$$SX2\_TR_{[cm]} = ((LX2POS_{[50\mu m]} - SX2\_CENT_{[50\mu m]})/\sqrt{2}) \times 0.005_{[cm/50\mu m]}. \quad (3.33)$$

The VDC X_{TR} positions for plane 1 and 2 are indicated in figure 3.8. The Y_{TR} positions in the VDC planes are extracted from the U plane positions in equations (3.16) to (3.20) on page 39. The Y_{TR} coordinates for the SASP VDCs are

$$SY1\_TR = Y1_{TR\ [cm]} = -(\sqrt{3}\,X1 - 2U1 - SY1\_CENT)_{[50\mu m]} \times 0.005_{[cm/50\mu m]}, \quad (3.34)$$

$$SY2\_TR = Y2_{TR\ [cm]} = -(\sqrt{3}\,X2 - 2U2 - SY2\_CENT)_{[50\mu m]} \times 0.005_{[cm/50\mu m]}. \quad (3.35)$$

These expressions were derived on page 39.

STH_TGT_TR, STH_VDC_TR:

In this section the angles θ_i at the target and θ_f at the VDC – STH_TGT_TR and STH_VDC_TR, respectively – are determined. In experiment E634, the SASP did not utilize a front end chamber, so that STH_TGT_TR must be determined using STH_VDC_TR. STH_VDC_TR is labelled as θ in figure 3.8 and is

$$STH\_VDC\_TR_{[mrad]} = \left(\frac{SDX12\_TR_{[cm]}}{100_{[cm/m]}\sqrt{2} \times SVDCDIST\_TR_{[m]} + SDX12\_TR_{[cm]}} \right)_{[rad]} \times 1000_{[\frac{mrad}{rad}]} \quad (3.36)$$

From the transfer matrix equation given in equation (2.1) we obtain

$$X_f = R_{11}X_i + R_{12}\theta_i + R_{16}\delta \tag{3.37}$$

$$\theta_f = R_{21}X_i + R_{22}\theta_i + R_{26}\delta. \tag{3.38}$$

Eliminating X_i from these equations and solving for θ_i, and recalling that $R_{12} = 0$ yields

$$\theta_i = \frac{R_{11}\theta_f - R_{21}X_f + (R_{16}R_{21} - R_{11}R_{26})\delta}{R_{11}R_{22}}. \tag{3.39}$$

The value of X_f is given by (3.14) and is calculated in the USR9 subroutine, along with the momentum deviation δ. This information, together with θ_f (STH_VDC_TR) from (3.36), permits calculation of θ_i (STH_TGT_TR). The following notational equivalences between the transfer matrix elements and NOVA terms exist:

$$\begin{array}{rcl} & & TRANSFER \\ \underline{MATRIX\ ELEMENT} & \Longrightarrow & \underline{NOVA} \\ \theta_f & = & STH\_VDC\_TR = SXFVECTOR(2) \\ X_f & = & SXF\_TR = SXF\_TR9 = SXFVECTOR(1) \\ \delta & = & SDEL9 = SXFVECTOR(6) \\ R_{ij} & = & SRij = SRMATRIX(q). \end{array}$$

The references to SXFVECTOR(n) indicate vector elements of vector SXFVECTOR which is evaluated in the NOVA user routine USR9. The reference to SRMATRIX(q) indicates each of the transfer matrix elements calculated in the NOVA user routine USRE. Using these equivalences, the following NOVA definition,

$$SRRR = SR16 \times SR21 - SR11 \times SR26 \tag{3.40}$$

and (3.39), we now have the desired expression for STH_TGT_TR,

$$STH\_TGT\_TR = \frac{SR11 \times STH\_VDC\_TR - SR21 \times SXF\_TR9 + SRRR \times SDEL9}{SR11 \times SR22}. \tag{3.41}$$

The small angle approximation used in (3.41) leads to a maximum error of about 2% since the possible STH_TGT_TR values do not exceed $\sim$ 100 mrad.

SPH_TGT_TR, SPH_VDC_TR:

To determine the angle ϕ at the target from its value at the VDCs, we consider the following relationship obtainable from the transfer matrix given in equation (2.1), valid for small SYL_TR (y_i, Y position at the target)

$$SPH\_TGT\_TR = \frac{SPH\_VDC\_TR}{SR44} \tag{3.42}$$

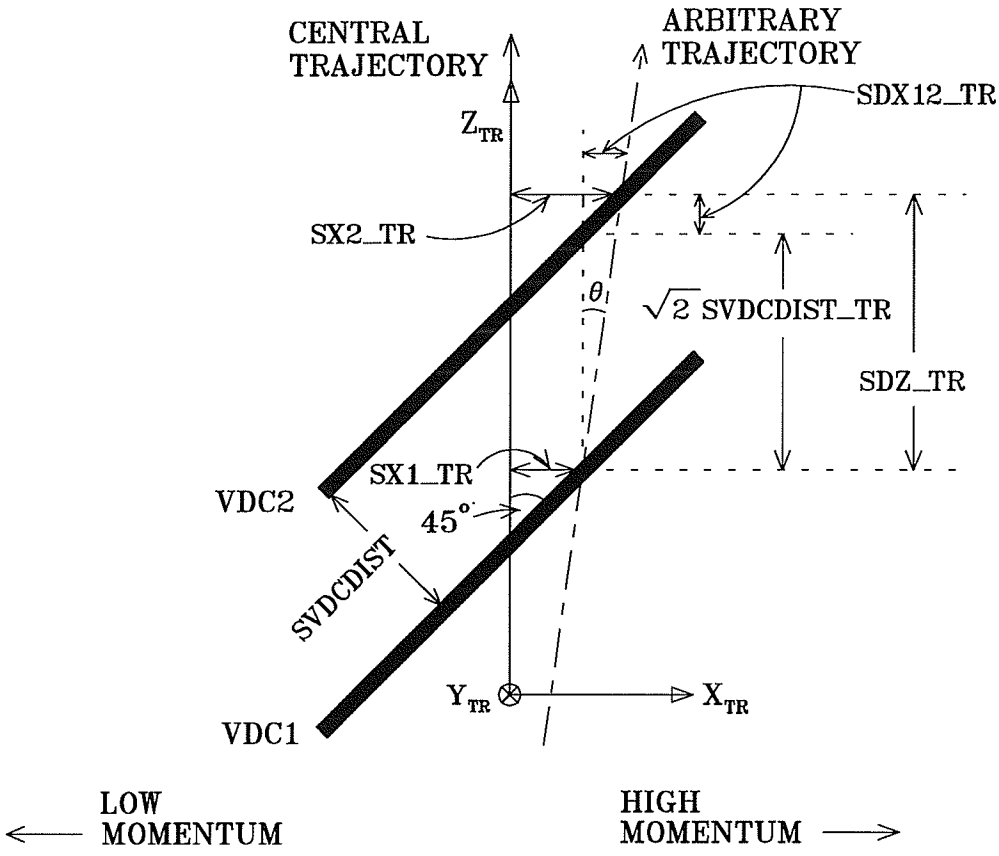

Figure 3.8: This figure shows a particle trajectory passing through SASP VDCs.

where SR44 is the R44 transfer matrix element for the SASP. This matrix element relates ϕ at the target to ϕ at the focal plane (near the VDC). By geometry,

$$SPH\_VDC\_TR_{[mrad]} = \frac{-(SDY12_{[mm/50\mu m]} \times 0.05_{[mm/50\mu m]})}{SDZ\_TR_{[m]}} \tag{3.43}$$

where

$$SDY12 = SY2 - SY1$$

and the minus sign in (3.43) is due to the fact that the VDC Y-coordinate measured quantities increase in a direction opposite to the Y_{TR} coordinate at the VDC (see figure 3.2). SDZ_TR is indicated in figure 3.8 [17]. We also write, referring to figure 3.8,

$$SVDCDIST\_TR_{[m]} = SVDCDIST_{[50\mu m]} \times 0.00005_{[m/50\mu m]}, \tag{3.44}$$

$$SDX12\_TR_{[cm]} = SX2\_TR_{[cm]} - SX1\_TR_{[cm]} \text{ and} \tag{3.45}$$

$$SDZ\_TR_{[m]} = \sqrt{2}\ SVDCDIST\_TR_{[m]} + \frac{SDX12\_TR_{[cm]}}{100_{[cm/m]}}. \tag{3.46}$$

Therefore, with both SDZ_TR and SDY12 determined, SPH_VDC_TR, and subsequently SPH_TGT_TR, can be calculated. The small angle approximation used in (3.43) is accept-

able since the ϕ-angle values used are less than $\sim$ 50 mrad.

3.5.2 MRS Variables

The definitions of coordinates at the top and bottom end of the MRS are analogous to those of the SASP, except where differences in axis orientation occur, as shown in figure 3.2.

RX0_TR, RY0_TR, RX1_TR, RY1_TR, RX2_TR, RY2_TR:

The MRS FEC coordinates in Transport notation are

$$RX0\_TR_{[cm]} = -(MX0POS_{[50\mu m]} - RX0\_CENT_{[50\mu m]}) \times 0.005_{[cm/50\mu m]} \quad (3.47)$$

and

$$RY0\_TR_{[cm]} = -(MY0POS_{[50\mu m]} - RY0\_CENT_{[50\mu m]}) \times 0.005_{[cm/50\mu m]}. \quad (3.48)$$

The MRS VDC1 Transport coordinates are

$$RX1\_TR_{[cm]} = -((MX1POS_{[50\mu m]} - RX1\_CENT_{[50\mu m]})/\sqrt{2}) \times 0.005_{[\frac{cm}{50\mu m}]} \quad (3.49)$$

$$RY1\_TR_{[cm]} = ((RY1_{[50\mu m]} - RX1\_CENT_{[50\mu m]}) \times 0.005_{[cm/50\mu m]}. \quad (3.50)$$

Similarly, for the VDC2 plane we have

$$RX2\_TR_{[cm]} = -((MX2POS_{[50\mu m]} - RX2\_CENT_{[50\mu m]})/\sqrt{2}) \times 0.005_{[\frac{cm}{50\mu m}]} \quad (3.51)$$

$$RY2\_TR_{[cm]} = ((RY2_{[50\mu m]} - RY2\_CENT_{[50\mu m]}) \times 0.005_{[cm/50\mu m]}. \quad (3.52)$$

RTH_TGT_TR, RTH_VDC_TR:

RTH_TGT_TR is given as

$$RTH\_TGT\_TR = \frac{(RTH\_VDC\_TR - RR26 \times RDELTA\_TR)}{RR22} \quad (3.53)$$

where RR22 is the MRS R_{22} transfer matrix element which relates θ_i at the target to θ_f at the focal plane (near the VDC). RR26 relates θ_i and δ_i. RTH_VDC_TR is evaluated in the same way as STH_VDC_TR; see equation (3.36). An expression for RDELTA_TR is derived from the transfer matrix for the MRS. Thus we have

$$RTH\_VDC\_TR_{[mrad]} = \left(\frac{RDX12\_TR_{[cm]}}{100_{[cm/m]}\sqrt{2} \times RVDCDIST\_TR_{[m]} + RDX12\_TR_{[cm]}} \right)_{[rad]} \times 1000_{[\frac{mrad}{rad}]} \quad (3.54)$$

where RDX12_TR = RX2_TR - RX1_TR and RDELTA_TR is given in NOVA as

$$RDELTA\_TR_{[cm]} = \frac{RXF\_TR_{[cm]}}{RR16}. \quad (3.55)$$

RPH_TGT_TR, RPH_VDC_TR:

Now let us determine the angle ϕ both at the target and at the MRS VDCs. At the target,

$$RPH\_TGT\_TR = \frac{RPH\_VDC\_TR}{RR44} \tag{3.56}$$

where RR44 is the R_{44} transfer matrix element for the MRS and it relates ϕ_i at the target to ϕ_f at the focal plane. Again, the assumption is that the Y position at the target is small.

RPH_VDC_TR is defined as

$$RPH\_VDC\_TR_{[mrad]} = \frac{RDY12_{[50\mu m]} \times 0.05_{[mm/50\mu m]}}{RDZ\_TR_{[m]}} \tag{3.57}$$

where

$$RDY12 = RY2 - RY1.$$

In parallel to the SASP case for SDZ_TR, RDZ_TR is defined as

$$RDZ\_TR_{[m]} = \sqrt{2}\ RVDCDIST\_TR_{[m]} + RDX12\_TR_{[cm]}/100_{[cm/m]} \tag{3.58}$$

where RVDCDIST_TR is the Transport units version (in meters) of RVDCDIST (in 50 μm).

3.6 Missing Mass Calculations

The mass of the residual (undetected) nucleus in the three-body reaction is referred to as the 'missing mass'; the NOVA variable used for this was DRMASS. However, in the kinematically complete three-body $^{12}C(\vec{p}, d\pi^+)^{11}B$ reaction where the momenta of both the deuteron and the pion are measured, the missing momentum and energy can be calculated. From this the missing mass can be determined as described below.

A typical missing mass spectrum for this reaction is shown in figure 3.9. The ground state, 2.12 MeV ($\frac{1}{2}-$), 4.45 MeV ($\frac{5}{2}-$) and 5.02 MeV ($\frac{3}{2}-$) excited states and the continuum are indicated in the figure.

3.6.1 Formulation

The standard coordinate system used for kinematics calculations for polarization measuring experiments is known as the Madison frame of reference. This coordinate system places the origin for kinematics calculations at the target, as shown in figure 3.10 on page 50. Note that for experiment E634, the Madison convention, which would require that the SASP angles be negative, was not followed strictly since the SASP angle values used in analysis were positive.

The use of two spectrometers makes possible a full kinematic determination for all bodies involved in three-body reactions. The SASP was used to detect the pions and the MRS used to detect the deuterons. Considering a generic three-body reaction,

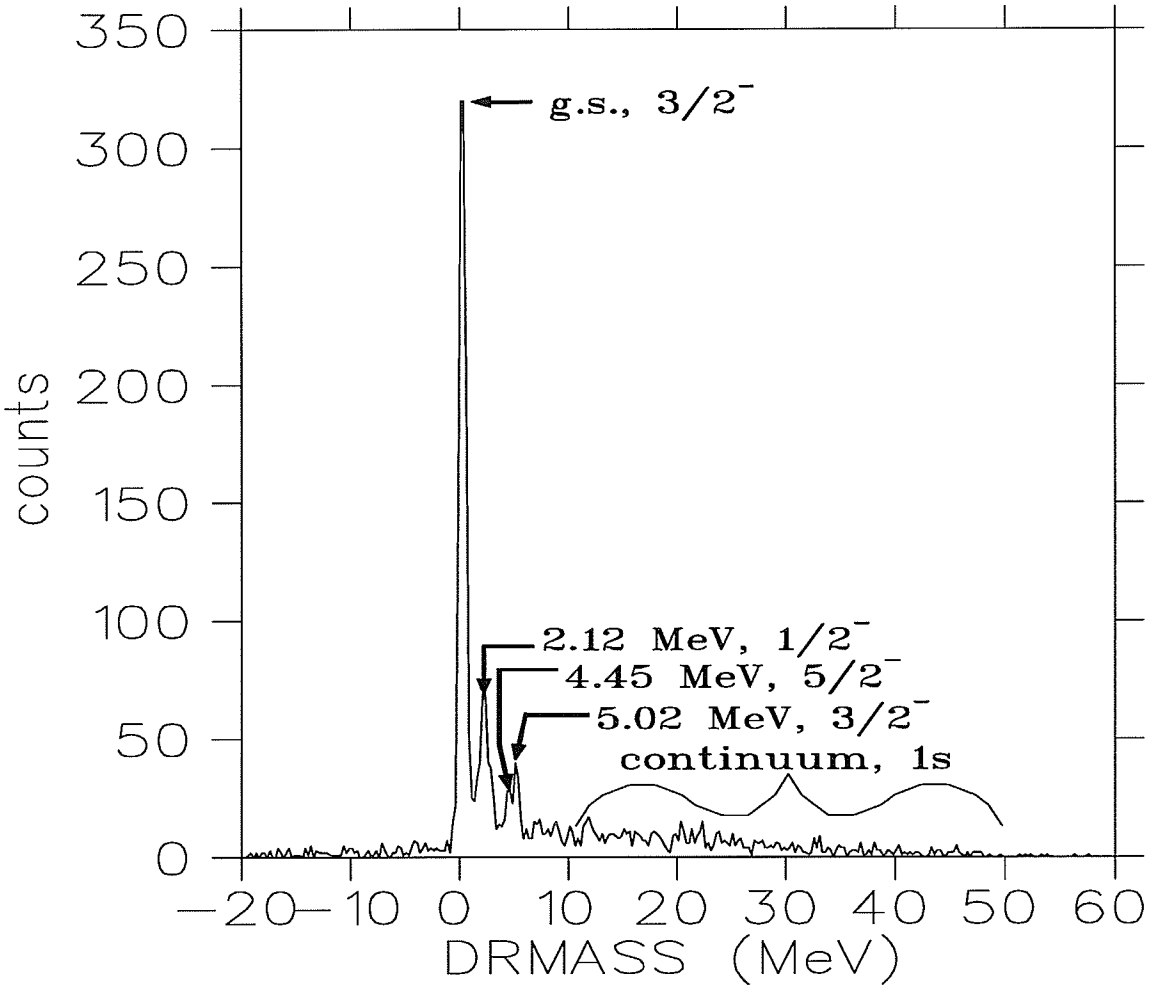

Figure 3.9: This is a missing mass spectrum for $^{12}\mathrm{C}(\vec{p}, d\pi^+)^{11}\mathrm{B}$, showing the four excited states and the $1s$ continuum state of $^{11}\mathrm{B}$. The recoil particle ground state rest mass is subtracted from the DRMASS definition so that in the missing mass spectrum the ground state will be at zero MeV.

THREE-BODY KINEMATICS FOR DASS EXPERIMENT		
REACTANT	ENERGY	MOMENTUM
A (target nucleus)	E_2 = target mass	$p_2 = 0$ (stationary target)
$\vec{p}$ (proton from cyclotron beam)	E_1 = beam energy	p_1 = beam momentum
d (MRS-detected particle)	$E_3 = \sqrt{p_3^2 + m_3^2}$	p_3 = MRS-measured deuteron momentum
π^+ (SASP-detected particle)	$E_4 = \sqrt{p_4^2 + m_4^2}$	p_4 = SASP-measured pion momentum
B (recoil nucleus)	E_5 unknown	p_5 unknown

Table 3.2: This table lists the known and unknown variables in the E634 DASS three-body reaction.

$$\begin{array}{cccccc} \mathrm{A} & (\vec{p}, & \mathrm{d} & \pi^+) & \mathrm{B}, \\ \uparrow & \uparrow & \uparrow & \uparrow & \uparrow \\ 2 & 1 & 3 & 4 & 5 \end{array}$$

we arbitrarily number the particles one through five. These numbers will be referred to in the following discussion.

3.6.2 Calculation

Table 3.2 lists the kinematic variables that are measured and those that need to be determined by calculation during analysis. All the masses are known except for the recoil nucleus mass. Using the known quantities, the recoil nucleus energy (E_5) and momentum (p_5) can be determined. From this the recoil mass can be calculated using

$$m_5 = \sqrt{E_5^2 - p_5^2}. \tag{3.59}$$

Energy conservation gives

$$E_5 = E_1 + E_2 - E_3 - E_4. \tag{3.60}$$

Likewise, momentum conservation dictates

$$\vec{p}_1 + \vec{p}_2 = \vec{p}_3 + \vec{p}_4 + \vec{p}_5\ . \tag{3.61}$$

Note that the momentum of the beam proton, $\vec{p}_1$, only has a Z-component (as indicated in figure 3.11 on page 52), so

$$\vec{p}_1 = p_1\hat{k}. \tag{3.62}$$

From equation (3.61) we have

$$\begin{aligned} \vec{p}_5 &= \vec{p}_1 - \vec{p}_3 - \vec{p}_4 \\ &= \vec{p}_1 - p_3\hat{n}_{MRS} - p_4\hat{n}_{SASP} \end{aligned} \tag{3.63}$$

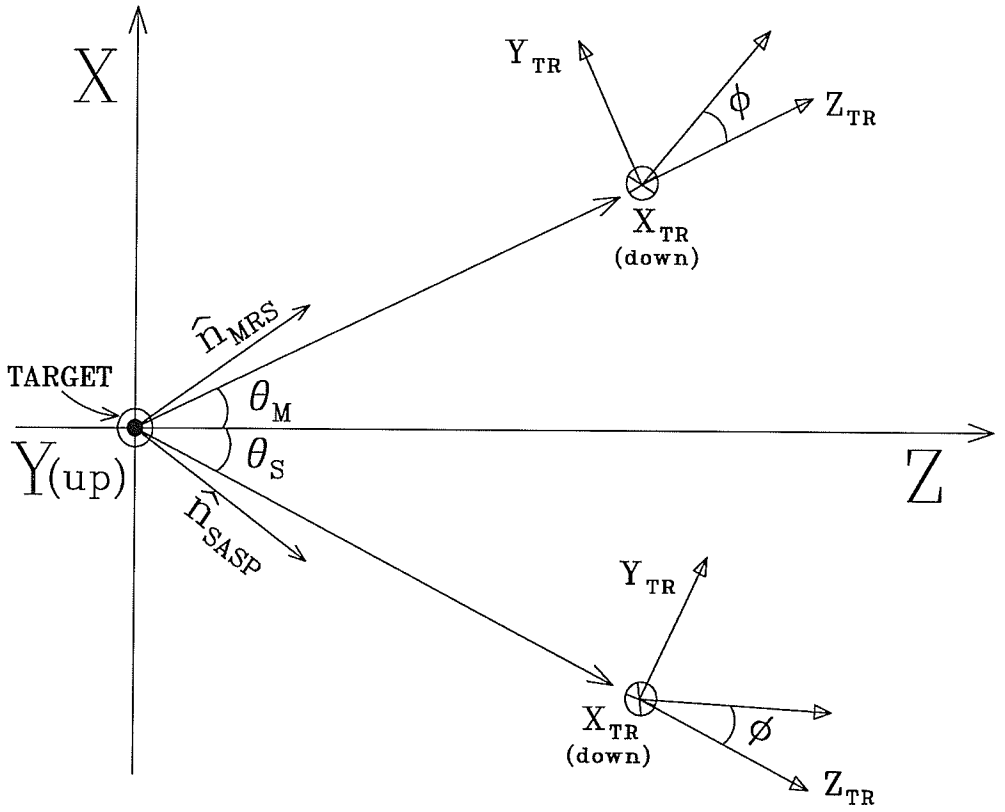

Figure 3.10: Madison and Transport coordinate systems for particle trajectories traversing the SASP and MRS are depicted here. The unit vectors $\hat{n}_{MRS}$ and $\hat{n}_{SASP}$ are oriented in the direction of an arbitrary particle trajectory.

where $\hat{n}_{MRS}$ and $\hat{n}_{SASP}$ are unit vectors along the actual trajectories for a specific event passing through the MRS and the SASP, respectively. This is shown in figure 3.10. It is emphasized that these unit vectors are not necessarily in the nominal directions of the central trajectories of the two spectrometers. The expressions for $\hat{n}_{MRS}$ and $\hat{n}_{SASP}$ are derived in appendix A. Squaring the recoil nucleus momentum vector gives

$$p_5^2 = p_1^2 + p_3^2 + p_4^2 - 2(\vec{p}_1 \cdot \hat{n}_{MRS})p_3 - 2(\vec{p}_1 \cdot \hat{n}_{SASP})p_4 + 2p_3p_4(\hat{n}_{MRS} \cdot \hat{n}_{SASP}). \quad (3.64)$$

With θ_S and θ_M as the SASP and MRS detector angles in the Madison frame as shown in figure 3.10 (but with θ_S positive) [17], angles with subscripts 'SASP' and 'MRS' describing particle trajectories through the respective spectrometers and the definitions of $\hat{n}_{SASP}$ and $\hat{n}_{MRS}$, we extract the X,Y and Z components of $\vec{p}_5$ from (3.63) as follows

$$\begin{aligned} p_{5x} &= -p_3 \frac{(\sin\theta_M + \phi_{MRS}\cos\theta_M)}{\sqrt{1+\phi_{MRS}^2+\theta_{MRS}^2}} \\ &\quad - p_4 \frac{(-\sin\theta_S + \phi_{SASP}\cos\theta_S)}{\sqrt{1+\phi_{SASP}^2+\theta_{SASP}^2}} \end{aligned} \quad (3.65)$$

$$
\begin{aligned}
p_{5y} &= -p_3\left[\frac{-\theta_{MRS}}{\sqrt{1+\phi_{MRS}^2+\theta_{MRS}^2}}\right] - p_4\left[\frac{-\theta_{SASP}}{\sqrt{1+\phi_{SASP}^2+\theta_{SASP}^2}}\right] \\
&= \frac{p_3\theta_{MRS}}{\sqrt{1+\phi_{MRS}^2+\theta_{MRS}^2}} + \frac{p_4\theta_{SASP}}{\sqrt{1+\phi_{SASP}^2+\theta_{SASP}^2}} \qquad (3.66)
\end{aligned}
$$

$$
\begin{aligned}
p_{5z} &= p_1 - p_3\left[\frac{\cos\theta_M - \phi_{MRS}\sin\theta_M}{\sqrt{1+\phi_{MRS}^2+\theta_{MRS}^2}}\right] \\
&\quad - p_4\left[\frac{\cos\theta_S + \phi_{SASP}\sin\theta_S}{\sqrt{1+\phi_{SASP}^2+\theta_{SASP}^2}}\right]. \qquad (3.67)
\end{aligned}
$$

Thus from (3.60) and (3.65) through (3.67), the energy and momentum of the undetected particle can be determined and the missing recoil mass calculated using (3.59). The NOVA expression for (3.60) is

$$ER = ((EB + TMASS) - EM) - ES \qquad (3.68)$$

where EB is the beam energy, TMASS is the target mass, EM is the MRS-detected deuteron energy and ES is the SASP-detected pion energy. If a dispersed beam is used, the energy of an incident proton is defined by its vertical position on the target as well as its nominal energy. This will be discussed in the next section.

3.6.3 Kinematic Description of Beam Dispersion

A proper expression for beam energy, E_1, includes a correction for the variation of incident projectile position on target. From figure 3.11, it is clear that

$$\Delta p = \frac{\partial p}{\partial x}\Delta X. \qquad (3.69)$$

As is discussed in §2.10, beam dispersion can be written in terms of

$$\Delta X/\delta = dispersion_{[cm/\%]}. \qquad (3.70)$$

Note that dispersion as discussed in this section refers to the dispersion magnitude. By combining this fact with equations (2.3) and (3.69), we get the following expression for Δp, the change in momentum of a particle along an arbitrary trajectory from the momentum of a particle along the central trajectory,

$$\Delta p = \frac{p_o}{100 \times dispersion}\Delta X. \qquad (3.71)$$

Therefore, the momentum of a particle following an arbitrary trajectory is

$$
\begin{aligned}
p &= p_o + \Delta p = p_o + \frac{p_o}{100 \times dispersion}\Delta X \\
&= p_o\left[1 + \frac{\Delta X}{100 \times dispersion}\right] \qquad (3.72)
\end{aligned}
$$

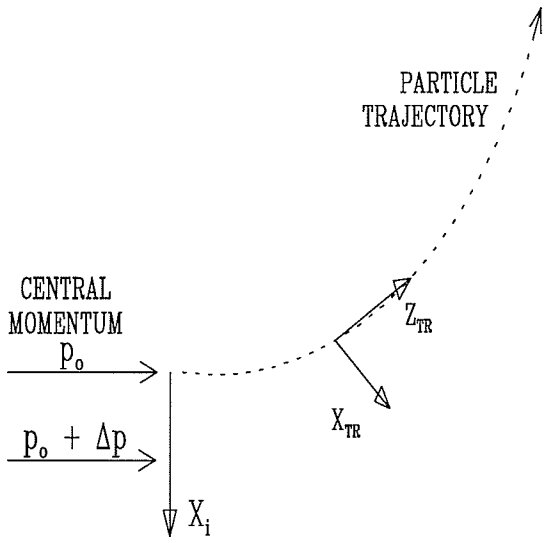

Figure 3.11: The momentum-X displacement relation illustrating beam dispersion is illustrated here.

where ΔX is the X-position at the target. This was calculated using MRS FEC information as follows

$$\Delta X = RXI\_TR_{[cm]} = RX0\_TR_{[cm]} - \frac{RTH\_TGT\_TR_{[mrad]} \times RFECDIST\_TR_{[m]} \times 100_{[cm/m]}}{1000_{[mrad/rad]}}, \quad (3.73)$$

where RX0_TR is the X-coordinate measured in the FEC, RTH_TGT_TR is the trajectory angle (θ) of the deuteron measured in the X_{TR}-Z_{TR} plane (in mrad), and RFECDIST_TR is the distance (in meters) between the target and the MRS FEC. Therefore, equation (3.71) becomes

$$\Delta p = PBD = \frac{RXI\_TR \times p_o}{100 \times dispersion}. \quad (3.74)$$

The SASP did not use a front end chamber for experiment E634 and therefore the X-position at the target was determined from the MRS FEC alone, as given in equation (3.73). Thus,

$$SXI\_TR_{[cm]} = RXI\_TR_{[cm]} = \Delta X. \quad (3.75)$$

From

$$E^2 = m^2 + p^2 \quad \text{and} \quad E = T + M \quad (3.76)$$

we can write

$$\Delta E = \Delta T = \frac{p}{E}\Delta p. \quad (3.77)$$

The energy of the beam particle at central momentum was written in the NOVA definition as

$$EB0 = (BMASS + TB) - TBCORR, \quad (3.78)$$

where TB is the nominal beam kinetic energy, BMASS is the proton mass, and TBCORR is an adjustable parameter to correct for errors in the absolute energy calibration and energy losses in the target. The corrected beam energy, EB, and beam momentum, PB, are then

$$EB = EB0 + \Delta E \tag{3.79}$$

$$= EB0 + \frac{PB0}{EB0}\Delta p, \tag{3.80}$$

and

$$PB = PB0 + PBD, \tag{3.81}$$

where PB0 is the beam particle momentum for a central momentum particle,

$$PB0 = \sqrt{EB0^2 - BMASS^2}. \tag{3.82}$$

3.6.4 Momentum P_π and P_d

Absolute momentum calibrations for each spectrometer have been performed in separate measurements. These are discussed on page 58 and page 62 for the SASP and MRS, respectively, and these calibrations were used to determine p_π and p_d.

3.7 Event Reconstruction

Event reconstruction is a trace back of the particle's path through the spectrometer. Reconstructing the event provides information crucial to the identification of the outgoing particles. It also identifies those events which did not originate at the target and those which pass through the spectrometer in an anomalous fashion. Empirical corrections were applied to correct for inadequate calibrations, energy loss effects and higher order aberrations in the SASP.

3.7.1 Event Coordinates

Wire chamber information was used to trace the particles' paths through the spectrometers. The coordinates calculated for the event reconstruction are listed in table 3.3. All target position and VDC coordinates used for kinematics calculations employ Transport dimensions, as indicated by '$_{TR}$'. Recall that for experiment E634, the MRS utilized a front end chamber whereas the SASP did not.

Target Position

For the MRS, the X and Y positions at the target are given (in NOVA nomenclature) by

$$RXI\_TR = RX0\_TR - (RTH\_TGT\_TR \times RFECDIST\_TR)/10, \tag{3.83}$$

$$RYI\_TR = (RYF\_TR - RR34 \times RPH\_TGT\_TR)/RR33. \tag{3.84}$$

VARIABLE DESCRIPTION	NOVA NAME (and equation reference)	
	MRS	SASP
Position at target	*RXI_TR* (3.83), *RYI_TR* (3.84)	*SXI_TR* (3.85), *SYI_TR* (3.86)
FEC X & Y coordinates	*RX0_TR* (3.47), *RY0_TR* (3.48)	— —
Focal plane position	*RXF* (3.29)	*SXF* (3.1)
VDC1 X & Y coordinates	*RX1_TR* (3.49), *RY1_TR* (3.50)	*SX1_TR* (3.32), *SY1_TR* (3.34)
VDC2 X & Y coordinates	*RX2_TR* (3.51), *RY2_TR* (3.52)	*SX2_TR* (3.33), *SY2_TR* (3.35)

Table 3.3: The coordinates calculated for E634 event reconstruction are listed in this table.

The expression for RXI_TR is also given in equation (3.73) on page 52 and is discussed in greater detail there. RX0_TR is the X position at the MRS FEC and RFECDIST_TR is the distance (in meters) between the target and the MRS FEC. Equation (3.84) is derived directly from the transfer matrix given in equation (2.1). RTH_TGT_TR and RPH_TGT_TR, θ_i and ϕ_i at the target, respectively, are derived in equations (3.53) and (3.56) of §3.5.2.

The SASP NOVA variables for the X and Y target positions are

$$SXI\_TR = RXI\_TR \tag{3.85}$$

$$SYI\_TR = (SYF\_TR - SR34 \times SPH\_TGT\_TR)/SR33. \tag{3.86}$$

The X position is set equal to that for the MRS since the SASP did not use a FEC. Equation (3.86) is derived from the transfer matrix given in equation (2.1).

FEC Coordinates

The MRS FEC coordinates MX0POS and MY0POS are the raw FEC data for the X and Y planes. This data is then used to calculate the FEC positions in terms of Transport coordinates RX0_TR and RY0_TR as was shown in equations (3.47) and (3.48) on page 46.

Focal Plane Position

The SASP focal plane position is discussed in detail in §3.3. The MRS focal plane is discussed in §3.4, with RXF given in equation (3.29).

Corrections to compensate for aberrations and improper calibrations were applied to SXF to improve energy resolution in the missing mass calculation. The corrected focal plane positions are discussed in §3.7.2.

VDC Coordinates

The X and Y coordinates for both VDC planes are discussed in §3.5.1 for the SASP and §3.5.2 for the MRS. The SASP VDC coordinates are given in equations (3.32), (3.33), (3.34) and (3.35) on page 43. The MRS VDC coordinates are given in equations (3.49), (3.50), (3.51) and (3.52) on page 46.

3.7.2 Empirical Resolution Corrections

At the time of analysis, a SASP momentum calibration for the spectrometer's application to the low momentum pions of experiment E634 was not available. Instead, the existing calibration based on proton elastic scattering was incorporated into the NOVA user routine USR9 which was used for experiment E634. Unfortunately, because of saturation effects, the field does not scale linearly over the large momentum acceptance of the SASP, resulting in a dependence of the missing mass on focal plane position. A second effect is that of optical aberrations in SASP; the correction in the focal plane position due to the angle θ at the target is particularly large.

To compensate for these shortcomings, empirical resolution corrections were manually performed. Since a suitable MRS momentum and field calibration was applied to the analysis, the need for empirical corrections to the missing mass was due primarily to the SASP and not the MRS. Therefore, correction efforts concentrated on SASP variables.

Two histograms were examined: HDRMDEL_N, a plot of SDEL (the SASP focal plane position) versus DRMASS (missing mass), and HSTH_DRMASS, a plot of the SASP θ_i at the target (STH_TGT_TR) versus DRMASS. The loci in these plots were manually straightened by adding appropriate correction factors determined from a curve fit to the original bowed loci. For approximately half of the runs, empirical correction of the loci in the HDRMDEL_N plot alone was sufficient to produce an acceptable energy resolution in the missing mass spectrum. For the other runs, the loci in both the HSTH_DRMASS and HDRMDEL_N were corrected. An example of the latter is run number 53; 'before' and 'after' stages of empirical correction are shown in figure 3.12.

The empirical correction was deduced as follows. The uncorrected missing mass variable is defined in NOVA as

$$\texttt{DRMASS0} = \texttt{SQRT(ER}**2 - \texttt{PRSQ)} - \texttt{RMASS} \tag{3.87}$$

where ER = energy of recoil particle (see equation (3.68) on page 51)
PRSQ = $p_x^2 + p_y^2 + p_z^2$, the sum of the squares of the X,Y,Z components of recoil particle momentum
RMASS = recoil particle ground state rest mass.

The recoil particle ground state rest mass is subtracted from the DRMASS definition so that in the missing mass spectrum (see page 48) the ground state will be at zero MeV. For

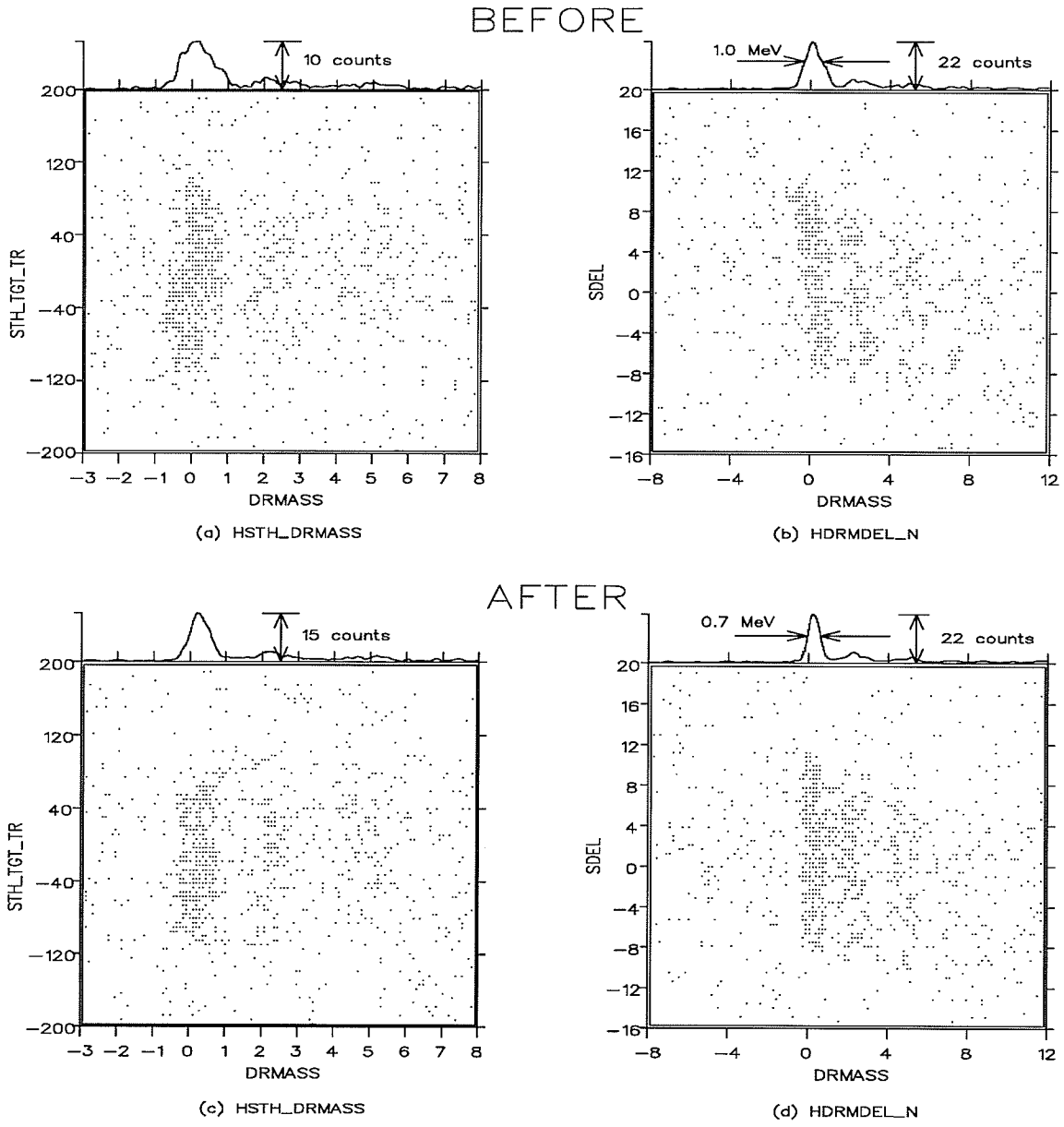

Figure 3.12: These plots demonstrate the effects of empirical corrections applied to θ at the target for SASP (STH_TGT_TR) and the SASP focal plane position (SDEL). Plots (a) and (b) show these plots before corrections are applied, plots (c) and (d) show the resulting plots after corrections are applied.

more details on the missing mass calculations, see §3.6. Figure 3.12(c) and 3.12(d) show both plots after the following corrections applied to the missing mass variable, DRMASS, are made:

$$\begin{aligned} \texttt{DRMASS} = {} & \texttt{DRMASS0} + \texttt{A} * \texttt{SDEL} + \texttt{B} * \texttt{SDEL} * *2 + \texttt{C} * \texttt{SDEL} * *3 \\ & + \texttt{AS} * \texttt{STH\_TGT\_TR} + \texttt{BS} * \texttt{STH\_TGT\_TR} * *2 + \texttt{CS} * \texttt{STH\_TGT\_TR} * *3 \\ & + \texttt{DS} + \texttt{FS} * \texttt{STH\_TGT\_TR} * *4 + \texttt{GS} * \texttt{STH\_TGT\_TR} * *5, \end{aligned} \tag{3.88}$$

where the following coefficients were used,

```
A  = 0.0324
B  = 1.11716E-03
C  = -2.55847E-05
AS = -0.0114
BS = -3.00720E-04
CS = 3.76564E-06
DS = -0.92565E-07
FS = 1.27197E-07
GS = 6.91328E-10
```

The resulting narrowing of the peaks in HDRMDEL_N and HSTH_DRMASS is apparent. For example, the FWHM of the ground state peak in the missing mass spectrum HDRMDEL_N before applied corrections was 1.0 MeV and after corrections had decreased to 0.7 MeV.

3.8 Calibrations

Proper energy and momentum calibration of the MRS and SASP is required to achieve correct missing mass results.

3.8.1 Beam Energy Calibration

Preliminary missing mass calculations revealed that the ground state (with the recoil particle ground state rest mass subtracted) was not situated at exactly 0 MeV. This was because the beam energy from the cyclotron is not known to better than approximately 1 MeV. To compensate for this uncertainty, the analysis utilized a correction factor, the NOVA parameter TBCORR, which shifted the missing mass ground state to its proper location. TBCORR is discussed in §3.6.3.

3.8.2 SASP Calibrations

Acceptance Calibration

A SASP acceptance scan using the $pp \rightarrow d\pi^+$ reaction at 500 MeV and SASP detection angle of 60° on a CH_2 target was obtained in a separate measurement in November 1994.

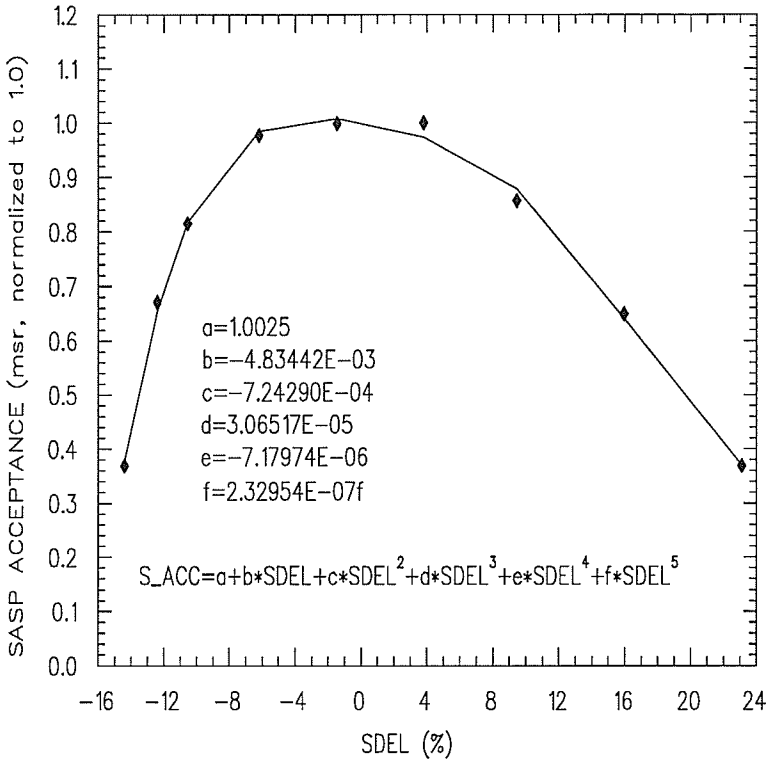

Figure 3.13: Shown is a fit to data for SASP experimental acceptance yields from $pp \rightarrow d\pi^+$ data corrected for pion decay. The data is normalized to unity at the peak of the curve.

The experimental yields were corrected for pion decay using the pion decay parameterization which is discussed in the upcoming subsection "Pion Decay Length". A fit to the data is shown in figure 3.13. This acceptance information, together with the MRS acceptance and pion survival efficiency, is used to calculate the detection efficiency on an event-by-event basis. These three factors together comprise the NOVA variable RSEFF, and are determined in the user routine USRQ (see appendix F).

Momentum Calibration

The SASP momentum calibration relating SDEL to SXF_TR, as given in the NOVA subroutine USR9, was obtained from the scattering of 200 MeV protons from ^{208}Pb. However, due to nonlinear effects in the magnet, this momentum calibration was not correct for the much lower momentum pions of experiment E634, and subsequent corrections were required. Separate corrections were used for 500 MeV and 371 MeV. For 500 MeV,

$$SDEL_{NEW} = (0.960912 \times SDEL9 + 2.43876E-03 \times SDEL9^2) - 6.55873E-05 \times SDEL9^3 \tag{3.89}$$

and for 371 MeV,

$$SDEL_{NEW} = (0.957065 \times SDEL9 + 1.52063E-03 \times SDEL9^2) - 5.14050E-05 \times SDEL9^3 \tag{3.90}$$

were used, where SDEL9 is the expression for SDEL as calculated by NOVA subroutine USR9. This SDEL is determined from a fit to the relationship between δ (in %) and SXF_TR. The SASP central momentum is $50.311 \times B_{SASP}$, and hence the momentum is given by

$$P_{SASP} = (50.311 \times B_{SASP}) \times \left(1.00 + \frac{SDEL}{100}\right). \tag{3.91}$$

Figures 3.14(a) and 3.14(b) show plots of the differences between SDEL_{NEW} (the empirically corrected SDEL) and SDEL9 (SDEL calculated using the USR9 subroutine), plotted as a function of SDEL9. The empirically corrected SDEL_{NEW} value was the value of SDEL used for E634 analysis.

Measurements were made in April 1995 to establish a new momentum calibration for the SASP using 120 MeV pions from the $^{12}\text{C}(p,\pi^+)^{13}\text{C}^*$ reaction at 280 MeV. This was an absolute calibration, using the MRS to determine the absolute beam energy. For more details, see appendix B. Figure 3.14(c) shows the difference between this new calibration, SDEL_{CAL}, and SDEL9, plotted as a function of SDEL9. Comparing figures 3.14(a) and (b) with (c), we see that the general nature of the empirical corrections are verified. However, the calibration from USR9 also produces a systematic offset of $\sim 1\%$.

Pion Decay Length

The SASP effective pion length was determined using a Monte Carlo program. From the survival probability of pions of a given SDEL and SASP central momentum P_0, the effective length, EFF_L, can be extracted from

$$\begin{aligned} PROB &= \exp\left(-\frac{m_\pi EFF\_L}{P_\pi c\tau}\right) \\ &= \exp\left(-\frac{139.57 \times EFF\_L}{P_\pi \tau\_c}\right), \end{aligned} \tag{3.92}$$

where $\tau\_c = 780.4$ cm, and P_π is the pion momentum corresponding to the given SDEL [14]. Figure 3.15 shows results of equation (3.92) calculated for various central momenta ranging from 80 to 500 MeV/c. For more details on pion effective length, please see appendix C.

3.8.3 MRS Calibrations

Acceptance Calibration

Acceptance scan data were recorded for a $^{12}\text{C(p,p')}^{12}\text{C}$ study conducted with the MRS in November 1994. Over the course of the experiment, it was discovered that the focal plane polarimeter cage (FPP) was incorrectly oriented. This cage houses the S1 and S2

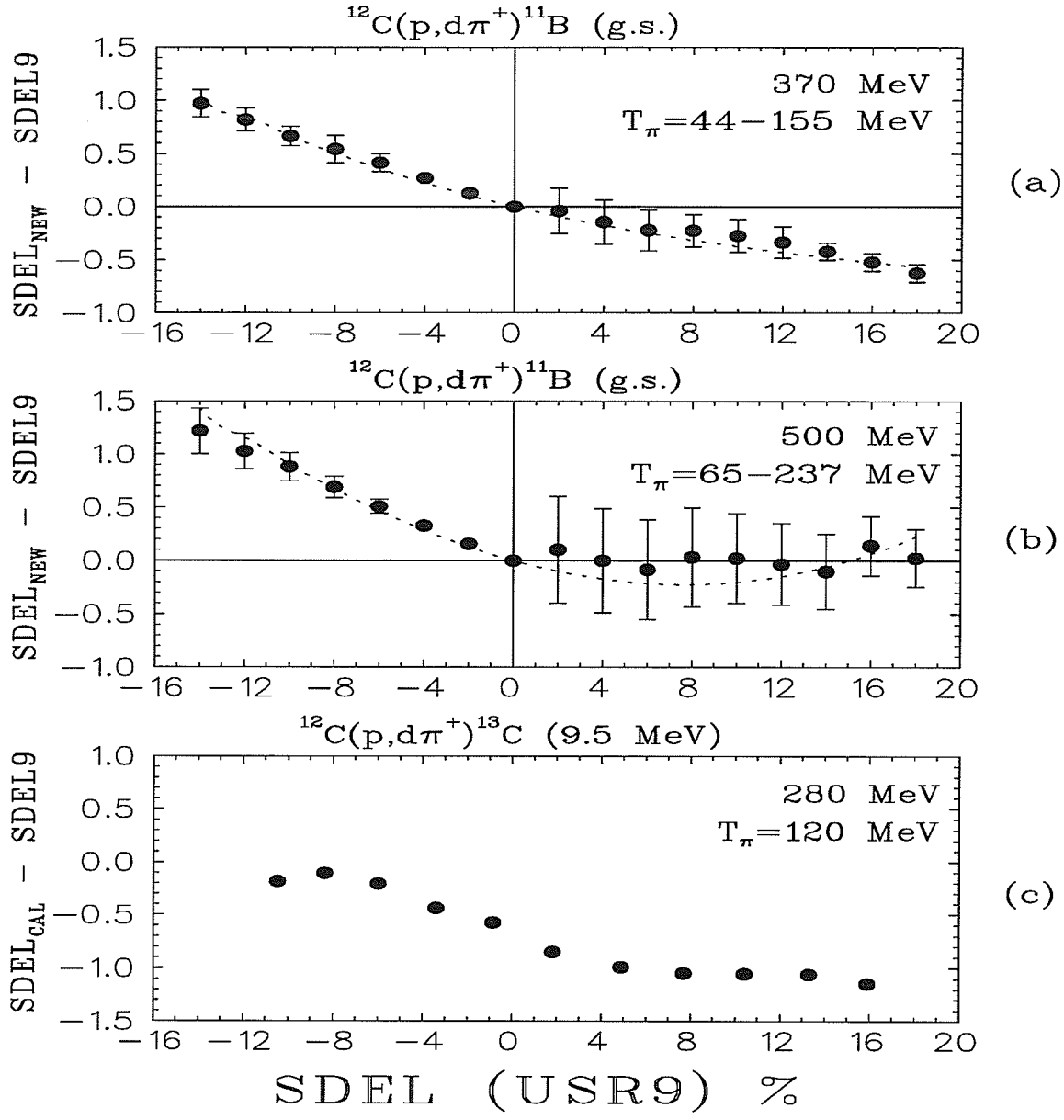

Figure 3.14: These plots show the variation of different SDEL values versus SDEL9 (SDEL calculated using the USR9 subroutine): (a), (b) show the difference between empirically corrected SDEL, $SDEL_{NEW}$, and SDEL9, at beam energies 370 MeV and 500 MeV, respectively; (c) shows the difference between calibrated SDEL value and SDEL9, at 280 MeV beam energy.

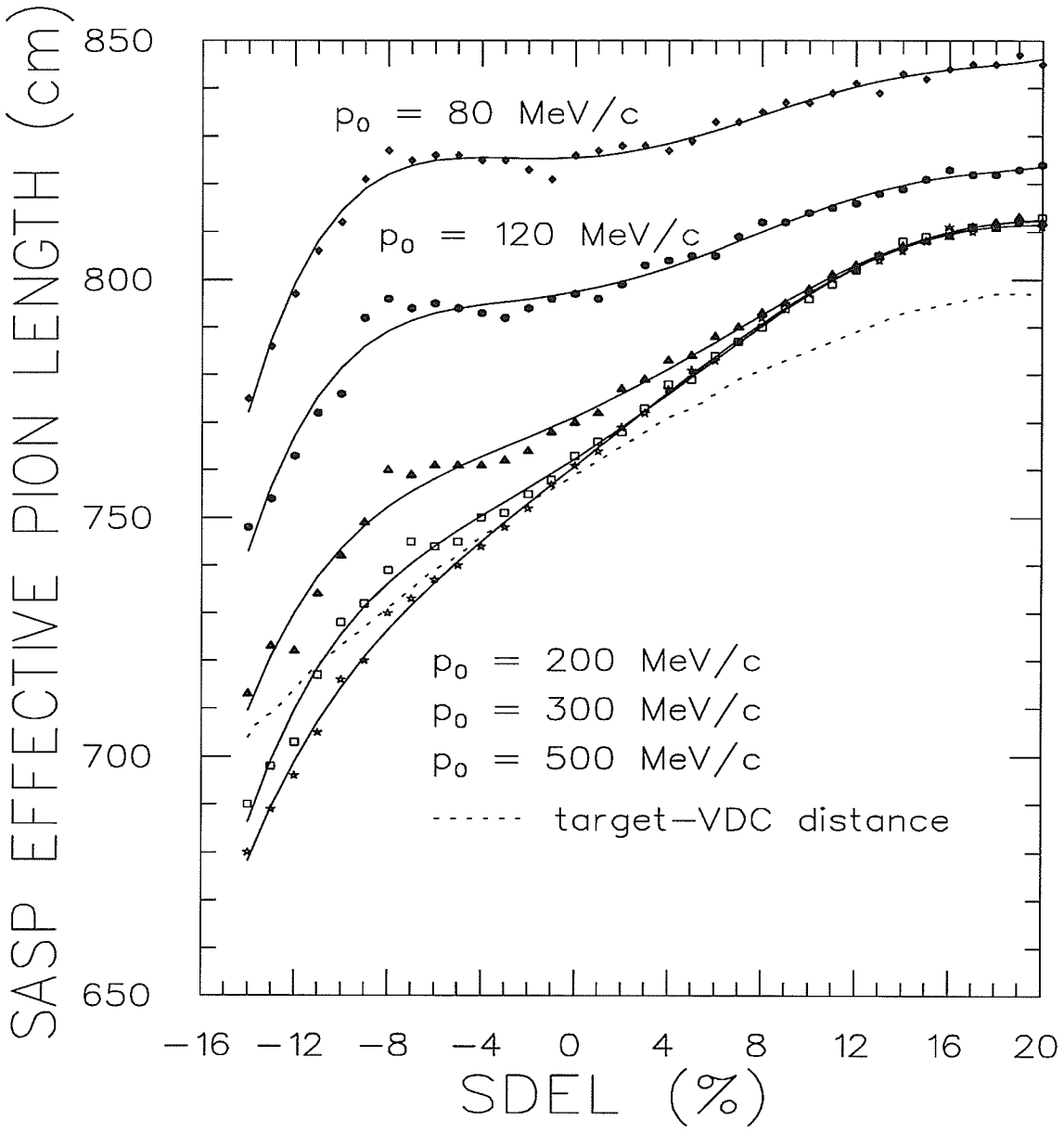

Figure 3.15: The SASP effective pion length versus SDEL is plotted in this figure for various central pion momenta.

scintillators and thus improper positioning of the FPP cage adversely affects the acceptance defined by these scintillators. This improper FPP orientation was in use during experiment E634 in August 1994. To investigate the resulting effect, acceptance scans were carried out for both the proper and improper FPP orientation [19]. The plots in figures 3.16 and 3.17 illustrate the MRS acceptance scans with the correct and incorrect FPP cage orientation [17]. The total number of data points selected for the two scans were 67 and 82 respectively. Analysis was carried out for the ground state, 4.44 MeV state and 9.64 MeV states of ^{12}C. A central ray located at RXF = 16475 (50 μm units) was assumed for the RDEL calculations. RDEL is the usual percentage momentum deviation ($= \delta = \left(\frac{p-p_o}{p_o}\right) \times 100\%$), and the momentum expressed in terms of the magnetic field and focal plane position is given in the following section. Curve fit information is included in the plots.

The acceptance in the plots in figures 3.16 and 3.17 is normalized to 1.0 at the peak of the curves. With the FPP cage in the correct orientation, optimum acceptance (that portion of the acceptance curve which is flattest) is centered at the RDEL range of -6% to +6%, while for improper FPP cage orientation is shifted to the RDEL range of -3% to +7%.

Momentum Calibration

Analysis of the November 1994 MRS calibration data has lead to the absolute momentum calibration

$$\frac{P_{MRS}}{B_{MRS}} = 92.750 - 7.79613E-04 \times RXF + 1.66265E-09 \times RXF^2, \qquad (3.93)$$

where RXF is the MRS focal plane position (in 50 μm units). The relationship between P_{MRS}/B_{MRS} and RXF is shown in figure 3.18. The MRS momentum calibration relating to equation (3.93) was not available at the time of experiment E634 analysis. Rather, the P_{MRS}/B_{MRS} ratio used for E634 was

$$\frac{P_{MRS}}{B_{MRS}} = 92.733 - 7.75068E-04 \times RXF + 1.56389E-09 \times RXF^2, \qquad (3.94)$$

which is very similar to equation (3.93). Further discussion of the absolute momentum calibration given in equation (3.93) can be found in appendix B.

3.8.4 SASP and MRS Solid Angles

Tests to confirm that the solid angle cuts imposed on the SASP and MRS data were defining appropriate solid angles were conducted. These tests consisted of setting various cuts on the X0 and Y0 FEC positions for the MRS, and on the extrapolated θ and ϕ angles at the target for the SASP. A total of 23 "IF" statements were introduced into the NOVA operation sequence. These statements essentially acted as scalers for the solid angle cuts and indicated the event passage through these cuts.

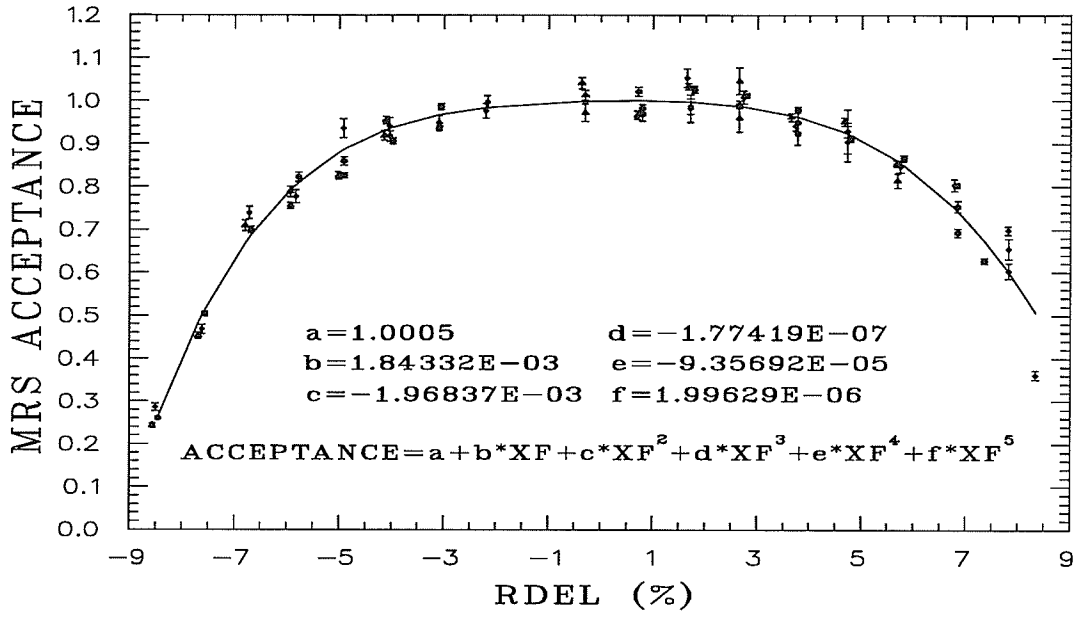

Figure 3.16: This figure shows the MRS acceptance for proper FPP cage orientation.

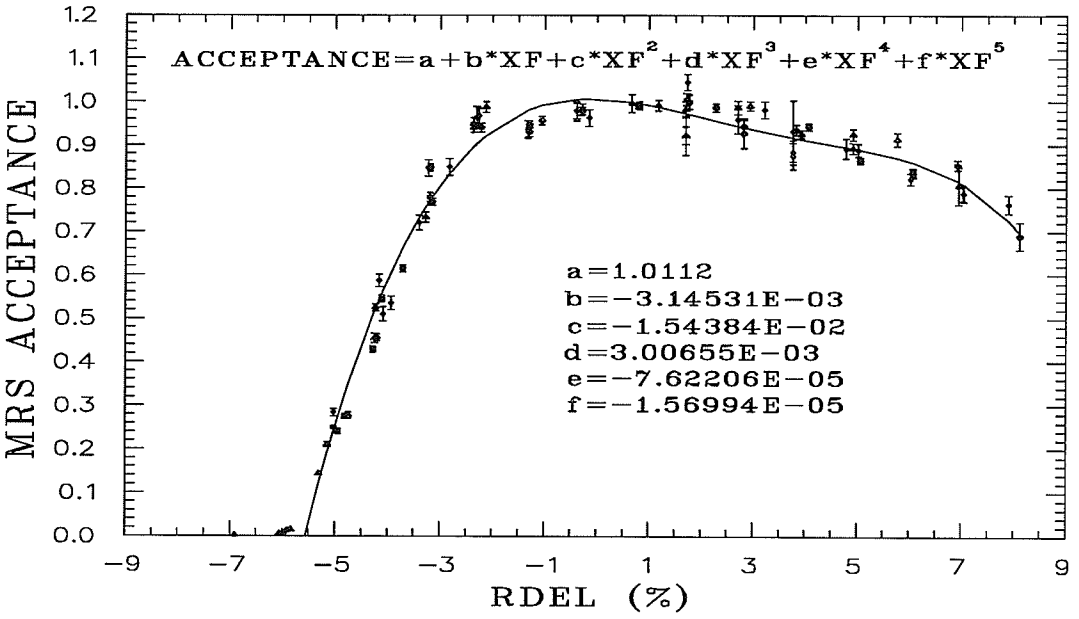

Figure 3.17: This figure shows the MRS acceptance for improper FPP cage orientation.

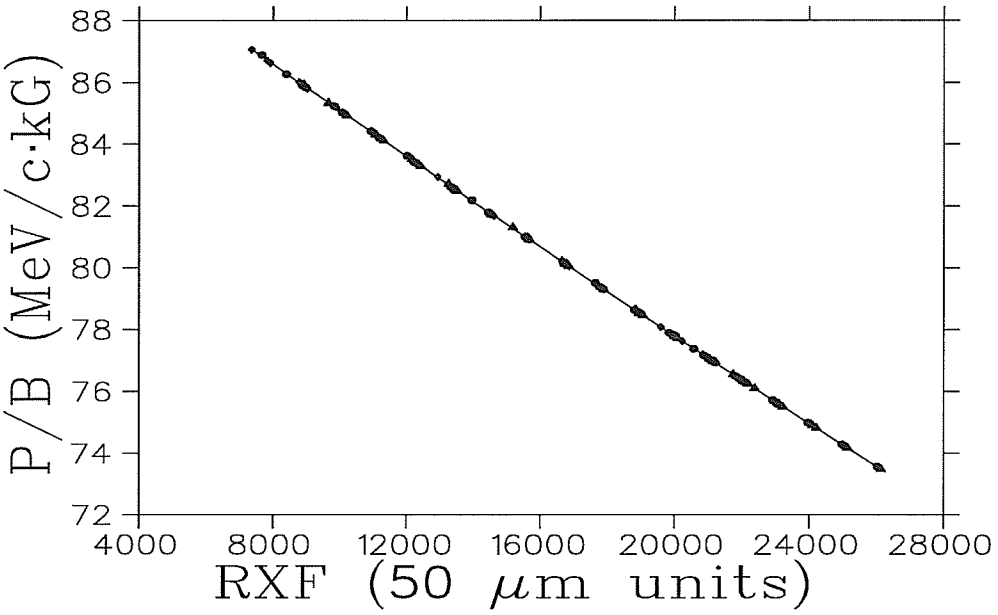

Figure 3.18: The MRS momentum calibration from November 1994 data is shown here.

SASP Solid Angle

From the known cross section of the $pp \rightarrow d\pi^+$ reaction, the SASP solid angle at the peak of the acceptance was determined to be 12.0 msr. The solid angle (in msr) as a function of SDEL is then simply 12 times the ordinate of the curve in figure 3.13.

Figure 3.19 shows the relations between event throughput and solid angle openings for three typical E634 runs using the carbon target. The angle reconstruction is not ideal, as shown by the nonlinearity in the curves. A solid angle of 12 msr was assumed and the various cuts on the SASP solid angle are in reasonable agreement with this value. This agreement is discussed in the following paragraphs.

The SASP solid angle is defined by

$$\Delta\Omega = (R\Delta\phi)(R\Delta\theta)/R^2 = \Delta\phi\Delta\theta, \tag{3.95}$$

where ϕ and θ are the reconstructed angles at the target (SPH_TGT_TR and STH_TGT_TR, respectively). For example, a possible $\theta - \phi$ combination that would satisfy a 12 msr solid angle value could be $\Delta\theta$ = 173 mrad and $\Delta\phi$ = 69 mrad. The actual cuts used in NOVA were wide open at $\Delta\theta$=309 mrad and Δ ϕ=113 mrad.

To test whether or not all valid events were properly passed, cuts having θ = 69, 149, 229 mrad and ϕ = 23, 53, 83 mrad were applied individually and in combination. Assuming the values of $\Delta\theta$ = 173 mrad and $\Delta\phi$ = 69 mrad for a 12 msr solid angle yielded predictions of 40% and 86% event passage through the $\Delta\theta$=69 and $\Delta\theta$=149 cuts and 33% and 77% passage through the $\Delta\phi$=23 and $\Delta\phi$=53 cuts. This compares favourably with the

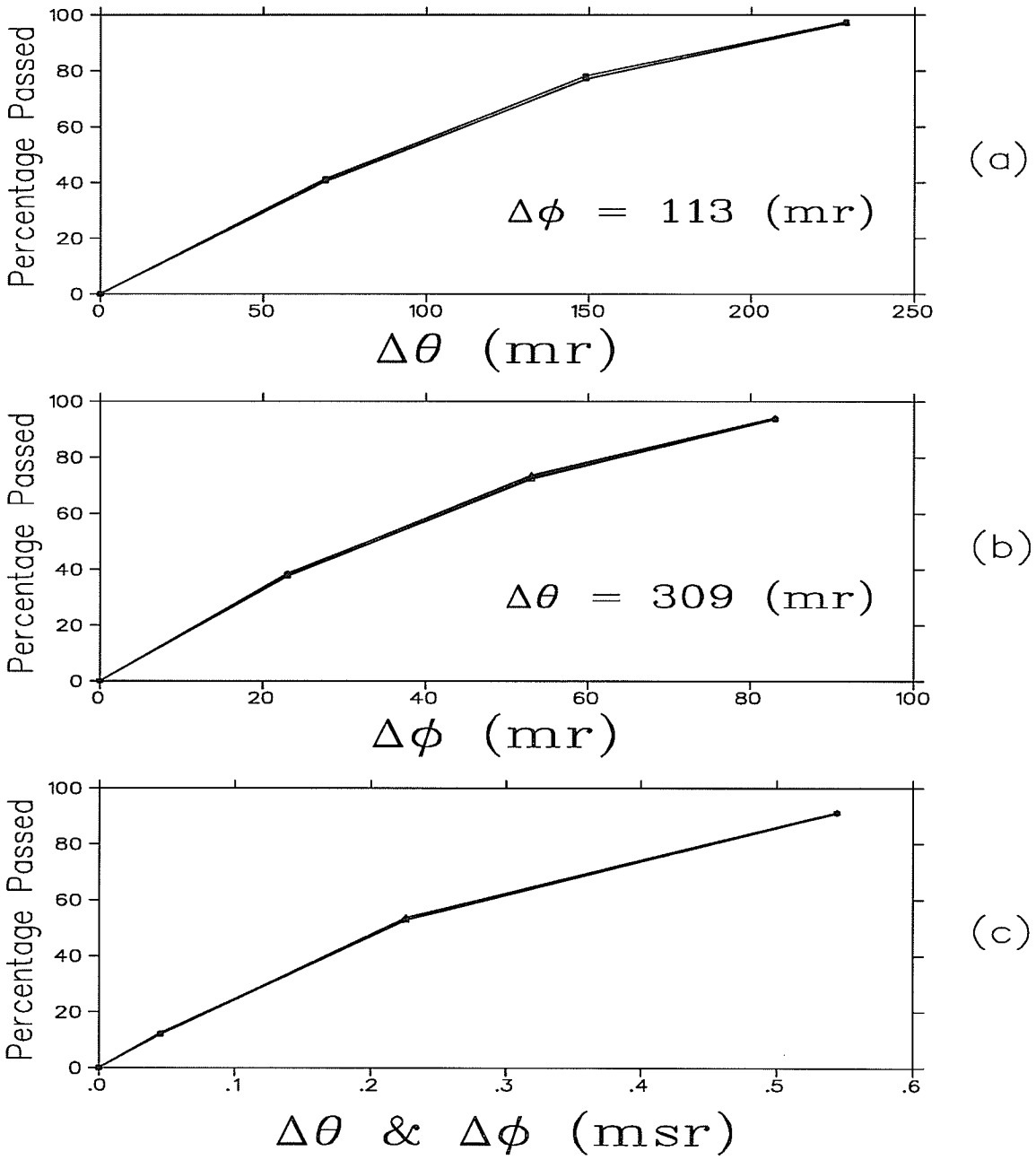

Figure 3.19: Plots of solid angle tests for the SASP for three runs are shown here: (a) has cuts on θ only, (b) has cuts on ϕ only and (c) has cuts on θ and ϕ combined. The horizontal scale in (c) is expressed relative to the maximum solid angle defined by the largest cuts on θ and ϕ.

results in figure 3.19(a) and (b). For the combined cuts of $\Delta\theta$=69, $\Delta\phi$=23 and $\Delta\theta$=149, $\Delta\phi$=53, the resulting '$\Delta\theta\&\Delta\phi$' cuts are

$$\frac{69}{309} \times \frac{23}{113} = 0.045 \text{ and } \frac{149}{309} \times \frac{53}{113} = 0.226. \tag{3.96}$$

These '$\Delta\theta\&\Delta\phi$' values are thus expressed relative to the maximum solid angle defined by the largest cuts on θ and ϕ.

On the assumption that the $\Delta\theta$ = 173 mrad and $\Delta\phi$ = 69 mrad cut corresponds to the full solid angle of 12 msr, the predictions are that 13% and 66% of the events should pass the combined cuts of $\Delta\theta$=69, $\Delta\phi$=23 and $\Delta\theta$=149, $\Delta\phi$=53, respectively. Figure 3.19(c) shows comparable results of approximately 12% and 54%. This demonstrates that cuts of these proportions or wider would not exclude valid events localized within the 12 msr solid angle.

MRS Solid Angle

For the MRS, openings of 600, 400, 300 and 200 (50μm units) were defined for the X0 FEC position, and openings of 800, 600, 400 and 200 (50μm units) were defined for the Y0 FEC position. An X0 opening of 600 (50μm units) and a Y0 opening of 800 (50μm units) corresponds to a 3.0 cm by 4.0 cm aperture and is assumed to constitute a wide open case. This translates to a solid angle of

$$\Delta\Omega_{MRS} = (3_{[cm]} \times 4_{[cm]})/63^2_{[cm]} = 3.02\ msr, \tag{3.97}$$

where the FEC-to-focal plane distance (NOVA variable RFECDIST_TR) is 63 cm. This value of $\Delta\Omega_{MRS}$ is larger than expected. If the aperture size is reduced by one-half, one would expect a 50% reduction in event throughput for a reduction in either the X0 or Y0 dimension, or, a 25% reduction if both dimensions are reduced simultaneously. The same three E634 runs were used to generate these solid angle plots as was done for the SASP. Figure 3.20 shows the relations between event throughput and solid angle openings for these runs. From figure 3.20(a) we see that at 50% of the wide open X0 cut, 60% of the valid events pass. Figure 3.20(b) shows that at 50% of the wide open Y0 cut, 50% of the valid events pass. Figure 3.20(c) shows that the combination of a 50% cut on each of X0 and Y0 as calculated by

$$\frac{300}{600} \times \frac{400}{800} = 0.25, \tag{3.98}$$

and gives an event passage of 30%. These 'ΔX&ΔY' values are thus expressed relative to the maximum solid angle defined by the largest cuts on X and Y.

Thus, these results are compatible with our expectations and show that the MRS yield is linearly proportional to the calculated solid angle. Comparing the event passage through a FEC aperture decreased by 50% (in the X0 dimension) to the assumed 100% passing

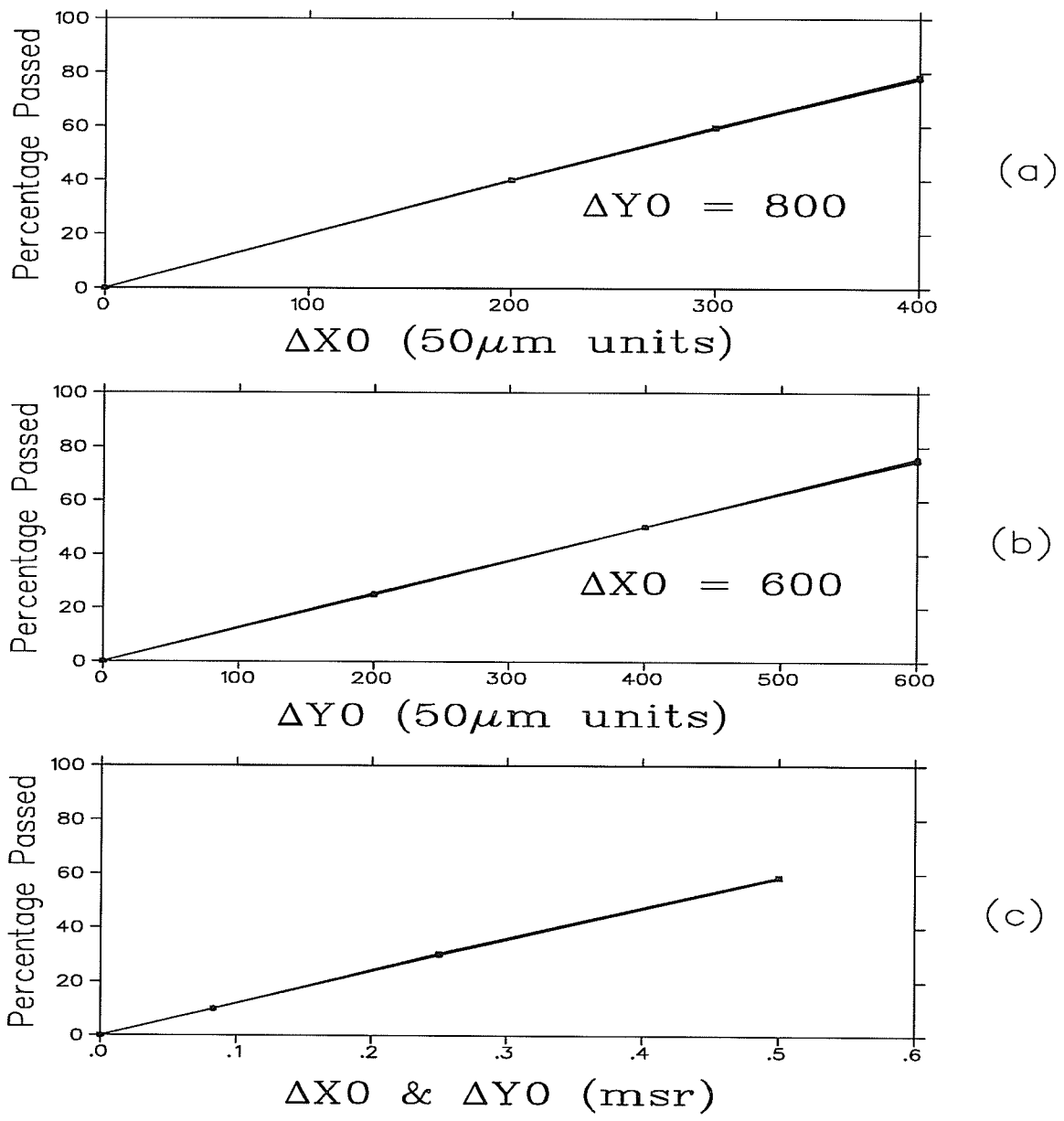

Figure 3.20: Plots of solid angle tests for the MRS for three E634 runs are shown here: (a) has cuts on X0 only, (b) has cuts on Y0 only and (c) has cuts on X0 and Y0 combined. The horizontal scale in (c) is expressed relative to the maximum solid angle defined by the largest cuts on X and Y.

through a full aperture, we have

$$\frac{\Delta\Omega_{MRS}}{3.02/2} = \frac{100}{60} \rightarrow \Delta\Omega_{MRS} = 2.51\ msr, \tag{3.99}$$

and thus the effective solid angle is determined to be 2.51 msr. This value is certainly consistent with that expected for the particular experimental setup used for E634.

3.8.5 Beam Flux and SEM and Polarimeter Calibration

The proton flux used in the cross section and analyzing power calculations was measured with a secondary emission monitor (SEM) and an in-beam polarimeter (IBP). The SEM can be used as a total current monitor. It consists of an array of foils in an evacuated container placed in the path of the proton beam. Alternating foils are positively charged and these attract electrons knocked out by penetrating beam protons. The current is then measured from the collected electron charge. A Faraday cup is used to calibrate the SEM.

Similarly, the IBP can also be used as a total current monitor. The current monitoring principle of the IBP is based on *pp*-elastic scattering from a polyethylene foil. Protons from this scattering are observed by one of four arms, each consisting of three plastic scintillators. There is a 'left', 'right', 'top' and 'bottom' arm, and asymmetries between the left and right arms and between the top and bottom arms can be measured.

The total number of protons with spin up and spin down, as given by the SEM is,

$$\begin{aligned} PROT_{\uparrow} &= (SEM_{\uparrow}/C_{SEM})/1.602 \times 10^{-10} nC \\ PROT_{\downarrow} &= (SEM_{\downarrow}/C_{SEM})/1.602 \times 10^{-10} nC \end{aligned} \tag{3.100}$$

where C_{SEM} = calibration constant for the SEM (see table 3.4) and
$SEM_{\uparrow}$, $SEM_{\downarrow}$ = SEM total counts for spin up, down.

Table 3.4 shows the SEM and polarimeter calibration constants used in determining the IBP/SEM counts ratio. The IBP and SEM counting rates were determined using equations (3.101) and (3.102) respectively,

$$Rate_{IBP} = 44.17 - \left(\frac{T_p}{100}\right)(1.171 - \left(\frac{T_p}{100}\right)1.250) \tag{3.101}$$

$$\frac{counts_{SEM}}{counts_{FCup}} = \frac{dE}{dx}(Al) \times 0.30738 \tag{3.102}$$

where the units or definitions are as follows,

T_p = proton energy in MeV,
ρ_{CH_2} = areal density of IBP CH_2 target (1.37 mg/cm^2),
Rate_{IBP} = IBP counting rate in counts/nC/mg/cm^2 CH_2,
counts_{SEM} = counts on SEM scaler (1 count = 10^{-10}C),
counts_{FCup} = counts on Faraday cup scaler (1 count = 10^{-10}C),
dE/dx = energy loss of electrons in aluminum, in MeV/g/cm^2. [20]

ENERGY MeV	C_{IBP} $counts/nC$	C_{SEM} $counts/nC$
371.2	78.15	7.654
500.7	95.41	6.639

Table 3.4: The In-Beam Polarimeter (IBP) and Secondary Emission Monitor (SEM) calibration constants are listed here.

Equation (3.101) is a result of a fit to calibration measurements from 200 MeV to 500 MeV and (3.102) is a result of averaged SEM calibration measurements.

In the program E634_ANAL.FOR (see appendix D), the polarimeter/SEM counts ratio, POL_SEM, is calculated as follows:

$$POL\_SEM = \frac{(IBP_{\uparrow} + IBP_{\downarrow})}{(SEM_{\uparrow} + SEM_{\downarrow})} \times \frac{C_{SEM}}{C_{IBP}} \tag{3.103}$$

where C_{SEM} = SEM calibration constant,
C_{IBP} = IBP calibration constant,
$POL_{\uparrow}$, $POL_{\downarrow}$ = IBP up, down counts,
$SEM_{\uparrow}$, $SEM_{\downarrow}$ = SEM up, down counts.

Figure 3.21(d) shows a plot of the IBP/SEM counts ratio, divided by the expected ratio, as a function of time over all the experimental runs. The expected ratio is deduced by obtaining the expected IBP and SEM count rates per unit charge from separate calibrations. Overall, the IBP/SEM counts ratio in figure 3.21(d) is fairly consistent for the duration of the experiment, with an average deviation between the SEM and polarimeter counts of approximately 3%. This discrepancy may be attributed to the condition of the IBP target. The IBP target is very sensitive to the beam current and to the position of the beam on the target. IBP target thickness and the quality of the vacuum housing the SEM target may also be responsible for a discrepancy between the SEM and polarimeter counts. The effect of the beam tune change from dispersed at 500 MeV to achromatic at 370 MeV is noticeable in figure 3.21(a) and figure 3.21(d) at about 55 hours when the 370 MeV runs commence. Note also that an achromatic beam will cause degradation of the IBP target more quickly than a dispersed beam.

Because of the IBP target's susceptibility to degradation, the SEM was assumed to provide a more reliable measure of beam charge. Comparing figures 3.21(a) and 3.21(b), one can readily see that the SEM counts more consistently than the IBP. Thus, in the cross section calculations, the number of spin up and down protons impinging on the target was extracted from the SEM counts.

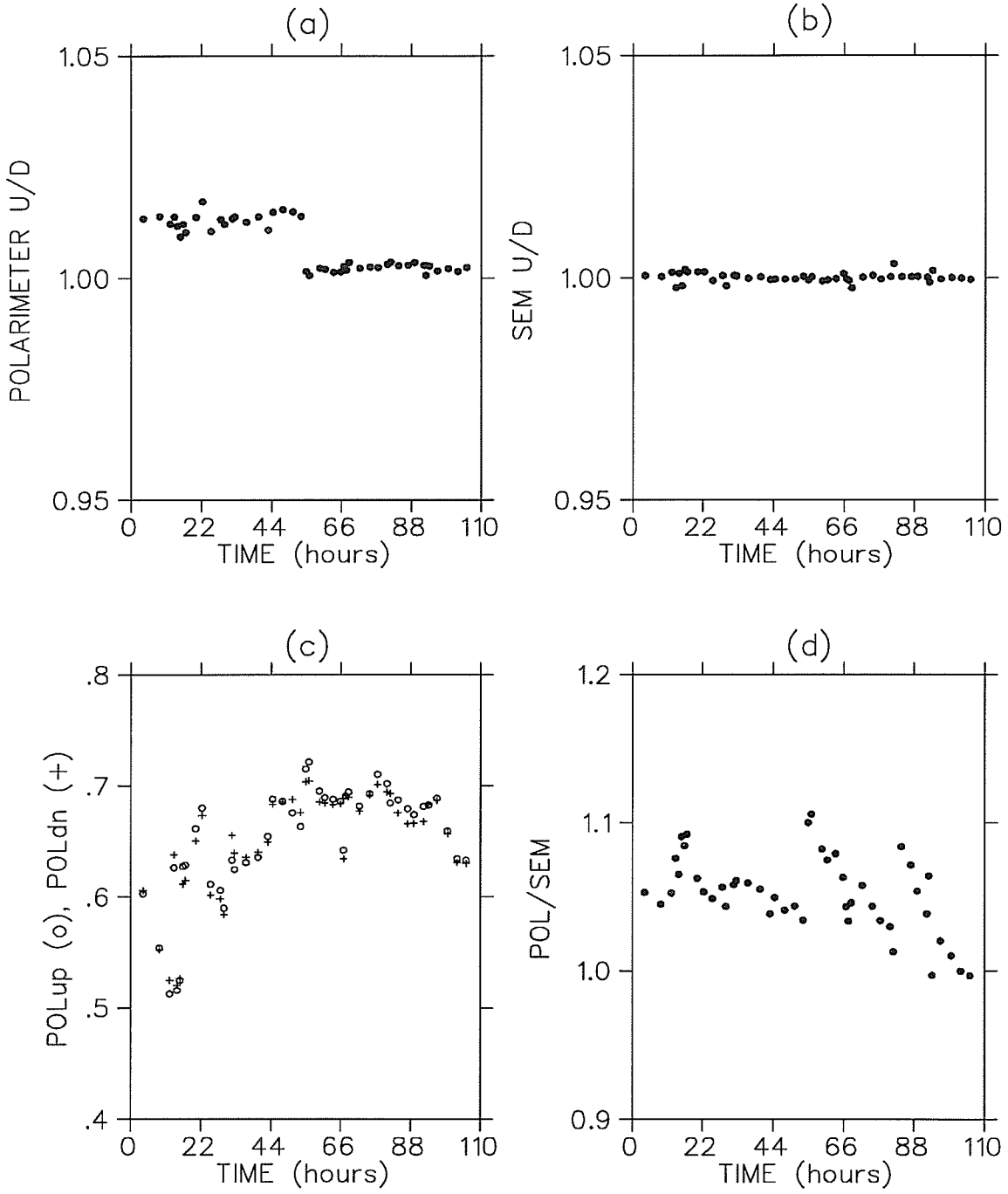

Figure 3.21: These plots show polarimeter and SEM counts in various forms: (a) polarimeter spin up/down ratio, (b) SEM spin up/down ratio, (c) spin up (circles) and down (crosses) polarization as determined by the polarimeter and (d) polarimeter/SEM ratio; the X-axis range on all plots covers the duration of the E634 experiment.

3.8.6 Spin Off Correction

Between polarized runs, short unpolarized runs were made throughout the experiment. The resulting 'spin off polarization' as a function of run time is shown in figure 3.22. This spin off polarization is a measure of the IBP's instrumental asymmetry. Extrapolations from these unpolarized runs were made, so that the estimated spin off polarization could be subtracted from the polarized runs. All of the polarimeter data shown in figure 3.21 have been corrected for spin off polarization.

3.8.7 Background Subtraction

The NOVA variable LTMRS represents the time difference between the activation of the MRS trigger and the SASP trigger. The NOVA analysis for E634 produced a histogram of the LTMRS variable, called HLTMRS. A sample of this histogram for one of the E634 runs is shown in figure 3.23. Peaks in HLTMRS coincide with cyclotron beam bursts (43 nanoseconds apart). The large peak corresponds to valid coincidence events between the SASP and MRS while the smaller peaks represent accidental coincidences with particles from other beam bursts. The dominant peak also contains accidental coincidence events and these random (background) events were subtracted directly in NOVA by the following method.

In the NOVA operation sequence used for E634 (listed in appendix G), software cuts on both the valid coincidence peak (LTMRS_P - 'p' for peak) and a peak containing only accidentals (LTMRS_R - 'r' for random) were made. Table 3.5 lists the histograms which were incremented when incoming DASS events satisfied either of these two cuts and table 3.6 gives a brief description of each these histograms. Examples of these histograms are shown in §4.1.

After differentiation between coincidence and random events was made, further cuts subdivided the events into spin up and spin down events. Unless otherwise specified, all histogram incrementation is by units of one. Fractional incrementation occurs when the spectrum is incremented by the variable RSEFF; RSEFF is the composite efficiency comprised of the SASP acceptance (S_ACC), MRS acceptance (R_ACC) and the SASP pion survival (SURVIV) fraction, that is,

```
RSEFF=R_ACC*S_ACC*SURVIV .
```

Thus, the increment is by a fractional amount proportional to the detection efficiency. The variables RSEFF, R_ACC, S_ACC and SURVIV are calculated by the NOVA user routine USRQ which is given in appendix F.

The background event subtraction was performed as part of the NOVA off-line analysis, by decrementing the appropriate spectra when an event satisfied the random event cut. Histograms such as HDRMDEL_N enabled an immediate assessment of the quantity of valid coincidence events.

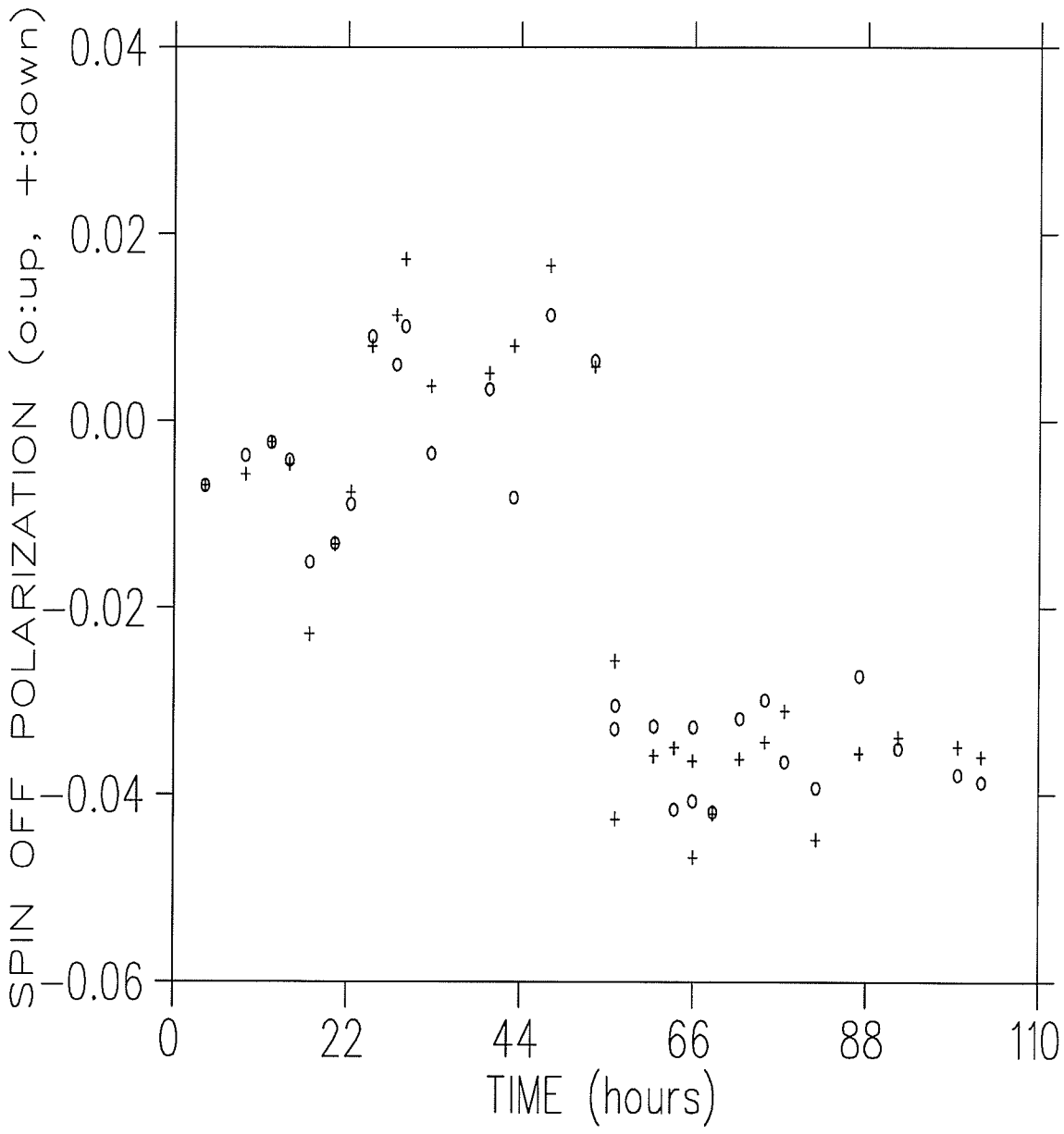

Figure 3.22: Spin off polarization versus run time for the duration of the E634 experiment is plotted here. The circles represent spin up, the crosses, spin down data. This apparent polarization is due to the IBP instrumental asymmetry.

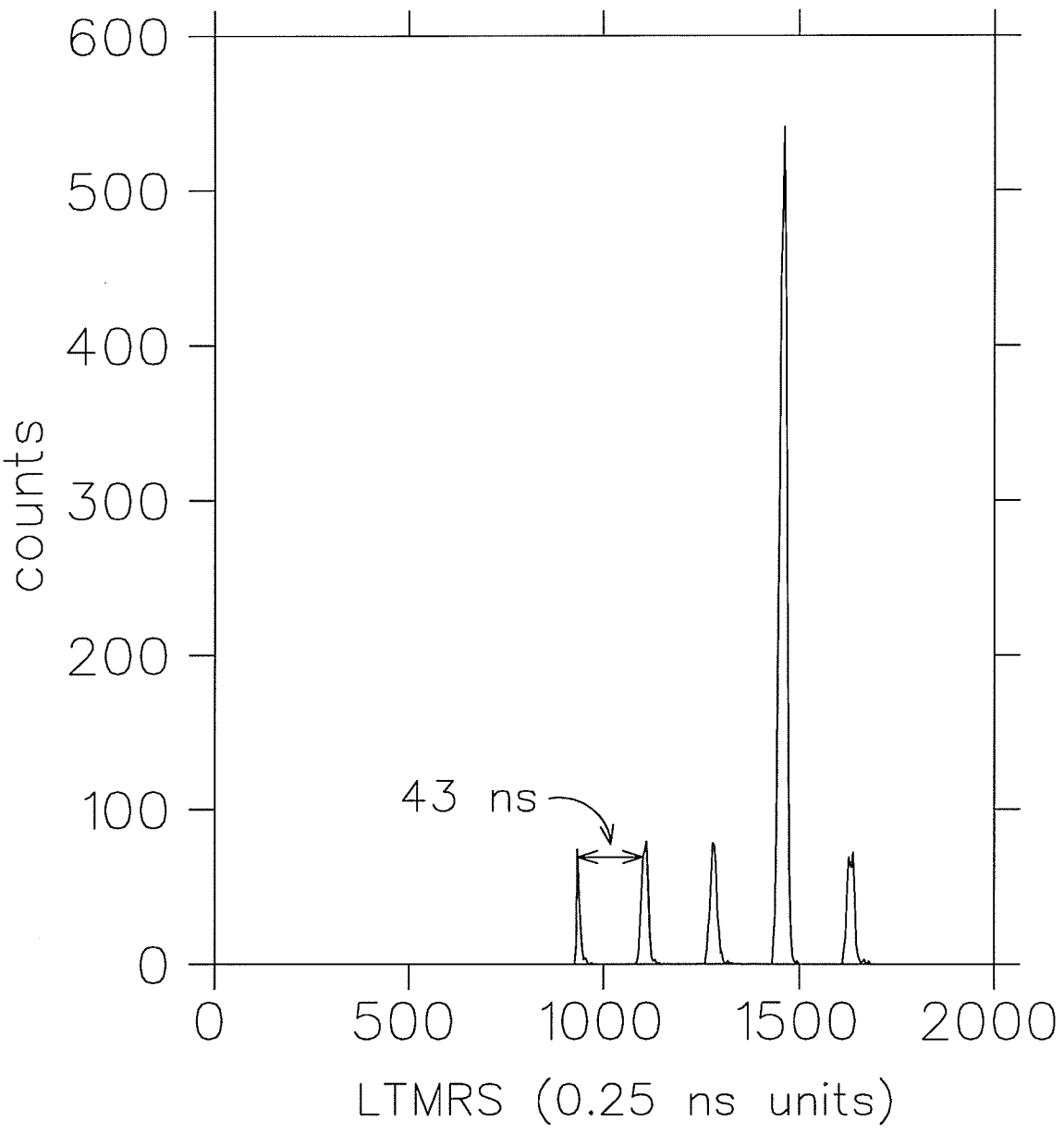

Figure 3.23: The HLTMRS spectrum showing the relative timing between the SASP and MRS is given above. The small peaks represent accidental deuteron-pion coincidences with pions and deuterons coming from other beam bursts. The large peak represents valid coincidence plus accidental events. Each proton beam burst is separated in time by 43 ns.

EVENTS ACCEPTED	HISTOGRAMS INCREMENTED	
	'LTMRS_P' coincidence events	'LTMRS_R' random events
SPIN UP AND DOWN	HDRMDEL_T	HDRMDEL_R
	HDRMDEL_N	HDRMDEL_N
	HDRMDEL_NC	
	HDRMDEL_NE	HDRMDEL_NE
	HDRMDEL_NEC	
	HSDELRACC	HSDELRACC
	HSDELSACC	HSDELSACC
	HSDELSURV	HSDELSURV
	HDRMASS_P	HDRMASS_R
SPIN UP ONLY	HDRMDEL_U	HDRMDEL_U
	HDRMDEL_UC	
	HDRMDEL_UE	HDRMDEL_UE
	HDRMDEL_UEC	
	HDRMASS_PU	HDRMASS_RU
SPIN DOWN ONLY	HDRMDEL_D	HDRMDEL_D
	HDRMDEL_DC	
	HDRMDEL_DE	HDRMDEL_DE
	HDRMDEL_DEC	
	HDRMASS_PD	HDRMASS_RD

Table 3.5: This table lists the histograms incremented upon satisfaction of the LTMRS_P and LTMRS_R conditions given in the NOVA operation sequence. LTMRS_P corresponds to peak events of the LTMRS histogram, representing valid coincidence events. The LTMRS_R condition corresponds to random events (background). For a description of the histograms, see table 3.6.

HISTOGRAM	DESCRIPTION
HDRMDEL_T	'T' indicates *total* events; accidentals were *not* subtracted
HDRMDEL_R	'R' indicates *random* events; only accidental events are displayed
HDRMDEL_N	'N' indicates *net* events; accidentals *were* subtracted
HDRMDEL_NC	'C' indicates *continuum*; the DRMASS scale extends to 60 MeV, allowing observation of continuum (1s) states (which lie in the 10 - 50 MeV excitation energy range)
HDRMDEL_NE	'E' indicates *efficiency* ; incremented by composite efficiency RSEFF
HDRMDEL_NEC	same as HDRMDEL_NE but using continuum DRMASS scale
HSDELRACC	incremented by R_ACC; represents MRS focal plane acceptance
HSDELSACC	incremented by S_ACC; represents SASP focal plane acceptance
HSDELSURV	incremented by SURVIV; represents the pion survival fraction
HDRMASS_P	bins spin up and down events satisfying LTMRS_P condition
HDRMASS_R	bins spin up and down events satisfying LTMRS_R condition
HDRMDEL_U	spin up events
HDRMDEL_UC	spin up events binned on a continuum DRMASS scale
HDRMDEL_UE	spin up efficiency spectrum, incremented by RSEFF
HDRMDEL_UEC	same as HDRMDEL_UE, but using a continuum DRMASS scale
HDRMASS_PU	bins spin up events satisfying LTMRS_P condition
HDRMASS_RU	bins spin up events satisfying LTMRS_R condition
HDRMDEL_D	spin down events
HDRMDEL_DC	spin down events binned on a continuum DRMASS scale
HDRMDEL_DE	efficiency spectrum, incremented by RSEFF
HDRMDEL_DEC	same as HDRMDEL_DE, but using a continuum DRMASS scale
HDRMASS_PD	bins spin down events satisfying LTMRS_P condition
HDRMASS_RD	bins spin down events satisfying LTMRS_R condition

NOTES: Histograms whose names start with ...
'HDRMDEL' are 2D plots of SDEL versus DRMASS
'HSDEL' are 1D plots of SDEL counts.
'HDRMASS' are 2D plots of SDEL versus DRMASS

Table 3.6: This table briefly describes the histograms listed in table 3.5. Unless otherwise specified, the incrementation of each histogram is by units of one.

Normalized Yield per Pixel

Because of the large variations of the detection efficiency (RSEFF) between events, a normalized yield which corrected for this efficiency was calculated on a pixel by pixel basis. It is often the case that in the two dimensional histograms (HDRMDEL_N, HDRMDEL_NE, etc.) there were two or three events per pixel. To quantify the normalized yield, let n be the value per pixel in the HDRMDEL_N spectrum. The corresponding pixel in the HDRMDEL_NE spectrum contains the value $\Sigma\eta_i$, where η_i = RSEFF$_i$. Defining an average value $\overline{\eta}$ for this pixel, we can write $\Sigma\eta_i = n\overline{\eta}$. The normalized yield for the pixel is then

$$\begin{aligned} Y &= \frac{1}{\eta_1}+\frac{1}{\eta_2}+\ldots \approx \frac{n}{\overline{\eta}} = \frac{n^2}{n\overline{\eta}} = \frac{n^2}{\Sigma\eta_i} \\ &= \frac{(pixel\ value\ in\ HDRMDEL\_N\ spectrum)^2}{pixel\ value\ in\ HDRMDEL\_NE\ spectrum}. \end{aligned} \tag{3.104}$$

Other corresponding pairs of spectra (HDRMDEL_U, HDRMDEL_UE and HDRMDEL_D, HDRMDEL_DE) were handled in the same manner. The calculations were performed by the E634_ANAL.FOR program, which is listed in appendix D.

3.9 Efficiencies

3.9.1 Wire Chamber Efficiencies

The wire chamber efficiencies for the SASP and MRS were read directly from the NOVA 'IF listing' after analysis of the data was complete. This 'IF listing' lists the scalers associated with all NOVA 'IF-THEN' conditions, indicating the percentage of events that have satisfied each condition. The two conditions of interest were

I. MMWOK: "multiwire okay" for the MRS; the NOVA definition is the logical combination of a hit on all four VDC planes as well as both FEC planes for events identified as deuterons. In NOVA it is given as

```
MMWOK=MVDC_OK&MFEC_OK,
      MVDC_OK=((MX1_OK&MX2_OK)&MU1_OK)&MU2_OK
      MFEC_OK=MX0_OK&MY0_OK .
```

The MRS wire chamber efficiency (for the FEC and VDCs) is defined as the ratio of events satisfying MMWOK divided by the number of events identified as deuterons.

II. LMWOK: "multiwire okay" for the SASP; the NOVA definition is the logical combination of a hit on all four VDC planes for events identified as pions. The NOVA definition is

```
LMWOK=LVDC_OK,
      LVDC_OK=((LX1_OK&LX2_OK)&LU1_OK)&LU2_OK .
```

The SASP wire chamber efficiency (for the VDCs) is defined as the ratio of events satisfying LMWOK divided by the number of events identified as pions.

These wire chamber efficiencies were used in the cross section calculations for each run.

The values for collective MRS wire chamber efficiency ranged from 40-60% while the majority of the SASP values were near 91-93% for all runs analyzed. Note that the MRS wire chamber efficiency includes the efficiency for both the FEC and the VDCs, which is the reason for a lower overall MRS chamber efficiency. The close proximity of the FECs to the scattering chamber and the high event rate environment typically causes the FECs to be less efficient than the VDCs.

3.9.2 NOVA Cuts on VDC and FEC Data

After the "multi-wire okay" cuts were satisfied, *meantime* cuts were imposed on the VDC and FEC data. These were done in NOVA by setting a cut around the peaks in the corresponding meantime (MT) histograms (HSVDCMT, HMVDCMT, HMFECMT).

For the VDCs, the "meantime" is the TDC value for a struck hypothetical wire which lies right at the intersection of the particle track and the wire plane. The drift chamber TDCs run in *common stop* mode and thus stop timing when the spectrometer event trigger is activated. The spectrometer event trigger is usually defined as a hit in the scintillator paddles, as was the case for experiment E634. Therefore, the VDC meantime essentially defines the start of the drift time and is a measure of the time required for a particle to pass between the VDC and scintillator paddles. Defining a region of acceptance around the peaks in the meantime plots serves to decrease background events that do not correspond to proper events.

The FEC "meantime" for the X or Y plane is the average of the following two drift times: the drift time between the particle track and the X (or Y) plane and the drift time between the same particle track and the offset X′ (or Y′) plane (see §2.4.1 for more details). This meantime pulse was part of the trigger for the MRS during experiment E634.

The meantime values for the FECs and the VDCs are calculated by the NOVA user routine USR1 using the TDC values of each wire in the drift chambers. Software cuts were used to place gates around the peaks in the meantime histograms. A greater amount of random background appears in the FEC meantime spectra compared to the VDC meantime spectra because of the FEC's close proximity to the target. This has yielded data passage through the FEC meantime cut, MFECMTCUT, of about 40% - 50% for most runs.

The FEC and VDC meantime cuts were combined into one cut called MEANTCUT as follows,

```
MEANTCUT=(MFECMTCUT&MVDCMTCUT)&LVDCMTCUT
```

and this was inserted into the NOVA OPSEQ. For most runs the passage through this cut ranged from 10% - 50%.

3.9.3 Computer Live Time

The data acquisition live time was determined using the *latch* (see page 14) and *busy* scaler readings. Their ratio provides a measure of the computer system live time for accepting input events,

$$n_{live} = \frac{latch}{event}, \tag{3.105}$$

which was used in the cross section calculation. The statistical error associated with this quantity is negligible.

3.10 Cross Section Calculation

The cross section for scattering to the left or right using a spin up polarized beam can be expressed in terms of the cross section for unpolarized beam ($d\sigma/d\Omega$) as

$$\frac{d\sigma}{d\Omega}(\uparrow) = \frac{d\sigma}{d\Omega}(1 + P(\uparrow)A_{N0}). \tag{3.106}$$

Similarly, the cross section using a spin down polarized beam can be expressed as

$$\frac{d\sigma}{d\Omega}(\downarrow) = \frac{d\sigma}{d\Omega}(1 - P(\downarrow)A_{N0}). \tag{3.107}$$

Manipulating these two expressions, one obtains the spin-averaged cross section that was used for E634 calculations:

$$\frac{d\sigma}{d\Omega}(A) = \frac{P(\downarrow)d\sigma/d\Omega(\uparrow) + P(\uparrow)d\sigma/d\Omega(\downarrow)}{P(\uparrow) + P(\downarrow)}, \tag{3.108}$$

where '$\uparrow$' and '$\downarrow$' refer to spin up and down states respectively. The spin up and down polarizations, $P(\uparrow)$ and $P(\downarrow)$, are positive numbers and were calculated using the in-beam polarimeter asymmetry and analyzing power, with a 'spin off polarization' subtraction made; see §3.8.6 on page 71.

The program E634_ANAL.FOR calculated the cross section for all the E634 runs. Four separate cross section calculations were performed, one for the total counts ($d\sigma/d\Omega(tot)$), spin up ($d\sigma/d\Omega(\uparrow)$), spin down ($d\sigma/d\Omega(\downarrow)$) and a cross section averaged over both spin up and down ($d\sigma/d\Omega(A)$). The only non-negligible source of random errors was the statistical error in the number of events. The expression for the error for total counts is derived below. The errors for spin up and spin down ($\varepsilon_{d\sigma/d\Omega(\uparrow)}$ and $\varepsilon_{d\sigma/d\Omega(\downarrow)}$) are also stated.

Let *CNET* equal the net counts (valid events minus accidentals). Then

$$d\sigma/d\Omega(tot) = CNET/Denom = CNET/(denom_{all}denom_{tot}) \tag{3.109}$$

where $denom_{all}$ is that part of the cross section denominator which is common to all three (total, spin up, spin down) cross sections. It is defined as

$$denom_{all} = d\Omega_{MRS}d\Omega_{SASP}n_t n_{live}(MMWOK/100)(LMWOK/100) \tag{3.110}$$

where $d\Omega_{MRS}$ = MRS solid angle
$d\Omega_{SASP}$ = SASP solid angle
n_t = number of target nuclei per cm^2
n_{live} = computer live time
$MMWOK/100$ = MRS wire chamber efficiency
$LMWOK/100$ = SASP wire chamber efficiency.

The $denom_{tot}$ part of the denominator is defined as

$$denom_{tot} = (prot_{up} + prot_{down}) \times EFFT \times RMRS \times \Delta P \tag{3.111}$$

where $prot_{up} + prot_{down}$ = total number of protons impinging on target
$EFFT$ = total efficiency as extracted from efficiency plot HDRMDEL_NE, comprising pion survival and spectrometer acceptance factors
$RMRS$ = an adjustment factor for MRS acceptance (a function of MRS focal plane position)
ΔP = pion momentum interval over which events were summed for the cross section calculation.

For the spin up and spin down cross sections, the expressions analogous to $denom_{tot}$ that were used were

$$denom_{up} = prot_{up} \times EFFT \times RMRS \times \Delta P, \tag{3.112}$$

$$denom_{down} = prot_{down} \times EFFT \times RMRS \times \Delta P. \tag{3.113}$$

The general expression for cross section error for total counts is then

$$\varepsilon_{d\sigma/d\Omega(tot)} = \frac{\varepsilon_{CNET}}{Denom} = \frac{\sqrt{CNET}}{Denom}. \tag{3.114}$$

However, if we define $CNET$ as $C_T - C_B$, where C_T is the total counts and C_B is the accidental event count, then

$$\varepsilon_{CNET} = \sqrt{\varepsilon_{C_T}^2 + \varepsilon_{C_B}^2}. \tag{3.115}$$

The statistical error ε_{C_T} is $\sqrt{C_T}$. The error in the background counts, ε_{C_B}, was not measured separately but was found to be quite small and represented by

$$\varepsilon_{C_B} = f \times C_T. \tag{3.116}$$

From the number of counts observed in various spectra, the following values of f were estimated:

$$f = \begin{cases} 0.02 & \text{for the ground state,} \\ 0.06 & \text{for the 2 MeV and 5 MeV states and} \\ 0.1 & \text{for the continuum part of the missing mass spectra.} \end{cases}$$

Therefore,

$$\varepsilon_{CNET} = \sqrt{C_T}\sqrt{1+f^2 C_T}. \tag{3.117}$$

Similarly, the errors for the spin up and spin down counts are

$$\varepsilon_{CNETup} = \sqrt{C_U}\sqrt{1+f^2 C_U} = \varepsilon_{d\sigma/d\Omega(\uparrow)} \text{ and} \tag{3.118}$$

$$\varepsilon_{CNETdn} = \sqrt{C_D}\sqrt{1+f^2 C_D} = \varepsilon_{d\sigma/d\Omega(\downarrow)}. \tag{3.119}$$

Letting ε_A be the error of the spin-averaged cross section, $d\sigma/d\Omega(A)$, the error calculation proceeds as

$$\begin{aligned}
\varepsilon_A^2 &= \varepsilon_{d\sigma/d\Omega(\uparrow)}^2 \left(\frac{\partial d\sigma/d\Omega(tot)}{\partial d\sigma/d\Omega(\uparrow)}\right)^2 + \varepsilon_{d\sigma/d\Omega(\downarrow)}^2 \left(\frac{\partial d\sigma/d\Omega(tot)}{\partial d\sigma/d\Omega(\downarrow)}\right)^2 \\
&= \varepsilon_{(\uparrow)}^2 \left(\frac{P(\downarrow)}{P(\uparrow)+P(\downarrow)}\right)^2 + \varepsilon_{(\downarrow)}^2 \left(\frac{P(\uparrow)}{P(\uparrow)+P(\downarrow)}\right)^2
\end{aligned}$$

and therefore (3.120)

$$\varepsilon_A = \frac{\sqrt{\varepsilon_{d\sigma/d\Omega(\uparrow)}^2 P(\downarrow)^2 + \varepsilon_{d\sigma/d\Omega(\downarrow)}^2 P(\uparrow)^2}}{P(\uparrow)+P(\downarrow)}. \tag{3.121}$$

The error calculations for the total, spin up and spin down cross section are performed in a similar fashion.

3.11 Analyzing Power Calculation

The analyzing power was calculated in E634_ANAL.FOR according to the expression

$$A_{N0} = \frac{d\sigma/d\Omega(\uparrow) - d\sigma/d\Omega(\downarrow)}{P(\downarrow)d\sigma/d\Omega(\uparrow) + P(\uparrow)d\sigma/d\Omega(\downarrow)}, \tag{3.122}$$

where 'P(↑)' and 'P(↓)' refer to spin up and down polarizations respectively, and these are positive numbers. This expression for the analyzing power is a consequence of equations (3.106) and (3.107).

With only the event counts contributing to the experimental error, the error associated with A_{N0} is calculated as follows,

$$\begin{aligned}
\varepsilon_{A_{N0}}^2 &= \varepsilon_{d\sigma/d\Omega(\uparrow)}^2 \left(\frac{\partial A_{N0}}{\partial d\sigma/d\Omega(\uparrow)}\right)^2 + \varepsilon_{d\sigma/d\Omega(\downarrow)}^2 \left(\frac{\partial A_{N0}}{\partial d\sigma/d\Omega(\downarrow)}\right)^2 \\
&= \frac{\varepsilon_{d\sigma/d\Omega(\uparrow)}^2}{(P(\downarrow)d\sigma/d\Omega(\uparrow)+P(\uparrow)d\sigma/d\Omega(\downarrow))^4} \\
&\quad \times (P(\downarrow)d\sigma/d\Omega(\uparrow)+P(\uparrow)d\sigma/d\Omega(\downarrow) - P(\downarrow)d\sigma/d\Omega(\uparrow)+P(\downarrow)d\sigma/d\Omega(\downarrow))^2 \\
&\quad + \frac{\varepsilon_{d\sigma/d\Omega(\downarrow)}^2}{(P(\downarrow)d\sigma/d\Omega(\uparrow)+P(\uparrow)d\sigma/d\Omega(\downarrow))^4} \\
&\quad \times (-(P(\downarrow)d\sigma/d\Omega(\uparrow)+P(\uparrow)d\sigma/d\Omega(\downarrow)) - P(\uparrow)d\sigma/d\Omega(\uparrow)+P(\uparrow)d\sigma/d\Omega(\downarrow))^2 \\
&= \frac{(P(\uparrow)+P(\downarrow))^2}{(P(\downarrow)d\sigma/d\Omega(\uparrow)+P(\uparrow)d\sigma/d\Omega(\downarrow))^4} \\
&\quad \times (\varepsilon_{d\sigma/d\Omega(\uparrow)}^2 d\sigma/d\Omega(\downarrow)^2 + \varepsilon_{d\sigma/d\Omega(\downarrow)}^2 d\sigma/d\Omega(\uparrow)^2)
\end{aligned} \tag{3.123}$$

and therefore

$$\varepsilon_{A_{N0}} = (P(\uparrow)+P(\downarrow))\frac{\sqrt{\varepsilon^2_{d\sigma/d\Omega(\uparrow)}d\sigma/d\Omega(\downarrow)^2+\varepsilon^2_{d\sigma/d\Omega(\downarrow)}d\sigma/d\Omega(\uparrow)^2}}{(P(\downarrow)d\sigma/d\Omega(\uparrow)+P(\uparrow)d\sigma/d\Omega(\downarrow))^2}. \quad (3.124)$$

Chapter 4

RESULTS AND DISCUSSION

4.1 NOVA Plots Generated From Analysis

A series of plots was made for each run for diagnostic purposes. What follows is a sample of that series for one of the E634 runs, run 53. Run 53 used a carbon target, beam energy of 500 MeV, MRS angle of 25° and SASP angle of 30°. It covered the momenta ranges for the pion and deuteron corresponding to 'box 3' in the kinematics plot shown in figure 1.2(c) on page 3.

Pions and deuterons were identified by energy loss in the paddle scintillators and by time of flight through the spectrometers. Figure 4.1(a) shows the HMPID spectrum which is the particle identification spectrum for the MRS-detected particle. The HSPID spectrum given in figure 4.1(b) and this is the particle identification spectrum for the SASP-detected particles. The particles in boxes labelled 1 and 4 in the figure 4.1 are deuterons and pions, respectively. Figure 4.2 displays the focal plane position in the SASP versus the focal plane position in the MRS. This is essentially a plot of pion momentum versus deuteron momentum. The various states of the ^{11}B nucleus are identified in the plot.

Figure 4.3 shows four plots of ϕ_{TR} and θ_{TR} plotted against DRMASS, for both spectrometers. These plots were used to check for optical aberrations which result in degradation of energy resolution in missing mass spectra. Empirical corrections were made based on these plots, as discussed in §3.7.2, and the plots shown in figure 4.3 have the corrections applied.

Figure 4.4 presents plots of SDEL (see page 29) versus DRMASS (see §3.6) showing total events in 4.4(a) and randoms only in 4.4(b). The X-projections at the top of the plots give an indication of the number of counts for each DRMASS channel.

Figure 4.5 contains various plots of SDEL versus DRMASS. The plots on the left hand column represent net events after subtraction of accidentals. The spectra on the right hand side are the corresponding efficiency spectra which are incremented by RSEFF for all valid coincidence events and decremented by RSEFF for random events. RSEFF is composed of the MRS acceptance, SASP acceptance and SASP pion survival fraction and

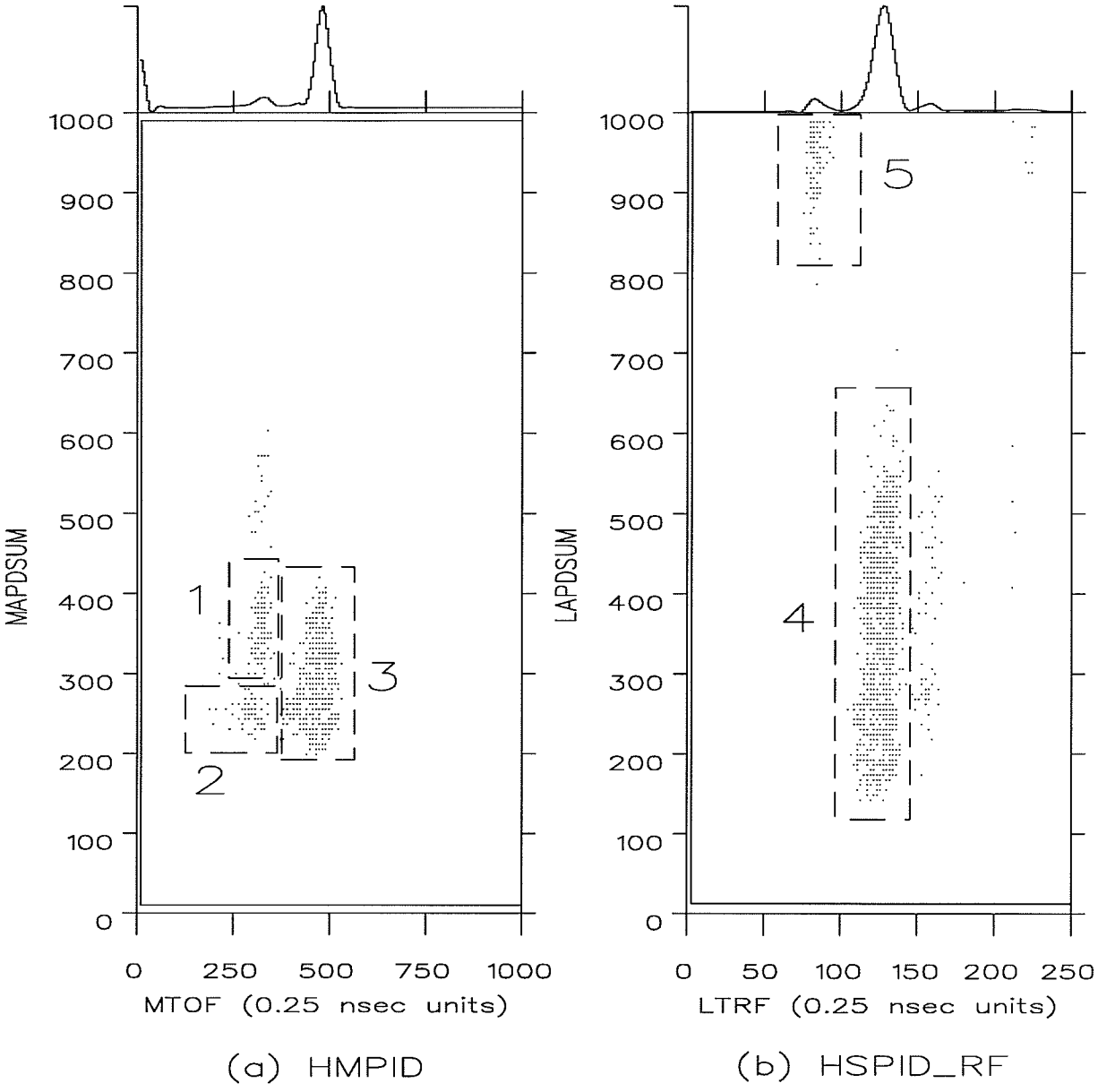

Figure 4.1: These spectra show the detected particles in (a) the MRS and (b) the SASP. The identified particles are: 1: deuterons, 2: accidental protons from other beam bursts, 3: scattered protons, 4: pions (π^+) and 5: accidental protons from other beam bursts. The Y-axis variable is the scintillator paddle sum for the MRS (MAPDSUM) and SASP (LAPDSUM); each is the sum of the digitized ADC counts for the charge in the signals in the individual paddles (comprising the paddle array), integrated over the time that the ADC gate signal is present. Thus, the vertical scales for the two plots give an indication of the amount of ionization that occurred in the scintillator array.

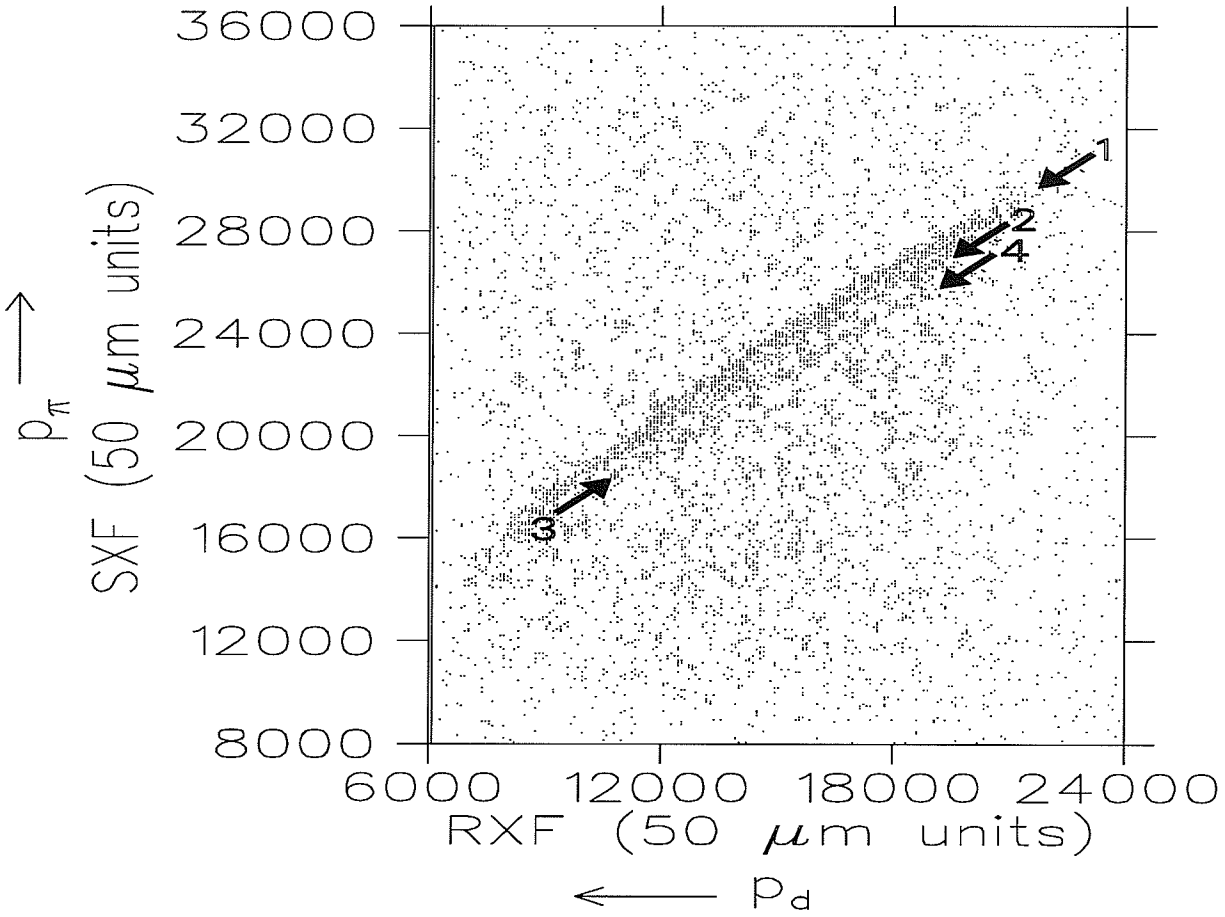

Figure 4.2: The above histogram represents a 'top view' of the missing mass spectrum; it is a plot of pion momentum versus deuteron momentum. The loci shown are identified as the following states of ^{11}B: 1, ground state; 2, first excited state, 2.12 MeV; 3, second excited state, 4.45 MeV; 4, third excited state, 5.02 MeV.

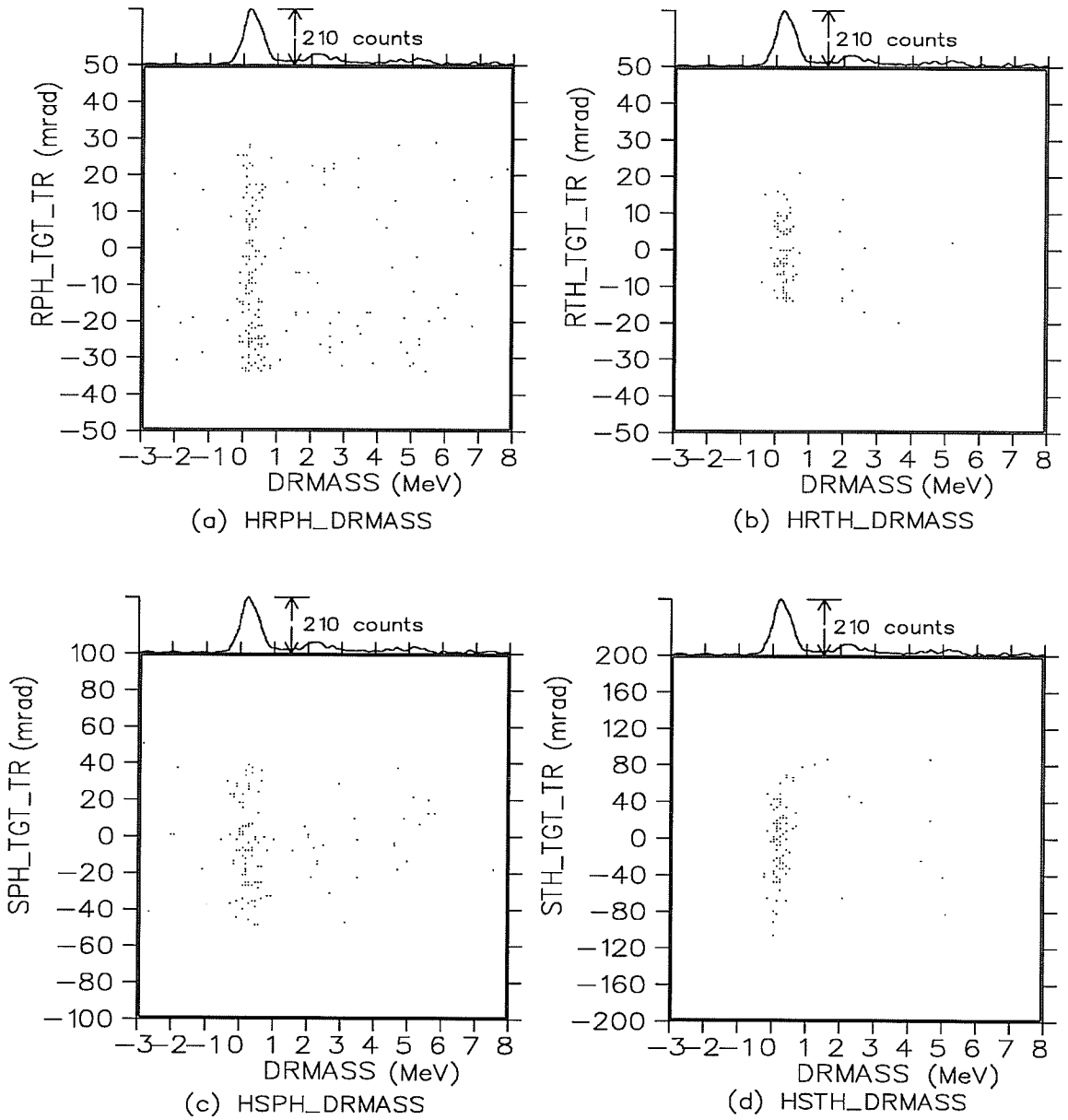

Figure 4.3: These four plots show the relation between ϕ and θ at the target and the missing mass, after empirical aberration corrections have been applied. The top two plots show this relation for the MRS, the bottom two for the SASP.

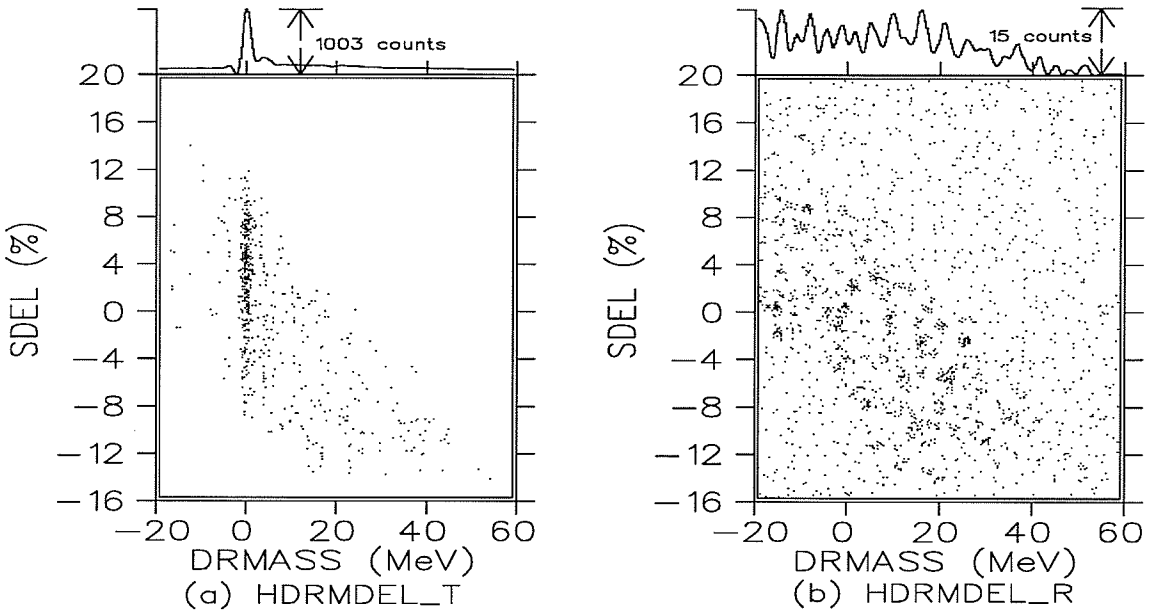

Figure 4.4: This figure contains plots of SASP focal plane position, SDEL, versus missing mass, DRMASS, showing (a) both true and random events (total events) and (b) only random events.

is discussed on page 71. Comparing the peak counts (indicated in the X-projections at the top of each plot) between the left and right columns gives an indication of the significance of the composite efficiency factor RSEFF. Figure 4.6 shows plots defined similarly to those in figure 4.5 except that the figure 4.6 plots extend their DRMASS-axis to include the continuum states.

Figure 4.7 provides an indication of the magnitude of the random events in comparison to the peak events, for the collective spin up and down events, spin up events only and spin down events only.

In figure 4.8, the spectra shown are incremented upon satisfaction of the LTMRS_P condition and decremented upon satisfaction of the LTMRS_R condition. The incrementation/decrementation is by variable units of (a) R_ACC, (b) S_ACC or (c) SURVIV. Thus, these plots provide a comparison between the magnitudes of these three efficiency factors. These variables are discussed on page 71 and calculated by NOVA user routine USRQ listed in appendix F.

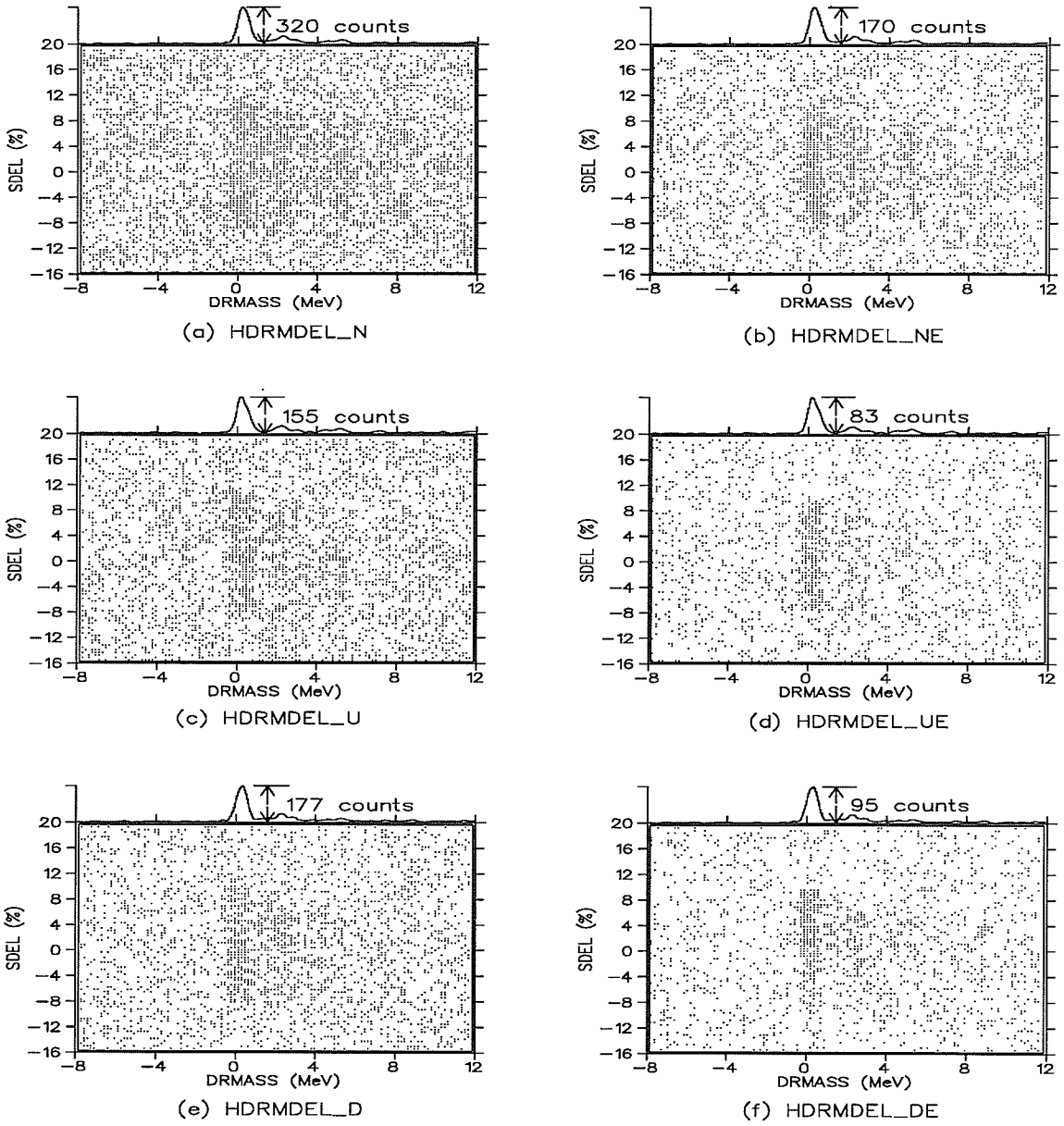

Figure 4.5: These are plots of SASP focal plane position, SDEL, versus missing mass, DRMASS. (a), (c) and (e) in the left column represent net events after subtraction of random events. (a) contains events for both spin up and down, (c) shows spin up events only and (e) contains spin down events only. Plots (b), (d) and (f) in the right column are the corresponding efficiency spectra incremented/decremented by all/random events.

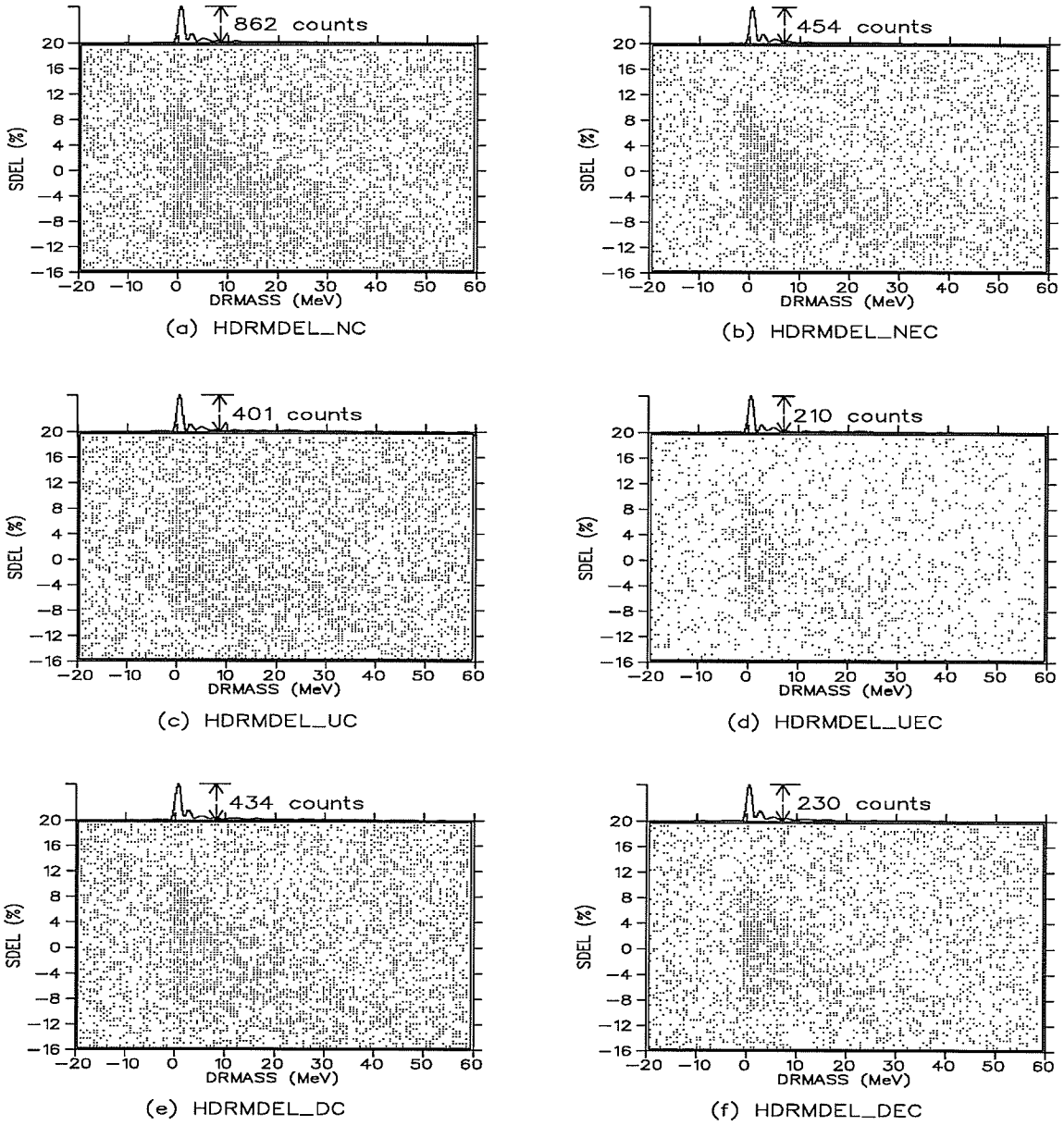

Figure 4.6: Plots of SASP focal plane position, SDEL, versus missing mass, DRMASS are given here. The details of this figure are the same as that for figure 4.5 except that here the missing mass scale is extended to include the continuum states.

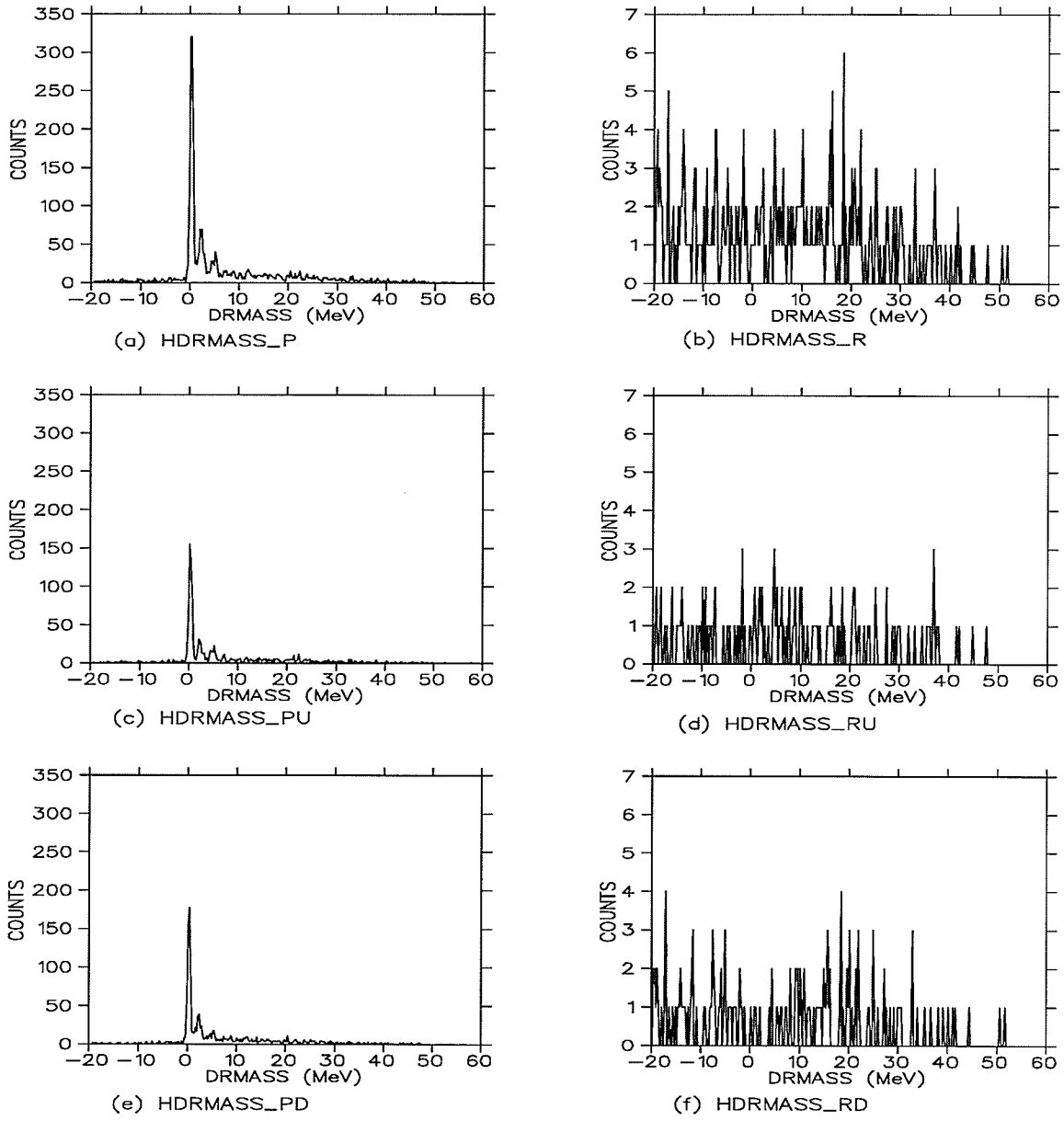

Figure 4.7: (a) shows the missing mass spectra incremented for events satisfying the LTMRS_P condition (a peak in the HLTMRS plot - see figure 3.23). (c) and (d) show the same but for spin up and down events respectively. (b) shows the missing mass spectra gated only on random events (satisfying the LTMRS_R condition) and (d) and (f) show random spin up and random spin down respectively.

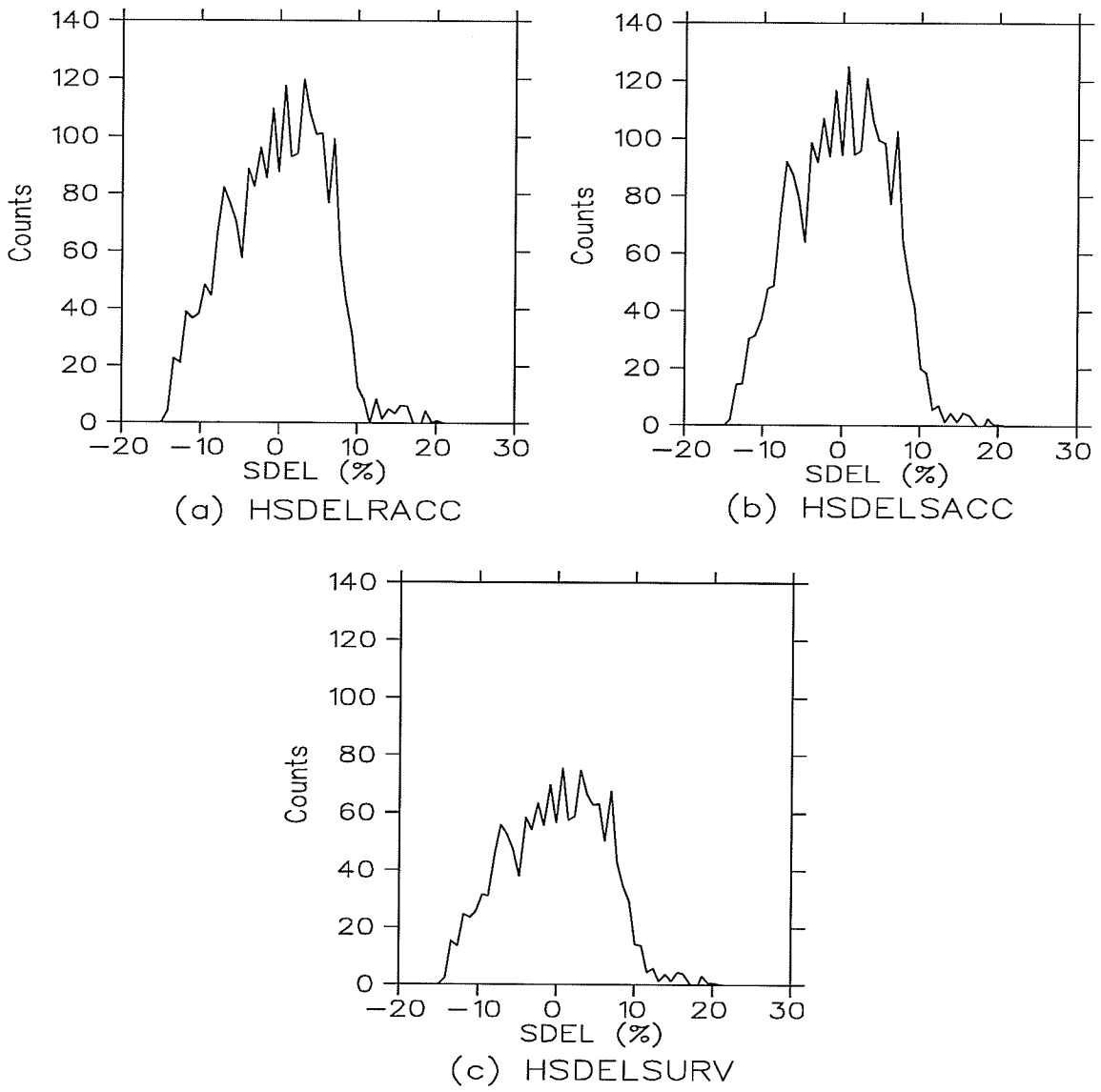

Figure 4.8: The above three spectra are incremented according to one of three efficiency factors: (a) MRS acceptance, (b) SASP acceptance and (c) the SASP pion survival fraction. The horizontal axes show the range of the SASP focal plane in terms of percent momentum deviation from central momentum. SDEL = 0% corresponds to the central momentum focal plane position.

4.2 Cross Sections and Analyzing Powers

The data in the HDRMDEL spectra in figures 4.5 and 4.6 was written to an output file for the subsequent calculation of the cross sections and analyzing powers. These spectra were HDRMDEL_N, HDRMDEL_U and HDRMDEL_D, representing all, spin up and spin down events, respectively, and the associated spectra containing the efficiency information are HDRMDEL_NE, HDRMDEL_UE and HDRMDEL_DE. This efficiency is the EFFT variable in equation (3.111). A second set of six similar spectra, with the missing mass scale extending from -20 MeV to 60 MeV, was used for analysis of the continuum region. The spectra were divided into sections, whose bin size in the SDEL variable was chosen on the basis of a compromise between counts and desired resolution in the pion momentum. The normalized yield for any bin in the two dimensional HDRMDEL plot was obtained by summing the same channel intervals in both the event plots and the efficiency plots. Random events had previously been subtracted from these spectra and, for the discrete states, represented no more than a few percent of the total events. The reading of spectra, binning of events, yield calculation and cross section and analyzing power calculations were all performed by the program E634_ANAL.FOR (see appendix D).

For brevity, only data for the ground state of the residual nucleus are investigated in this thesis. Also, the runs using the oxygen target are not explored here, since subtracting background events for these runs proved too cumbersome. Figures 4.9 through 4.11 show cross section and analyzing power results calculated from the experimental data. The plots for the four 500 MeV carbon target runs show two theoretical distorted wave impulse approximation (DWIA) curves representing the initial energy approximation (IEA) (solid line) and final energy approximation (FEA) (dashed line) models for the cross sections and analyzing powers. The short dashed curve in the analyzing power graphs represents the free $pp \rightarrow d\pi^+$ analyzing power. These theoretical models are discussed in §5.2.

The plots for the carbon runs show that the agreement between theory and experiment for the analyzing powers is generally better at θ_{MRS}=15° than at θ_{MRS}=25°. This is because the 15° deuteron angle corresponds to a lower momentum transfer as can be seen when comparing the p_{recoil} curves plotted for these two angles. At lower momentum transfer, the struck proton behaves like a quasifree object in the reaction and therefore we observe an analyzing power close to that of the free $pp \rightarrow d\pi^+$ analyzing power.

Results for the carbon target at 370 MeV beam energy are shown in figure 4.10. For this energy no DWIA calculations were available. Instead, a greatly simplified model (see discussion of PWIA model on page 97) was used. This model assumed that the cross section is proportional to $\left(\frac{d\sigma}{d\Omega}\right)_{pp\rightarrow d\pi^+} |\Phi(\vec{p})|^2$, where $\left(\frac{d\sigma}{d\Omega}\right)_{pp\rightarrow d\pi^+}$ is the differential cross section for the free $pp \rightarrow d\pi^+$ process and $\Phi(\vec{p})$ is the target proton momentum wave function. This is shown by the double line in the plots. The curve labelled T_{pp} represents the effective laboratory pp collision energy (with a free proton) that gives rise to the same

center of mass energy of the pion and deuteron system as in the $^{12}C(\vec{p}, d\pi^+)^{11}B$ reaction.

Figure 4.11 shows cross section and analyzing power results for the runs using the deuterium target at beam energies of 370 MeV and 500 MeV. The $^2H(p, d\pi^+)n$ reaction is a simple case of the $A(\vec{p}, d\pi^+)B$ reaction.

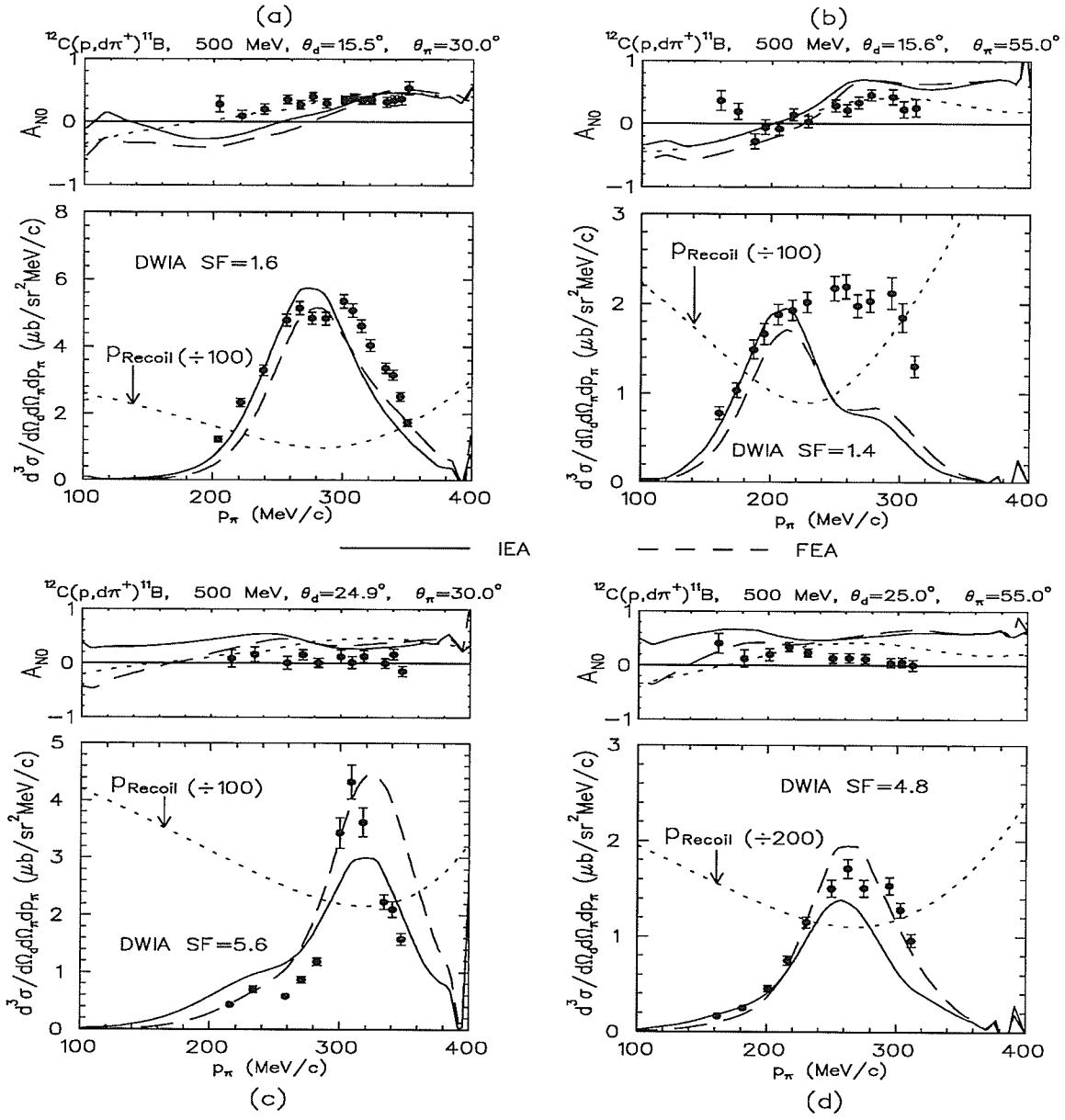

Figure 4.9: These plots show the cross section and analyzing power results for 500 MeV carbon target runs with the following MRS and SASP angle combinations: (a) MRS=15.5°, SASP=30.0°, (b) MRS=15.6°, SASP=55.0°, (c) MRS=24.9°, SASP=30.0°, (d) MRS=25.0°, SASP=55.0°. The short dashed curve in the analyzing power graphs represents the free $pp \rightarrow d\pi^+$ analyzing power. P_{recoil} represents the momentum of the recoil target nucleus; its value is read off the vertical scale in MeV/c, by multiplying by the reduction factor as specified in the plots (ie, 100, 200).

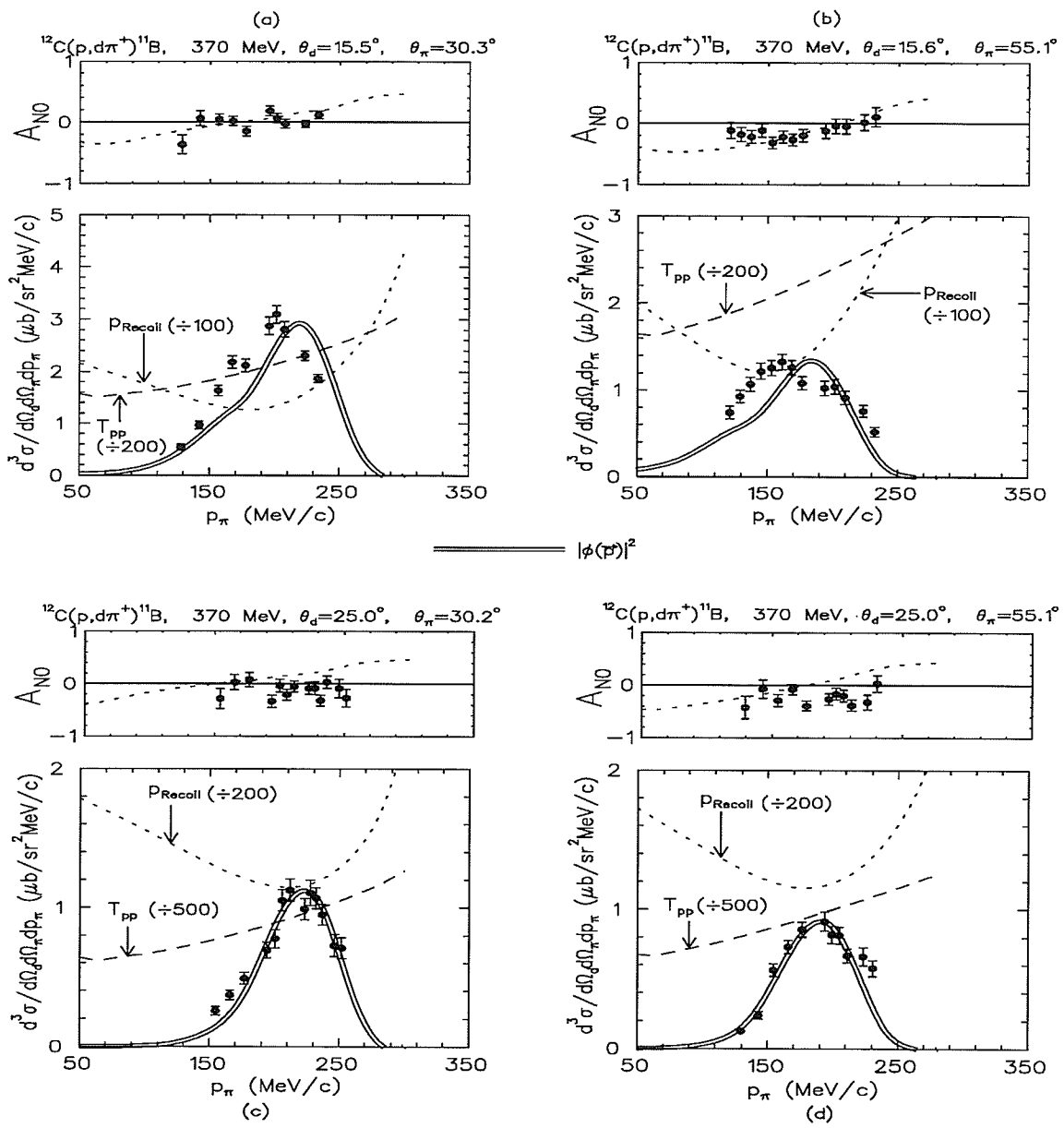

Figure 4.10: The above plots illustrate cross section and analyzing power results for 370 MeV carbon target runs with the following MRS and SASP angle combinations: (a) MRS=15.5°, SASP=30.3°, (b) MRS=15.6°, SASP=55.1°, (c) MRS=25.0°, SASP=30.2°, (d) MRS=25.0°, SASP=55.1°. Other details are the same as for figure 4.9.

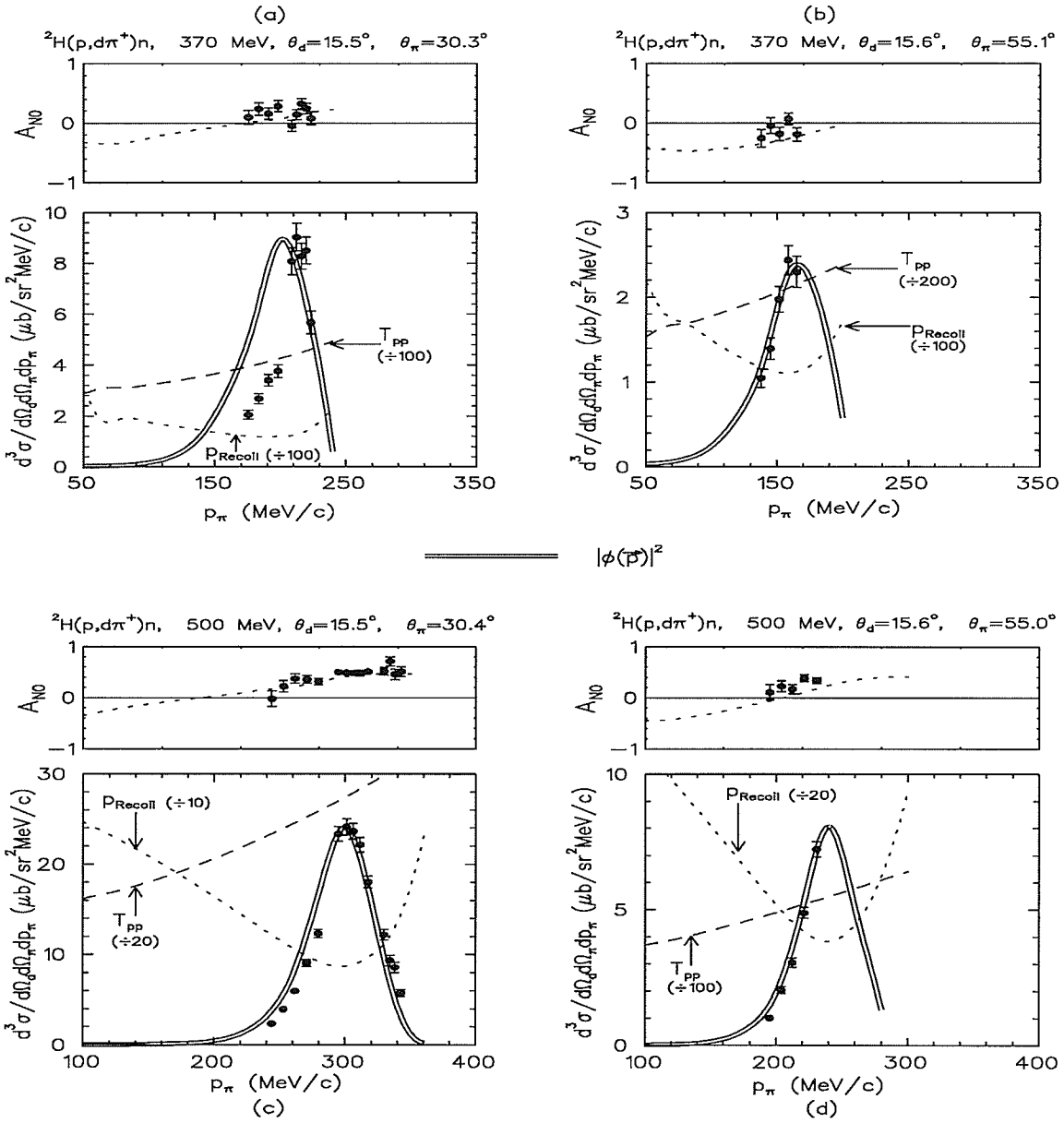

Figure 4.11: These plots show cross section and analyzing power results for deuterium target runs with the following beam energies and MRS and SASP angle combinations: (a) 370 MeV, MRS=15.5°, SASP=30.3°, (b) 370 MeV, MRS=15.6°, SASP=55.1°, (c) 500 MeV, MRS=15.5°, SASP=30.4°, (d) 500 MeV, MRS=15.6°, SASP=55.0°. Other details are the same as for figure 4.9.

Chapter 5

THEORY

Previous experiments involving exclusive A$(\vec{p},\pi^+)$B reactions lead us to believe that the dominant underlying process for these reactions is the $pp \rightarrow d\pi^+$ process which itself is dominated by the intermediate formation of the Δ_{1232} [5]. The theoretical approach in analyzing the $(\vec{p},d\pi^+)$ reaction is to imbed the fundamental $pp \rightarrow d\pi^+$ process in a DWIA description of the reaction. The following sections discuss this link, the DWIA and $pp \rightarrow d\pi^+$ models and the fit to cross section and analyzing power data.

5.1 DWIA Model

The pion-absorption reaction, $(\pi^+,2p)$, is known to proceed predominantly through absorption on quasi-deuteron pairs, $\pi d \rightarrow pp$ for example, and this may be viewed as roughly related to the time-reversed $(\vec{p},d\pi^+)$ reaction and has been shown to be reasonably well understood by the distorted wave impulse approximation (DWIA) theory [21]. The DWIA model takes into account the distortion of the plane waves by the interaction between the incident particle and target. A further feature of the impulse approximation theory is that it assumes that the incident particle interacts with one nucleon at a time, that the amplitude of the incident wave reaching each nucleon in the target nucleus is unaffected by the presence of the other nucleons (it is the imaginary part of the optical potential that accounts for any nucleon interaction), and that the binding energies of the target nucleons are very much less than the incident energy [22]. The reactions studied here clearly satisfy the impulse approximation since: (1) the separation energies for the removal of a neutron and proton from a ^{12}C nucleus are 18.721 and 15.956 MeV, respectively, and the incident proton energies of 370 MeV and 500 MeV are much greater than these binding energies; and (2) the quasifree nature of the ^{12}C$(\vec{p},d\pi^+)^{11}$B reaction, at least at low momentum transfer, implies that the target nucleon is unaffected by the presence of the other nucleons [22].

5.2 Comparison of Theory with Experimental Results

The plots of cross sections and analyzing powers are given in §4.2 on pages 93 through 95. The plots for the 500 MeV runs with the ^{12}C target show initial and final energy approximation (IEA and FEA) curves for the cross section. The fact that the $pp \rightarrow d\pi^+$ process involves a bound target proton implies that the process is *off-shell*, that is, energy and momentum are not conserved within the two nucleon system. Thus, both the IEA and FEA models of cross section are plotted to illustrate the possible extremum of cross section data. For most of the four 500 MeV ^{12}C plots, the cross section data does indeed fall between these two approximations.

The spectroscopic factor associated with the fits of the cross section data to the DWIA model is also given in plots in figure 4.9, and has values ranging from 1.4 to 5.6. From other experiments, one expects a value of about 2.5 for the proton occupancy of the $p_{3/2}$ shell. The reason for the wide range of values from the present reaction is not clear. The theoretical fit to the data varies in quality, but the overall shape of the theory-based curve is broadly consistent with the data points. These theoretical calculations are preliminary, and greater investigation of different parameter sets is required to see the sensitivity of the cross sections and analyzing powers to changes in the parameters.

The DWIA model calculations were not available for the remaining ^{12}C and ^{2}H target runs at the time of analysis. The cross section data for these runs is instead compared with a simplified plane wave impulse approximation (PWIA) model which replaces the distorted momentum distribution with the square of the momentum wave function, $|\Phi(\vec{p})|^2$. This model for the theoretical cross section is given by

$$\frac{d^3\sigma}{d\Omega_d d\Omega_\pi dp} = C_k \left(\frac{d\sigma}{d\Omega}\right)_{pp\rightarrow d\pi^+} \sum_{p_{mt}} |\Phi(p_{mt})|^2 \tag{5.1}$$

where C_k = a kinematic factor (set to a constant value for simplicity - normally it is only slowly varying over the region of interest)

$\Phi(p_{mt})$ = momentum wave function at the momentum p defined by the momentum transfer

$\left(\frac{d\sigma}{d\Omega}\right)_{pp\rightarrow d\pi^+}$ = differential cross section for $pp \rightarrow d\pi^+$. This was calculated by a program called 3_BODY_A.FOR, written by W. R. Falk [17].

For ^{12}C, a harmonic oscillator wave function was assumed, leading to the result

$$|\Phi(p)|^2 = p^2 e^{-p^2/v}. \tag{5.2}$$

For the deuteron, a Hulthen-type wave function was assumed, and for the pion a plane wave model was assumed. Predictions of this simplified model are shown in figures 4.10 and 4.11.

Discrepancies between the data and this model are most likely due to an inadequacy of the simple PWIA model; the PWIA model ignores the interaction between the particles

with the result that the overall normalization is not a reliable quantity. The overall shape, however, is consistent between the data and the model.

Chapter 6

RECOMMENDATIONS and CONCLUSION

6.1 Recommendations

Although the results achieved from the data analysis were certainly reasonable, there are aspects that could be improved upon in subsequent experimentation and analysis. Some of these are included below.

- Using a thinner target (for each of ^{12}C, CD_2 and ^{16}O) would be advantageous as it would result in the deuterons losing less energy before entering the MRS, thereby improving resolution.
- It would be best to use a dispersed beam for the 370 MeV runs as well as the 500 MeV runs to improve resolution. This was not done at the outset because an adequate dispersed beam tune at 370 MeV was not available at the time of the experiment. Surprisingly, the resolution for the 370 MeV runs seemed better than the resolution for the 500 MeV runs. The deuteron energy loss would be greater at 370 MeV than for 500 MeV, thus resulting in poorer energy resolution for the lower energy; so, the actual improvement in resolution for the 370 MeV runs is especially puzzling.
- To observe the correlation between beam dispersion and the resulting energy dispersion, a histogram of DRMASS versus X_i (particle position at the target) could be incorporated into the NOVA analysis. If a correlation between these two variables is observed, perhaps further empirical corrections could be made.
- The event rates were limited by the MRS FEC capabilities. Perhaps upgraded FEC technology could improve this situation.
- During analysis, the most suitable MRS and SASP calibrations, transfer matrix elements and aberration optimization calculations should be employed. Not all the optimum analysis elements were available at the time of E634 analysis.

6.2 Conclusion

The first high resolution study of the $(\vec{p}, d\pi^+)$ reaction on nuclei has been carried out. Using the two TRIUMF spectrometers, the MRS and SASP, enabled a full kinematic reconstruction of the three-body reactions studied. The reactions examined were $^{12}C(\vec{p}, d\pi^+)^{11}B$ and $^{2}H(\vec{p}, d\pi^+)n$, at 500 and 370 MeV beam energies. The MRS was used to detect deuterons while the SASP detected pions. The purpose of the experiment was to investigate the degree to which reactions of $A(\vec{p}, d\pi^+)B$ type proceed via the quasifree $pp \rightarrow d\pi^+$ process and how this process is modified by the nuclear medium. This was carried out by calculating the associated cross sections and analyzing powers and looking for characteristics of a quasifree process.

The $^{2}H(\vec{p}, d\pi^+)n$ reaction provided a simple case of the $A(\vec{p}, d\pi^+)B$ reaction. In regions of low momentum transfer, the observed analyzing powers for both beam energies and the four spectrometer angle combinations followed the free $pp \rightarrow d\pi^+$ analyzing power theoretical curve (dashed line) fairly closely.

The theoretical cross section model used for the $^{2}H(\vec{p}, d\pi^+)n$ and $^{12}C(\vec{p}, d\pi^+)^{11}B$ reactions at 370 MeV beam energy employed a simple PWIA model based on the square momentum wave function for the reaction. This provided an adequate fit to the cross section data.

For the ^{12}C target runs at 500 MeV, DWIA calculations employing the IEA and FEA assumptions provided fits to the analyzing power and cross section data. For the A_{N0} plots, a curve representing the free $pp \rightarrow d\pi^+$ analyzing power was also included for comparison. At the MRS angle of 15.5°, the analyzing power data fits the free $pp \rightarrow d\pi^+$ curve better than the IEA or FEA curves. This indicates that the free $pp \rightarrow d\pi^+$ process aptly describes the $^{12}C(\vec{p}, d\pi^+)^{11}B$ reaction at these momenta and angles. The analyzing power fit at the MRS angle of 25.0° was not as good; here the momentum transfer is higher and not as well characterized by the free $pp \rightarrow d\pi^+$ mechanism. The data points do, however, lie within the range of the initial and final energy approximations.

The effect of the nuclear medium in the $pp \rightarrow d\pi^+$ process manifests itself in this experiment. For the $^{12}C(\vec{p}, d\pi^+)^{11}B$ reactions, the deuteron detection angle, and in turn, the amount of momentum transfer, plays a significant role in the agreement of data with theory. In the simpler $^{2}H(\vec{p}, d\pi^+)n$ reactions, the data fit is fairly consistent for all spectrometer angle combinations.

Although the agreement of data with theory varies in quality, the free $pp \rightarrow d\pi^+$ process has been shown to predominate in the lower momentum transfer experiments. The effects of the nuclear medium upon this process is apparent when comparing the results of the $^{2}H(\vec{p}, d\pi^+)n$ and $^{12}C(\vec{p}, d\pi^+)^{11}B$ reactions. These results will provide important information for planning subsequent experiments that will examine a much greater region of the allowed phase space, beyond the quasifree region [5].

Bibliography

[1] S. S. M. Wong. *Introductory Nuclear Physics.* Prentice-Hall, Inc., 1990.

[2] D. H. Perkins. *Introduction to High Energy Physics.* Addison-Wesley Publishing Company, Inc., 1987.

[3] G. Friedlander, J. Kennedy, E. Macias, and J. Miller. *Nuclear and Radiochemistry.* John Wiley & Sons, Inc., 1981.

[4] W. R. Falk. Phenomenological $pp \rightarrow d\pi^+$ model of A$(\vec{p},\pi^+)$B reactions. *Physical Review C*, 50(3):1574–1593, September 1994.

[5] W. R. Falk. E634 experiment proposal: Investigation of the (p,dπ^+) reaction in the quasifree region, December 1990.

[6] E634 experiment logbook, August 1994. TRIUMF.

[7] S. Yen. Optics of the Q-Q-Clamshell Second Arm Spectrometer. TRIUMF Design Note, TRI-DN-88-10, February 1988.

[8] K. Hicks. Medium Resolution Spectrometer (MRS) manual. Revision 2.0, July 1988.

[9] The "DASSHELP" on-line VMS help for SASP/MRS/DASS experimenters at TRIUMF.

[10] J. A. Chakhalyan. The TRIUMF Second Arm Spectrometer System (SASP). Master's thesis, University of British Columbia, April 1995.

[11] P.Kitching et al. Quasifree nucleon-nucleon scattering. *Advances in Nuclear Science*, 15(43):58–61, 1985.

[12] P. W. Green. Introduction to the NOVA data analysis system, March 1991. TRIUMF document no. TRI-DNA-91-1.

[13] P. W. Green. ECL, 1992. TRIUMF Preliminary Draft (unpublished).

[14] K. M. Furutani. *Pion Production From Few Nucleon Systems in the Region of the Δ_{1232} Resonance.* PhD thesis, University of Manitoba, December 1991.

[15] TRIUMF Data Acquisition Software Group. Twotran reference manual. TRIUMF document, 1989.

[16] S. Yen. Private communication. TRIUMF.

[17] W. R. Falk. Private communication. University of Manitoba.

[18] M. A. Punyasena, S. Yen, M. Hartig, and Y. Ke. Empirical determination of the focal surface and first order transfer matrix elements of the SASP. TRIUMF, December 1994.

[19] SASP development runs logbook.

[20] 4B IBP calibration notes (appendix A and B), March 1985.

[21] A.A.Cowley and P.G.Roos et al. Quasifree subthreshold pion production in the reaction $^{12}C(p, d\pi^+)^{11}B$. *Physical Review C*, 45(4):1745–1747, April 1992.

[22] D. F. Jackson. *Nuclear Reactions.* Methuen & Co. Ltd., 1970.

[23] S. Kowalski and H. A. Enge. *RAYTRACE.* MIT, 1986.

Appendix A

Calculation of Unit Vectors for Particle Trajectories Through the SASP and MRS

The following is a derivation of a unit vector in the direction of a particle trajectory traversing either of the two DASS spectrometers. These unit vectors are termed $\hat{n}_{SASP}$ and $\hat{n}_{MRS}$ and are utilized in the missing mass calculations of §3.6. The Madison system is the frame of reference adhered to, wherein the origin is situated at the target. This is illustrated in figure 3.10 on page 50. The central trajectories of the MRS and SASP as measured in the Madison frame using spherical coordinates correspond to θ_M, $\phi_M = 0$ for the MRS, and θ_S, $\phi_S = \pi$ for the SASP.

Each spectrometer has its own Transport coordinate system for which angles of a given trajectory are defined with respect to the central ray as discussed in §3.2;

θ is measured in the $X_{TR} - Z_{TR}$ plane (the positive θ direction is downwards from the central trajectory) and

ϕ is measured in the $Y_{TR} - Z_{TR}$ plane (see figure 3.10).

Let $\vec{r}$ be a vector measured along the central particle trajectory (in either spectrometer) and $\vec{R}$ be the vector along the actual trajectory. We adopt the following for angle interpretation:

$\theta_{M/S}$ = detection angle θ (in radians) for the MRS/SASP,
$\phi_{M/S}$ = ϕ (in radians) for the MRS/SASP,
θ = θ_{TR} converted to radians (from mrad), in the $X_{TR} - Z_{TR}$ transport plane,
ϕ = ϕ_{TR} converted to radians (from mrad), in the $Y_{TR} - Z_{TR}$ Transport plane.

A vector along a trajectory through the SASP can be characterized in the Transport coordinate system by

$$\vec{R} = \vec{r} + r(\sin\phi)\hat{Y}_{TR} + r(\sin\theta)\hat{X}_{TR}, \tag{A.1}$$

and since the angles θ and ϕ in the Transport system are typically of the order of milliradians, we make the approximation

$$\sin\theta \simeq \theta$$

and

$$\sin\phi \simeq \phi.$$

This gives us

$$\vec{R} = \vec{r} + r\phi\hat{Y}_{TR} + r\theta\hat{X}_{TR}. \tag{A.2}$$

Figure 3.10 indicates that in the Madison system a vector along the central ray traversing the SASP is given by

$$\vec{r} = -r(\sin\theta_S)\hat{i} + r(\cos\theta_S)\hat{k}. \tag{A.3}$$

The Transport unit vectors $\hat{X}_{TR}$ and $\hat{Y}_{TR}$ can be written in terms of Madison unit vectors $\hat{i}, \hat{j}, \hat{k}$ and θ_S as follows

$$\begin{aligned} \hat{X}_{TR} &= -\hat{j} \\ \hat{Y}_{TR} &= \cos\theta_S\hat{i} + \sin\theta_S\hat{k}. \end{aligned} \tag{A.4}$$

Using equations (A.3) and (A.4) , we can write equation (A.2) in terms of Madison coordinates, used for kinematic calculations, as

$$\begin{aligned} \vec{R} &= r[-\sin\theta_S\hat{i} + \cos\theta_S\hat{k} + \phi\cos\theta_S\hat{i} + \phi\sin\theta_S\hat{k} + \theta(-\hat{j})] \\ &= r[(-\sin\theta_S + \phi\cos\theta_S)\hat{i} + (\cos\theta_S + \phi\sin\theta_S)\hat{k} - \theta\hat{j}]. \end{aligned} \tag{A.5}$$

Squaring this trajectory vector gives

$$\begin{aligned} R^2 &= r^2[\sin^2\theta_S - 2\phi\sin\theta_S\cos\theta_S + \phi^2\cos^2\theta_S + \cos^2\theta_S \\ &\quad -2\phi\sin\theta_S\cos\theta_S + \phi^2\cos^2\theta_S + \theta^2] \\ &= r^2[1 + \phi^2 + \theta^2] \end{aligned} \tag{A.6}$$

and therefore the magnitude of $\vec{R}$ is

$$R = r\sqrt{1 + \phi^2 + \theta^2}. \tag{A.7}$$

From this we have an expression for $\hat{n}_{SASP}$, the unit vector along an arbitrary trajectory traversing the SASP:

$$\hat{n}_{SASP} = \frac{\vec{R}}{R} = \frac{(-\sin\theta_S + \phi\cos\theta_S)\hat{i} + (\cos\theta_S + \phi\sin\theta_S)\hat{k} - \theta\hat{j}}{\sqrt{1 + \phi^2 + \theta^2}}. \tag{A.8}$$

For a particle trajectory through the MRS, a similar procedure is followed. Transport conventions dictate that a vector along a trajectory through the MRS is characterized in the same way as for the SASP, as given in (A.2).

From figure 3.10, we see that in the Madison system a vector along the central ray traversing the MRS is given by

$$\vec{r} = r\sin\theta_M\hat{i} + r\cos\theta_M\hat{k}. \tag{A.9}$$

The transport unit vectors $\hat{X}_{TR}$ and $\hat{Y}_{TR}$ can be written in terms of Madison unit vectors $\hat{i}, \hat{j}, \hat{k}$ and θ_M as follows

$$\begin{aligned} \hat{X}_{TR} &= -\hat{j} \\ \hat{Y}_{TR} &= \cos\theta_M\hat{i} - \sin\theta_M\hat{k}. \end{aligned} \tag{A.10}$$

Using (A.9) and (A.10), we can write equation (A.2) in terms of the Madison coordinates as

$$\begin{aligned} \vec{R} &= r[\sin\theta_M\hat{i} + \cos\theta_M\hat{k} + \phi\cos\theta_M\hat{i} - \phi\sin\theta_M\hat{k} + \theta(-\hat{j})] \\ &= r[(\sin\theta_M + \phi\cos\theta_M)\hat{i} + (\cos\theta_M - \phi\sin\theta_M)\hat{k} - \theta\hat{j}]. \end{aligned} \tag{A.11}$$

Squaring this trajectory vector gives

$$\begin{aligned} R^2 &= r^2[\sin^2\theta_M + 2\phi\sin\theta_M\cos\theta_M + \phi^2\cos^2\theta_M + \cos^2\theta_M \\ &\quad - 2\phi\sin\theta_M\cos\theta_M + \phi^2\sin^2\theta_M + \theta^2] \\ &= r^2[1 + \phi^2 + \theta^2] \end{aligned} \tag{A.12}$$

and thus the magnitude of $\vec{R}$ is

$$R = r\sqrt{1 + \phi^2 + \theta^2}, \tag{A.13}$$

which is the same as for the SASP, as one would expect.

From this we have an expression for the $\hat{n}_{MRS}$, the unit vector along an arbitrary trajectory traversing the MRS:

$$\hat{n}_{MRS} = \frac{\vec{R}}{R} = \frac{(\sin\theta_M + \phi\cos\theta_M)\hat{i} + (\cos\theta_M - \phi\sin\theta_M)\hat{k} - \theta\hat{j}}{\sqrt{1 + \phi^2 + \theta^2}}. \tag{A.14}$$

Appendix B

MRS Momentum Calibration

Absolute energy and momentum calibrations for the MRS were obtained through analysis of data taken in January 1995 and November 1994, respectively. An absolute calibration of the MRS at a single focal plane position was also determined from the January 1995 data and this result compared to the absolute momentum calibration given in equation (3.93) on page 62. The details of these calibrations are presented below.

I. Absolute Cyclotron Beam Energy Calibration
(REFERENCE: BL4B OPTICS Logbook, Vol. 4, January 10, 1995)

Target = CD_2, 8.52 mg/cm^2, target angle = 0°
MRS angle = 15.44°
Nominal Beam Energy = 313.1 MeV
This beam energy results in nominal energies of about 287.7 MeV and 42.8 MeV for protons and pions respectively.

(1) MRS Magnetic Field Ratio:
The MRS magnetic field ratio for protons from pp scattering events and pions from $pp \rightarrow d\pi^+$ was measured for a given energy and scattering angle at the same focal plane position RXF (measured in 50μm units). This ratio is sensitive to beam energy and very insensitive to the exact scattering angle.

Table B.1 provides the data for the determination of this ratio. First, the pion's focal plane position from a $pp \rightarrow d\pi^+$ reaction at a given magnetic field setting was measured. Second, the magnetic field corresponding to the same focal plane position for a proton from an elastic pp scattering experiment was deduced by interpolation between measured positions surrounding the desired focal plane position. Hence, the MRS magnetic field ratio is given by

$$B_{(pp\ elastic)}/B_{(pp\rightarrow d\pi^+)} = 9.8437/1.4349 = 6.8602. \qquad \text{(B.1)}$$

PARTICLE	RUN	B_{MRS}	RXF (50μm units)
π	150	1.4349	16780
p	151	9.6522	14558
p	153	9.8401	16738
p	extrapolated		
	to RXF=16780	9.8437	16780

Table B.1: These measurements were used to determine absolute beam energy calibration.

T_{beam} (MeV)	P_p (MeV/c)	E_p (MeV)	-dP	Corrected P_p	Corrected $P_p/P(\pi)$
308	781.28	1220.97	0.21	781.07	7.2081
310	784.11	1222.78	0.21	783.90	7.0210
312	786.94	1224.60	0.21	786.73	6.8524
314	789.76	1226.41	0.21	789.55	6.6985
T_{beam} (MeV)	P_π (MeV/c)	E_π (MeV)	-dP	Corrected P_π	
308	108.58	176.83	0.22	108.36	
310	111.86	178.86	0.21	111.65	
312	115.02	180.86	0.21	114.81	
314	118.08	182.82	0.21	117.87	

Table B.2: These quantities were used to determine the kinematically corrected P_p/P_π ratio. The columns titled 'corrected' show quantities corrected for energy losses incurred at the target and at the FEC, as specified in equation (B.2).

(2) Kinematics and Energy Loss:

The energy loss of a proton or pion in the target is:	0.030 MeV
The energy loss of a proton or pion through the FEC is:	0.103 MeV
Total energy loss:	0.133 MeV

Therefore,

$$dP = (E/P)dT,\ dT = -0.133 \text{ MeV}. \tag{B.2}$$

Table B.2 lists the data used to determine the proton-pion momentum ratio, corrected for energy losses incurred at the target and in the FEC.

(3) Interpolating the last column in table B.2 for the P_p/P_π value of 6.8602 gives $T_p = 311.9$ MeV. Note that this calculation assumes that the magnetic field behaves linearly.

II. Absolute MRS Calibration at a Single Point:
(REFERENCE: BL4B OPTICS Logbook, Vol. 4, January 10, 1995)

(1) Pb(p,p)Pb scattering was used where an angle-insensitive momentum could be established at the above value of $T_p = 311.9$ MeV.

Target = ^{208}Pb, 17.8 mg/cm^2, target angle = 0 °
Beam energy and MRS angle as above (311.9 MeV, 15.44 °)
The ^{208}Pb run considered here is run 155. The result: At B_{MRS} = 10.100 kG, RXF = 14543 (50μm units).

(2) Kinematics and Energy Loss:

The energy loss of a proton in target is:	0.032 MeV
The energy loss of a proton through FEC is:	0.103 MeV
Total energy loss:	0.135 MeV

Therefore,

$$dP = (E/P)dT = 0.20 \text{ MeV/c}. \tag{B.3}$$

At 15.44° and 311.9 MeV, the scattered proton momentum is 826.01 MeV/c, and the corrected proton momentum is therefore 825.81 MeV/c.

(3) Results Summary: B_{MRS} = 10.100 kG, RXF = 14543 50μm units, P = 825.81 MeV/c.

III. MRS Momentum Calibration:
(REFERENCE: SASP DEVELOPMENT Logbook, Vol. 5, November 1994)

(1) New focal plane calibration data were obtained in connection with the acceptance scans. The ground state, 4.44 MeV, and 9.64 MeV states from the ^{12}C (p,p') ^{12}C reaction were used, for a total of 149 data points. The data set comprised approximately 60 runs. The analysis was done by Mona Benjamintz. Approximately 82 data points represent measurements where the focal plane polarimeter cage (FPP) had the wrong orientation (the orientation during experiment E634), with the remaining 67 data points taken using the correct orientation. For reasons which are not clear, the latter data set provided a calibration curve whose deviations of individual points from the fitted curve were much less than for the former data set.

The NOVA analysis was carried out with the acceptance cuts wide open. A constant kinematic correction RCKIN=-5.0 was used throughout and peak positions and areas extracted from the spectrum HMXFK (a histogram of RXFK – kinematically corrected MRS focal plane position). Relevant NOVA definitions are given below.

```
RXF=RQ1/RQ2
  RQ1=RVDCDIST*RX1C-RFOCAL_F*RDX12
  RQ2=RVDCDIST-RDX12*RTAN_DELTA
      RVDCDIST=5472.0000
      RX1C=MX1POS+RX1C0
          MX1POS=MDRIFTVEC(20)
```

```
            RX1C0=5472.0000
            RFOCAL_F=-1000.0000
            RDX12=RX1C-MX2POS
            RTAN_DELTA=0.0000
  RXFK=((RXF+RCKIN*RPH_TGT_TR)+RCXI*RXI_TR)
            +RCY0Q*(MY0POS-RY0_CENT)**2
  RCKIN=-5.0000
  RCXI=0.0000
  RCY0Q=0.0000
  RPH_TGT_TR=(RY0_TR/(RFECDIST_TR*1.00000E+02))*1.00000E+03
    RY0_TR=-(MY0POS-RY0_CENT)*5.00000E-03
      MY0POS=MDRIFTVEC(28)
      RY0_CENT=800.0000
    RFECDIST_TR=0.6430
```

Target = CD_2 10.8 mg/cm^2, target angle = 0°
MRS scattering angle = 25.01 °
Beam Energy = 278.796 MeV (see page 9 of logbook)

The energy loss of a proton in the target is:	0.041 MeV
The energy loss of a proton through the FEC is:	0.109 MeV
Total energy loss (dT):	0.150 MeV

Therefore,

$$dP = (E/P)dT = 0.24 \text{ MeV/c}, \tag{B.4}$$

and corrected momenta for each of the ground state (P1), 4.44 MeV state (P2) and 9.64 MeV state (P3) are:

P1 = 767.32-0.24=767.08 MeV/c,
P2 = 760.35-0.24=760.11 MeV/c,
P3 = 752.13-0.24=751.89 MeV/c.

(2) A plot of P/B vs. RXF is shown in figure 3.18 given on page 62. The errors in the figure are given by:

d(P/B) ~ -0.00073 ×d(RXF), for RXF ~ 16,475, or
d(P/B)/(P/B) ~ (-9.0E-06) ×d(RXF), for RXF ~ 16,475 and P/B=80.357.

a. The statistical error in the peak position:
$dX \sim 0.425 \times FWHM/\sqrt{(PeakArea)}$. This translates into an error of:
d(P/B)/(P/B)~ 3.8E-06 for FWHM=100 and Peak Area=10000, and
d(P/B)/(P/B)~ 1.9E-06 for FWHM=100 and Peak Area=40000.

b. Uncertainty in the vertical beam position on target:
Assume uncertainty in vertical position is 1 mm. Displacement along RXF is R11×1.414=-0.377×1.414=-0.53 mm, and 0.53 mm corresponds to 10.7 50μ m units.
Hence d(P/B)/(P/B)$\sim$ (-9.0E-06) × 10.7 = 9.6E-05.

c. The statistical peak position uncertainty would thus appear to be negligible in comparison to peak position shifts caused by slight vertical movements of the beam. The fit to the curve in figure 3.18 is given by:

$$P/B = 92.711 - 7.79286E-04 \times RXF + 1.66195E-09 \times RXF^2. \quad \text{(B.5)}$$

This fit was obtained using the 67 data points mentioned above. The average fractional deviation, $d(P/B)/(P/B)$, of these points from this curve is only about 5.0E-05. On the other hand, for the other 82 data points this deviation is about 4.0E-04. It is possible that this difference is the result of an unstable beam, or minor adjustments to the beam tune.

(3) Comparisons:

a. Result of II.(3): P/B = 825.81/10.100 = 81.763. Equation (B.5), evaluated at RXF = 14543 gives P/B = 81.729. The ratio of these two P/B values is 1.00042. This excellent agreement suggests that the beam energy as given above (278.796 MeV) is very close to the correct value.

b. RUN 153 (from I. 1.):
Momentum, corrected for energy loss, for 311.9 MeV is 786.59 MeV/c, with B = 9.8401, RXF = 16738. Thus, P/B = 786.59/9.8401 = 79.937. Equation (B.5) evaluated at RXF = 16738 gives P/B = 80.133. The ratio of these two P/B values is 0.99755.
This result is not as good as the 1.00042 value in 'a.' and may suggest that the momentum sensitivity to angle of pp scattering and the uncertainty in the angle are responsible. However, a change in angle of $\sim 0.4^\circ$ is required to bring this into line. This seems to be too large for the angle uncertainty; no further insights into this situation have arisen.

c. Comparison with focal plane calibration in previous use:
The expression appearing in some earlier NOVA's is:

$$\begin{aligned} P &= (B/9.43794) \times (878.42 + RXF \times \\ &\quad (-0.00734191 + 1.48141E-08 \times RXF)) \quad \text{(B.6)} \\ \text{or, } P/B &= 93.073 - 0.000777914 \times RXF + \\ &\quad 1.56963E-09 \times RXF^2. \quad \text{(B.7)} \end{aligned}$$

Results from equations (B.5) and (B.7) are compared in table B.3.

RXF	EQN. (B.7) P/B	EQN. (B.5) P/B	RATIO
6000.0	88.462	88.095	1.00416
8000.0	86.950	86.583	1.00424
10000.0	85.451	85.084	1.00431
12000.0	83.964	83.599	1.00437
14000.0	82.490	82.127	1.00442
16000.0	81.028	80.668	1.00447
18000.0	79.579	79.222	1.00450
20000.0	78.143	77.790	1.00453
22000.0	76.719	76.371	1.00455
24000.0	75.307	74.965	1.00456
26000.0	73.908	73.573	1.00456

Table B.3: A comparison between old and new expressions for the P/B ratio is shown here.

The ratio in table B.3 indicates that, in addition to $\sim 0.4\%$ difference in normalization of these curves, there is also a difference in their slopes, amounting to a difference of the above ratio of 0.04% over the length of the focal plane.

(4) As a final renormalization to the exact value of the Pb(p,p)Pb result, we multiply equation (B.5) by the factor 1.00042 (from III.(3)a.), to give the final absolute calibration

$$P/B = 92.750 - 7.79613E-04 \times RXF + 1.66265E-09 \times RXF^2$$

$$\text{thus, } P/B = 80.357 \text{ at } RXF = 16475 \tag{B.8}$$

Appendix C

SASP Effective Pion Length

A Monte Carlo program written by W. R. Falk called USR0:[FALK.DASS.MC] PI_DECAY_MC.FOR (on the TRIUMF VMS system) calculates the effective pion length through the SASP. In summary, this program selects a distribution of randomly generated rays which fall within the following positional criteria: $\theta \in$ [-100,100]mrad, $\phi \in$ [-40,40]mrad, and $SDEL \in$ [-15%,20%]. The RAYTRACE [23] program then guides these rays through the spectrometer, and for a given θ, ϕ and δ, calculates the effective pion length from the target up to the point of intersection between the SASP focal plane and transport coordinate system. The program PI_DECAY_MC.FOR determines the pion path length from this point onwards through the top end of the spectrometer, taking pion decay into consideration.

The angles θ, ϕ and δ are calculated in transport units by the NOVA user routine USRE, which also calculates all but the R_{5j} terms in the transfer matrix. The R_{5j} terms are related to particle path length through the spectrometer and are thus calculated using PI_DECAY_MC.FOR.

The portion of the path length calculated by the RAYTRACE program is given by the following expression,

$$L = A + B\theta + C\theta^2 + D\phi^2, \tag{C.1}$$

where this length has the transport dimensions of centimeters. Table C.1 lists the coefficients corresponding to equation (C.1) for various values of *SDEL*. Plots of these coefficients versus *SDEL* values can be found in the file USR0:[FALK.DASS.MC] SASP_LENGTH.PCM. It is assumed that if the pion decays before reaching VDC2, the event will be lost, since the track reconstruction would not trace back to the target and survive the cuts imposed on it at that end of the spectrometer. This may not be completely adequate, since muons from the decay of the high energy pions may have a trajectory that deviates only slightly from that of the pion. The maximum opening angle of the decay is given by equation (C.2),

$$sin^{-1}(\beta_\mu/\beta_\pi) = sin^{-1}(0.2714 \times E_\pi/P_\pi). \tag{C.2}$$

SDEL	A	B	C	D
-15.0	685.84	0.40518	-1.35529E-05	5.12839E-04
-10.0	690.05	0.42909	-8.89453E-06	4.77461E-04
-5.0	694.80	0.44983	2.15284E-05	4.49100E-04
0.0	699.90	0.46895	6.90097E-05	4.24688E-04
5.0	705.21	0.48773	1.31917E-04	4.03965E-04
10.0	710.61	0.50734	2.11342E-04	3.87701E-04
15.0	716.06	0.52858	3.01880E-04	3.76690E-04
20.0	721.53	0.55121	3.78637E-04	3.68003E-04

Table C.1: This table lists the coefficients for path lengths at various SDEL values.

PARAMETER	DESCRIPTION
SL0=700.0	Central path length from target to transport origin, cm
SZV2=59.0	Distance along central ray from transport origin to VDC2, cm
SZSP=107.5	Distance along central ray from transport origin to paddles, cm
SZS1=252.9	Distance along central ray from transport origin to S1, cm
VDCL=91.2	Half-length of VDC2, cm
VDCW=17.5	Half-width of VDC2, cm
SCPL=113.3	Half-length of scintillator paddles, cm
SCPW=30.5	Half-width of scintillator paddles, cm
SC1L=106.7	Half-length of scintillator S1, cm
SC1W=30.5	Half-width of scintillator S1, cm

Table C.2: Geometrical parameters used in program PI_DECAY_MC.FOR are listed in this table.

This, for example, gives an opening angle of 27.8° for P_π=100 MeV/c and 16.7° for P_π=400 MeV/c. The factor of 0.2714 is required to translate between the pion and muon momentum, since the opening angle is proportional to the energy of the pion-to-muon decay.

Beyond VDC2, the pion (if it survives) or the muon (if the pion decays) trajectories are traced back to see if they intersect with the array of five scintillator paddles or with the final S1 paddle. In PI_DECAY_MC.FOR, muon decay is treated in detail, transforming the isotropic decay in the pion rest frame to the laboratory frame. Geometrical parameters used are given in table C.2.

Since the scintillator paddles and S1 are not symmetrically placed with respect to the central ray, shifts defining the end of these devices were specified. These shifts are shown in table C.3.

From the Monte Carlo survival probability for pions of a given $SDEL$ and a given SASP central momentum P_0, the effective length, EFF_L, is extracted from the expression

$$PROB = \exp\left((-139.57 \times EFF\_L)/(\tau\_c \times P)\right). \qquad \text{(C.3)}$$

SCINTILLATOR CENTER SHIFT FACTORS
SCPLO=-(SCPL-25.0)
SCPHI=SCPL+25.0
SC1LO=-(SC1L-17.68)
SC1HI=SC1L+17.68

Table C.3: Shifts used to align the centers of the scintillation detectors with the central particle trajectory are given here.

P_0	A	B	C	D	E	F
80	825.5	0.258	0.1071E+00	0.6222E-02	-0.1020E-02	0.2688E-04
120	797.4	0.883	0.9080E-01	0.5041E-02	-0.8801E-03	0.2273E-04
200	771.2	2.240	0.6038E-01	0.3379E-02	-0.6428E-03	0.1500E-04
300	762.4	3.156	0.5863E-01	0.2296E-02	-0.7087E-03	0.1831E-04
500	760.8	3.891	-0.5778E-02	0.1357E-02	-0.4491E-03	0.1127E-04

Table C.4: The parameters of the fifth order fit to the SASP effective pion length are listed above.

Here τ_c = 780.4 cm, and P is the pion momentum corresponding to the given $SDEL$.

Results of these calculations are shown in figure 3.15 on page 57 for central momenta of 80, 120, 200, 300 and 500 MeV/c. The rises and bumps in the p_o curves are due to a pion missing the S1 scintillator while the muon does not miss it. Each of these curves was fitted to a fifth order polynomial in $SDEL$ with the results shown by the solid lines in the figure and given in table C.4.

The six resulting coefficients were next fitted to cubic equation as a function of P_0, providing a general expression

$$EFF\_L = f(SDEL, P_0), \tag{C.4}$$

so that pion decay lengths for any given $SDEL$ and P_0 can be calculated. The coefficients of this "parameterization of parameters" are listed in table C.5. In the NOVA analysis for experiment E634, the above parameterization, together with the SASP and MRS focal plane acceptances (see §3.8.2 and §3.8.3, respectively), were provided by the NOVA user routine USRQ, listed in appendix F. The SASP pion efficiency is then given by

$$ACCEPTANCE_{SDEL} \times \exp((-139.57 \times EFF\_L)/(\tau_c \times P)). \tag{C.5}$$

Test output of the parameterization given in table C.5 is shown in table C.6 [17].

Parameter A	Parameter B
FIT: A = AA + AB $\times P_0$ + AC $\times P_0^2$ + AD $\times P_0^3$	FIT: B = BB + BB $\times P_0$ + BC $\times P_0^2$ + BD $\times P_0^3$
COEFFICIENTS: AA = 906.60	COEFFICIENTS: BA = -1.6247
AB = -1.3081	BB = 2.59342E-02
AC = 3.85717E-03	BC = -3.79387E-05
AD = -3.64865E-06	BD = 1.62509E-08
Parameter C	**Parameter D**
FIT: C = CA + CB $\times P_0$ + CC $\times P_0^2$ + CD $\times P_0^3$	FIT: D = DB + DB $\times P_0$ + DC $\times P_0^2$ + DD $\times P_0^3$
COEFFICIENTS: CA = 0.18867	COEFFICIENTS: DA = 9.48187E-03
CB = -1.32423E-03	DB = -4.89838E-05
CC = 4.58248E-06	DC = 1.10364E-07
CD = -5.42283E-09	DD = -8.97919E-11
Parameter E	**Parameter F**
FIT: E = EA + EB $\times P_0$ + EC $\times P_0^2$ + ED $\times P_0^3$	FIT: F = FB + FB $\times P_0$ + FC $\times P_0^2$ + FD $\times P_0^3$
COEFFICIENTS: EA = -1.75380E-03	COEFFICIENTS: FA = 5.12961E-05
EB = 1.20465E-05	FB = -4.01958E-07
EC = -4.27421E-08	FC = 1.45585E-09
ED = 4.77286E-11	FD = -1.62380E-12

Table C.5: The parameters of the third order fit to the coefficients of the fit for the SASP effective pion length are given in the above table.

	P_0, MeV								
SDEL	50	80	100	120	150	200	300	400	500
-20.0	543.0	560.0	567.0	571.0	573.0	566.0	535.0	519.0	562.0
-16.0	743.0	727.0	717.0	707.0	695.0	677.0	653.0	644.0	650.0
-12.0	827.0	799.0	782.0	768.0	751.0	729.0	710.0	706.0	699.0
-8.0	852.0	822.0	805.0	790.0	772.0	752.0	736.0	736.0	726.0
-4.0	853.0	825.0	809.0	796.0	780.0	762.0	751.0	753.0	745.0
0.0	850.0	825.0	811.0	799.0	785.0	770.0	763.0	767.0	761.0
4.0	851.0	828.0	815.0	804.0	792.0	780.0	776.0	783.0	776.0
8.0	855.0	833.0	822.0	812.0	801.0	791.0	791.0	798.0	791.0
12.0	860.0	839.0	828.0	819.0	810.0	801.0	803.0	811.0	802.0
16.0	862.0	843.0	832.0	824.0	815.0	808.0	811.0	819.0	809.0
20.0	864.0	845.0	835.0	826.0	818.0	810.0	813.0	821.0	811.0
24.0	878.0	854.0	842.0	831.0	820.0	811.0	815.0	824.0	810.0

Table C.6: This table lists test output of parameterization of coefficients given in table C.4.

Appendix D

The E634_ANAL.FOR Program

The program E634_ANAL.FOR, written by W. R. Falk (University of Manitoba), processes the E634 output and produces quantities such as cross section and analyzing powers, and is given below.

```
C Program E634_ANAL.FOR, for analyzing E634 output from NOVA
C W.R. FALK, July 12, 1995
C *** LINK E634_ANAL+USRQ
IMPLICIT REAL*8(A-H,O-Z)
REAL*4 EFFVECTOR,BMRS,RDEL,BSASP,SDEL
DIMENSION AA(80,64,12),BB(80,64,12),UF(82),WMASS(80,12),
1   SUMS(15,12),FFI(7),NCHXX(25),EFFVECTOR(4)
DIMENSION EXC(10),LX1(10),LX2(10),NDEL(10),NCH(10,6)
DIMENSION CTOT(10,6),CTOU(10,6),CTOD(10,6),CEFT(10,6),
1 CEFU(10,6),CEFD(10,6),EFFT(10,6),EFFU(10,6),EFFD(10,6),
2 CXTOT(10,64),DEL(10,6),PPpi(10,6),TTpi(10,6),
3 DELI(10,6),PPII(10,6),PPIAV(10,6),TTII(10,6),TTIAV(10,6),
4 PDAV(10,6),DELR(10,6),QEFF(10,6),RMRS(10,6)
C
C-------------------------------------------------------------------------
C
C INPUT: UNIT 2 - Input file E634_RUNS.
C UNIT 3 - Input file E634_SCAL.
C                  copied from PRV20:[BENJAMIN.NOVA]E634SUMM2.TXT
C UNIT 5 - Input file ANAL#., where # is run number
C
C INPUT UNITS for SWRITE files from NOVA
C HDRMDEL_N.SWR  FOR011
C HDRMDEL_NE.SWR FOR012
C HDRMDEL_U.SWR  FOR013
```

```
C HDRMDEL_UE.SWR FOR014
C HDRMDEL_D.SWR  FOR015
C HDRMDEL_DE.SWR FOR016
C
C HDRMDEL_NC.SWR  FOR017
C HDRMDEL_NEC.SWR FOR018
C HDRMDEL_UC.SWR  FOR019
C HDRMDEL_UEC.SWR FOR020
C HDRMDEL_DC.SWR  FOR021
C HDRMDEL_DEC.SWR FOR022
C
C OUTPUT: UNIT 6 - All input information and final results
C UNIT 7 - Summary of final results
C UNIT 8 - Spectra for PLOTDATA plots
C UNIT 9 - Raw Spectra AA(I,J,K) and EFFICIENCIES for diagnostics
C
C-------------------------------------------------------------------------
C
dWMRS=0.0025 ! MRS solid angle, sr
dWSASP=0.012 ! SASP solid angle, sr
C
FFI(1)=0.0004 ! For error multiplier for g.s., (0.02)**2
FFI(2)=0.0036 ! For error multiplier for 2.12, (0.06)**2
FFI(3)=0.0036 ! For error multiplier for 5.02, (0.06)**2
FFI(4)=0.0100 ! For error multiplier for cont., (0.10)**2
C
C-------------------------------------------------------------------------
C
IPRINT=0 ! For output control on UNIT 9
READ(5,*) IRUN,NCHX,NCHY,DELO,DDELY,NEXC,RANDOM
IF(IRUN.LT.0) THEN
IPRINT=1 ! Print diagnostic output AA(I,J,K)
IRUN=-IRUN
ENDIF
DO I=1,NEXC
READ(5,*) EXC(I),LX1(I),LX2(I),NDEL(I),(NCH(I,J),J=1,6)
ENDDO
C IRUN = Run number (search for this in next READ)
C NCHY, NCHX = Number of channels in the SDEL vs. DRMASS plot
```

```
C DEL0 = SDEL value at channel 0
C DDELY = SDEL interval/channel
C NEXC = Number of excitation energy intervals for discrete
C states and continuum
C RANDOM = Number of RANDOM events in HDRMDEL_R in channels
C 30 to 80, for those runs where NOVA had a slight error.
C EXC(I) = Excitation energy for interval I
C LX1(I), LX2(I) = PEAK integration limits for interval I
C NDEL(I) = Number of intervals in SDEL for interval I
C NCH(I,J) = Starting channel of J'th SDEL interval (add 1 extra!)
C
WRITE(6,605) IRUN,NCHX,NCHY,DEL0,DDELY,NEXC,RANDOM,IRUN
605 FORMAT(' IRUN  NCHX  NCHY   DEL0   DDELY   NEXC  RANDOM '/
1 I4,2I6,F8.1,F8.3,I6,F8.0,70X,I4/)
WRITE(6,607)
607 FORMAT('      I    EXC    LX1  LX2   NDEL   '
1 '   (NCH(I,J),J=1,6)')
DO I=1,NEXC
WRITE(6,609) I,EXC(I),LX1(I),LX2(I),NDEL(I),(NCH(I,J),J=1,6)
ENDDO
609 FORMAT(1H ,I6,F8.2,I6,I5,I6,I6,5I4)
C
C--------------------------------------------------------------------------
C
C Next input file is always the same, namely E634_RUNS.
10 READ(2,*) NRUN,NTGT,TB,MIN,NBOX,THSASP,BSASP,THMRS,BMRS,
1 ASYMM_UP,ASYMM_DN
IF(NRUN.LT.IRUN) GO TO 10
IF(NRUN.NE.IRUN) GO TO 99
RAD=180.0/3.141593
STHM=DSIN(THMRS/RAD)
CTHM=DCOS(THMRS/RAD)
STHS=DSIN(THSASP/RAD)
CTHS=DCOS(THSASP/RAD)
Wpi=139.57
Wp=938.28
Wd=1875.629
C Select appropriate particle masses target particle densities:
GO TO (14,16,18),NTGT ! NTGT=1,2,3 respect. for 2H, 12C and 16O
```

```
14 Wt=1875.629 ! Target, 2H
Wr=939.57 ! Recoil, n
   TARG_N=(0.050/(2.0*2.0))*(6.023D+23)*2.0 ! 2H
GO TO 20
16 Wt=11174.958 ! Target, 12C
Wr=10252.635 ! Recoil, 11B
   TARG_N=(0.052/12.0)*(6.023D+23) ! 12C
GO TO 20
18 Wt=14895.207 ! Target, 16C
Wr=13969.055 ! Recoil, 15N
   TARG_N=(0.035/16.0)*(6.023D+23) ! 16O ??
20  CONTINUE
C
WRITE(6,622) NRUN,NTGT,TB,MIN,NBOX,THSASP,BSASP,THMRS,BMRS,Wt,Wr,
1 ASYMM_UP,ASYMM_DN,TARG_N
622 FORMAT('ONRUN  NTGT   TB   MIN  NBOX  THSASP  BSASP  THMRS ',
1'  BMRS      Wt          Wr     ASYMM_UP  ASYMM_DN    TARG_N'/
2 2I5,F7.1,2I5,F9.2,F7.3,F7.2,F7.3,2F11.3,2F10.4,D12.4 /)
C
C--------------------------------------------------------------------------
C Scaler information, wire chamber efficiencies
C Next input file is always the same, namely E634_SCAL.
25 READ(3,*) MRUN,POLLTU,POLRTU,POLLAU,POLRAU,SEMU,T6OU,
1 POLLTD,POLRTD,POLLAD,POLRAD,SEMD,T6OD,BUSY,EVENT,RMWOK,SMWOK
IF(MRUN.LT.IRUN) GO TO 25
IF(MRUN.NE.IRUN) GO TO 99
C
COMP_LIVE=BUSY/EVENT
WRITE(6,626) MRUN,POLLTU,POLRTU,POLLAU,POLRAU,SEMU,T6OU,
1               POLLTD,POLRTD,POLLAD,POLRAD,SEMD,T6OD,
2               BUSY,EVENT,COMP_LIVE,RMWOK,SMWOK
626 FORMAT('  RUN    L_TOT      R_TOT      L_ACC      R_ACC      ',
1 '  SEM       60_Hz'/' ',I4,6F11.0/'     ',6F11.0/
2 ' BUSY  EVENTS  COMP_LIVE  MMWOK  LMWOK : ',
3 2F12.0,F7.3,1X,2F6.1/)
C
C Polarization and beam normalization
IF(TB.EQ.371.2) THEN
ANCH2=0.4236 ! CH2 analyzing power
```

```
POLN=78.15 ! Counts/nC
SEM=7.654 ! Counts/nC
ENDIF
IF(TB.EQ.500.7) THEN
ANCH2=0.4659 ! CH2 analyzing power
POLN=95.41 ! Counts/nC
SEM=6.639 ! Counts/nC
ENDIF
POLSEM=POLN/SEM
C
PUP=ASYMM_UP/ANCH2 ! UP
PDN=-ASYMM_DN/ANCH2 ! DOWN polarization
C
POLU=(POLLTU+POLRTU-POLLAU-POLRAU)
POLD=(POLLTD+POLRTD-POLLAD-POLRAD)
POL_RAT=POLU/POLD
POL_SEM=((POLU+POLD)/(SEMU+SEMD))/POLSEM
SEM_RAT=SEMU/SEMD
PROT_UP=(SEMU/SEM)/(1.602D-10)
PROT_DN=(SEMD/SEM)/(1.602D-10)
C
WRITE(6,627) PUP,PDN,POL_SEM,POL_RAT,SEM_RAT,PROT_UP,PROT_DN
627 FORMAT('    PUP     PDN   POL_SEM   POL_RAT    SEM_RAT  ',
1 '  PROT_UP     PROT_DN '/2F8.4,F9.4,F10.4,F11.4,2D12.4/)
C
C-------------------------------------------------------------------------
C
C READ 12 64x80 spectra containing the results of the NOVA analysis.
C Adapted from the program SPEC_READ.FOR for reading 2D spectra created
C by the NOVA SWRITE command. W.R. Falk, June 2, 1995
C
NX=80
NY=64
M=NX+NY+4
C
DO K=1,12 ! K-loop
KK=K+10
C
C Read 2D spectrum
```

```
DO I=1,3 !Dummy READS
READ(KK,*) IJUNK
ENDDO
C
DO I=1,M !Dummy READS
READ(KK,*) QJUNK
ENDDO
C
II=NX+2
READ(KK,*) (UF(I),I=1,II) ! Underflow ROW - ignore
C
DO J=1,NY
READ(KK,*) AL,(AA(I,J,K),I=1,NX),AH
ENDDO
C
C Generate a 1D spectra of missing mass and form various sums
SUMT=0.0 ! Total
IT=0
SUMR=0.0 ! For RANDOM's correction
IR=0
SUMN=0.0 ! Negatives
IN=0
SUMP=0.0 ! Positives
IP=0
DO I=1,NX
SUM=0.0
DO J=1,NY
AIJ=AA(I,J,K)
SUM=SUM+AIJ
IT=IT+1
SUMT=SUMT+AIJ
IF(I.GE.30.AND.I.LE.80) THEN
IR=IR+1
SUMR=SUMR+AIJ
ENDIF
IF(AIJ.GT.0.0) THEN
IP=IP+1
SUMP=SUMP+AIJ
ENDIF
```

```
IF(AIJ.LT.0.0) THEN
IN=IN+1
SUMN=SUMN+AIJ
ENDIF
ENDDO
WMASS(I,K)=SUM
ENDDO
SUMS(1,K)=SUMT
SUMS(2,K)=IT
SUMS(3,K)=SUMN
SUMS(4,K)=IN
SUMS(5,K)=SUMP
SUMS(6,K)=IP
SUMS(7,K)=SUMR
SUMS(8,K)=IR
ENDDO ! K-loop
C
X=-8.125
DO I=1,NX
X=X+0.25
WRITE(8,802) I,X,(WMASS(I,K),K=1,6)
802 FORMAT(1H ,I5,F8.2,3X,6F8.1)
ENDDO
C
X=-20.50
DO I=1,NX
X=X+1.0
WRITE(8,802) I,X,(WMASS(I,K),K=7,12)
ENDDO
C
IF(IPRINT.EQ.1) THEN ! Diagnostic output
NCHXX(1)=5
DO I=2,25
NCHXX(I)=NCHXX(I-1)+3
ENDDO
KLOW=-5
DO N=1,2
KLOW=KLOW+6 ! 1,7
KHI=KLOW+1 ! 2,8
```

```
DO L=1,2
IF(L.EQ.1) WRITE(9,920) KLOW,IRUN
IF(L.EQ.2) WRITE(9,922) KHI,IRUN
WRITE(9,901) (NCHXX(I),I=1,25)
M=0
DO JJ=1,64
M=M+1
IF(M.EQ.8) THEN
WRITE(9,903)
M=0
ENDIF
J=65-JJ
IF(L.EQ.1) WRITE(9,910) J,(AA(I,J,KLOW),I=5,77,3)
IF(L.EQ.2) THEN
DO I=5,77,3
AIJ1=AA(I,J,KLOW)
AIJ2=AA(I,J,KHI)
BIJ=0.0
IF(AIJ1.NE.0.0) BIJ=AIJ2/AIJ1
BB(I,J,KHI)=BIJ
ENDDO
WRITE(9,912) J,(BB(I,J,KHI),I=5,77,3)
ENDIF
ENDDO
WRITE(9,914)
ENDDO
ENDDO
ENDIF
901 FORMAT('    J\I',I3,24I5/)
903 FORMAT(1H )
910 FORMAT(1H ,I4,25F5.1)
912 FORMAT(1H ,I4,25F5.2)
914 FORMAT(1H1)
920 FORMAT('     SPECTRUM',I3,' , TOTAL COUNTS         RUN',I3/)
922 FORMAT('     SPECTRUM',I3,' , EFFICIENCIES         RUN',I3/)
C
DO K=1,5,2
SUMS(9,K)=SUMS(1,K+1)/SUMS(1,K)    ! Raw efficiency, old
SUMS(9,K+1)=SUMS(9,K)
```

```
SUMS(10,K)=SUMS(9,K)
SUMS(10,K+1)=SUMS(10,K)
IF(RANDOM.NE.0.0) THEN
Y=SUMS(9,K)*SUMS(3,K)
Z=SUMS(1,K+1)+Y
SUMS(10,K)=Z/SUMS(1,K)    ! Corrected efficiency, old
SUMS(10,K+1)=SUMS(10,K)
ENDIF
SUMS(11,K)=SUMS(10,K)/SUMS(9,K)    ! Eff. correction factor
SUMS(11,K+1)=SUMS(11,K)
SUMS(12,K)=0.0
SUMS(12,K+1)=0.0
ENDDO
EFF_CFT=SUMS(11,1) ! Efficiency correction factor, ALL
EFF_CFU=SUMS(11,3) ! Efficiency correction factor, UP
EFF_CFD=SUMS(11,5) ! Efficiency correction factor, DOWN
CON_CF=(SUMS(7,K)-RANDOM)/SUMS(7,K) ! Cont. correct. factor
DO K=7,11,2
SUMS(9,K)=SUMS(1,K+1)/SUMS(1,K)    ! Raw efficiency, old
SUMS(9,K+1)=SUMS(9,K)
SUMS(10,K)=0.0
SUMS(10,K+1)=0.0
SUMS(11,K)=0.0
SUMS(11,K+1)=0.0
SUMS(12,K)=CON_CF ! Continuum correction factor
SUMS(12,K+1)=CON_CF
ENDDO
C
C Re-consideration of the efficiency calculation (June 13, 1995).
C Previously summed the quantities in the eff. plots. We should have
C used the reciprocals - ie. the yield per pixel
DO K=1,11,2
SUM=0.0
DO I=1,NX
DO J=1,NY
BB(I,J,K)=0.0
AIJ=AA(I,J,K)
CIJ=AA(I,J,K+1)
IF(CIJ.NE.0.0) THEN
```

```
BIJ=AIJ**2/CIJ ! Norm. yield for pixel
BB(I,J,K)=BIJ
SUM=SUM+BIJ
ENDIF
ENDDO
ENDDO
SUMS(13,K)=0.0
SUMS(13,K+1)=SUM
SUMS(14,K)=SUMS(1,K)/SUM
SUMS(14,K+1)=SUMS(14,K)
ENDDO
C
WRITE(6,640)
640 FORMAT('    K     SUMT     IT     SUMN     IN     SUMP     IP ',
1 '    SUMR     IR      EFFO    EFFC   E_C_F   R_C_F ',
2 '    YIELD   EFF_N '/)
DO K=1,12
WRITE(6,642) K,(SUMS(I,K),I=1,14)
642 FORMAT(1H ,I4,2X,8F8.1,4F8.3,F10.1,F8.3)
ENDDO
WRITE(6,644) EFF_CFT,EFF_CFU,EFF_CFD,CON_CF
644 FORMAT('0 EFF_CFT, EFF_CFU, EFF_CFD, CON_CF : ',4F9.4)
C
C--------------------------------------------------------------------------
C
C Form the sums for all the intervals involving the states in 11B :
C 0.00, 2.12 and 5.02 MeV.
C
IXU=3
IF(NEXC.LE.3) IXU=NEXC
DO IX=1,IXU
LXLOW=LX1(IX)
LXHI=LX2(IX)
DO J=1,NY
XSUM=0.0
                DO I=LXLOW,LXHI
XSUM=XSUM+AA(I,J,1)
ENDDO
CXTOT(IX,J)=XSUM
```

```
ENDDO
NDELTA=NDEL(IX)
DO JY=1,NDELTA
         CTOT(IX,JY)=0.0 ! Counts TOTAL
                CTOU(IX,JY)=0.0 ! Counts UP
                CTOD(IX,JY)=0.0 ! Counts DOWN
                CEFT(IX,JY)=0.0 ! Counts TOTAL reciprical efficiency
                CEFU(IX,JY)=0.0 ! Counts UP reciprical efficiency
                CEFD(IX,JY)=0.0 ! Counts DOWN reciprical efficiency
EFFT(IX,JY)=0.0
EFFU(IX,JY)=0.0
EFFD(IX,JY)=0.0
                DO I=LXLOW,LXHI
                JLOW=NCH(IX,JY)
                 JHI=NCH(IX,JY+1)-1
                DO J=JLOW,JHI
CTOT(IX,JY)=CTOT(IX,JY)+AA(I,J,1)
CEFT(IX,JY)=CEFT(IX,JY)+BB(I,J,1)
CTOU(IX,JY)=CTOU(IX,JY)+AA(I,J,3)
CEFU(IX,JY)=CEFU(IX,JY)+BB(I,J,3)
CTOD(IX,JY)=CTOD(IX,JY)+AA(I,J,5)
CEFD(IX,JY)=CEFD(IX,JY)+BB(I,J,5)
                        ENDDO
ENDDO
CEFT(IX,JY)=CEFT(IX,JY)/EFF_CFT  ! Correct TOTAL recip. effic.
CEFU(IX,JY)=CEFU(IX,JY)/EFF_CFU  ! Correct UP recip. effic.
CEFD(IX,JY)=CEFD(IX,JY)/EFF_CFD  ! Correct DOWN recip. effic.
IF(CEFT(IX,JY).EQ.0.0) GO TO 41
EFFT(IX,JY)=CTOT(IX,JY)/CEFT(IX,JY)  ! Efficiencies
41 IF(CEFU(IX,JY).EQ.0.0) GO TO 42
EFFU(IX,JY)=CTOU(IX,JY)/CEFU(IX,JY) ! Efficiencies
42 IF(CEFD(IX,JY).EQ.0.0) GO TO 43
EFFD(IX,JY)=CTOD(IX,JY)/CEFD(IX,JY) ! Efficiencies
43 CONTINUE
        ENDDO
        ENDDO
C
C       Form the sums for all the intervals involving the continuum in 11B :
C
```

```
IF(NEXC.LT.4) GO TO 53
DO IX=4,NEXC
        LXLOW=LX1(IX)
        LXHI=LX2(IX)
DO J=1,NY
XSUM=0.0
                DO I=LXLOW,LXHI
XSUM=XSUM+AA(I,J,7)
ENDDO
CXTOT(IX,J)=XSUM
ENDDO
        NDELTA=NDEL(IX)
        DO JY=1,NDELTA
                CTOT(IX,JY)=0.0  ! Counts TOTAL
                CTOU(IX,JY)=0.0  ! Counts UP
                CTOD(IX,JY)=0.0  ! Counts DOWN
                CEFT(IX,JY)=0.0  ! Counts TOTAL reciprical efficiency
                CEFU(IX,JY)=0.0  ! Counts UP reciprical efficiency
                CEFD(IX,JY)=0.0  ! Counts DOWN reciprical efficiency
EFFT(IX,JY)=0.0
EFFU(IX,JY)=0.0
EFFD(IX,JY)=0.0
                DO I=LXLOW,LXHI
                JLOW=NCH(IX,JY)
                 JHI=NCH(IX,JY+1)-1
                 DO J=JLOW,JHI
                                CTOT(IX,JY)=CTOT(IX,JY)+AA(I,J,7)
                                CEFT(IX,JY)=CEFT(IX,JY)+BB(I,J,7)
                                CTOU(IX,JY)=CTOU(IX,JY)+AA(I,J,9)
                                CEFU(IX,JY)=CEFU(IX,JY)+BB(I,J,9)
                                CTOD(IX,JY)=CTOD(IX,JY)+AA(I,J,11)
                                CEFD(IX,JY)=CEFD(IX,JY)+BB(I,J,11)
                        ENDDO
                ENDDO
IF(CEFT(IX,JY).EQ.0.0) GO TO 46
EFFT(IX,JY)=CTOT(IX,JY)/CEFT(IX,JY) ! Efficiencies
46 IF(CEFU(IX,JY).EQ.0.0) GO TO 47
EFFU(IX,JY)=CTOU(IX,JY)/CEFU(IX,JY) ! Efficiencies
47 IF(CEFD(IX,JY).EQ.0.0) GO TO 48
```

```
EFFD(IX,JY)=CTOD(IX,JY)/CEFD(IX,JY) ! Efficiencies
48 CONTINUE
                CTOT(IX,JY)=CTOT(IX,JY)*CON_CF   ! Corrected TOTAL counts
                CTOU(IX,JY)=CTOU(IX,JY)*CON_CF   ! Corrected UP counts
                CTOD(IX,JY)=CTOD(IX,JY)*CON_CF   ! Corrected DOWN counts
        ENDDO
        ENDDO
C
53 CONTINUE
Y=-16.28125
DO J=1,NY
Y=Y+0.5625
WRITE(8,805) J,Y,(CXTOT(IX,J),IX=1,NEXC)
805 FORMAT(1H ,I5,F8.2,3X,8F8.1)
ENDDO
C
C-------------------------------------------------------------------------------
C
C Spectrometer momentum intervals boundaries
PSC=50.311*BSASP ! SASP central momentum
DO I=1,NEXC
N=NDEL(I)+1
  DO J=1,N
K=NCH(I,J)-1
FK=K
SDEL=DEL0+FK*DDELY ! SDEL for lower boundary of interval
PS=PSC*(1.0+SDEL/100.0)
Ppi=PS
Epi=DSQRT(Ppi**2+Wpi**2)
DEL(I,J)=SDEL
PPpi(I,J)=Ppi
TTpi(I,J)=Epi-Wpi
ENDDO
ENDDO
C
C Spectrometer SDEL, momentum and energy intervals, and averages
DO I=1,NEXC
N=NDEL(I)
  DO J=1,N
```

```
DELI(I,J)=DEL(I,J+1)-DEL(I,J) ! Delta SDEL
PPII(I,J)=PPpi(I,J+1)-PPpi(I,J) ! Delta Ppi
PPIAV(I,J)=(PPpi(I,J+1)+PPpi(I,J))/2.0
TTII(I,J)=TTpi(I,J+1)-TTpi(I,J) ! Delta Tpi
TTIAV(I,J)=(TTpi(I,J+1)+TTpi(I,J))/2.0
ENDDO
ENDDO
C
C Calculation of deuteron momentum at center of interval and combined
C efficiencies from USRQ subroutine. This serves as a check, only!
E1=Wp+TB ! Incident proton energy
P1=DSQRT(E1**2-Wp**2)
PMC=80.357*BMRS
DO I=1,NEXC
W5=Wr+EXC(I)
N=NDEL(I)
  DO J=1,N
P4=PPIAV(I,J) ! Pion momentum
SDEL=(P4-PSC)*100.0/PSC
E4=DSQRT(Wpi**2+P4**2)
E=E1+Wt-E4
Px=P1-P4*CTHS
Py=P4*STHS
A=(E*E-Px**2-Py**2+Wd**2-W5**2)/2.0
B=Px*CTHM+Py*STHM
AAA=E*E-B*B
BBB=-2.0*E*A
CCC=A*A+(Wd*B)**2
Ed=(-BBB+DSQRT(BBB**2-4.0*AAA*CCC))/(2.0*AAA)
Pd=DSQRT(Ed**2-Wd**2)
PDAV(I,J)=Pd
RDEL=(Pd-PMC)*100.0/PMC
DELR(I,J)=RDEL
C Next three lines for Corrections for MRS acceptance
RRMRS=0.989+0.0171*RDEL
IF(RDEL.LT.-0.9) RRMRS=1.112+0.1494*RDEL
IF(RDEL.GT.7.6) RRMRS=6.395-6.917*RDEL
RMRS(I,J)=RRMRS
CALL USRQ(EFFVECTOR,BMRS,RDEL,BSASP,SDEL)
```

```
QEFF(I,J)=EFFVECTOR(4)
C WRITE(6,647) P4,Pd,SDEL,RDEL,(EFFVECTOR(ML),ML=1,4)
C 647 FORMAT(1H ,2F9.2,2F8.2,4F8.3)
ENDDO
ENDDO
C
WRITE(6,650)
650  FORMAT('0TOTAL COUNTS AND EFFICIENCIES FOR THE INTERVALS ',
1 'AND DETAILS ON THE MOMENTUM/ENERGY INTERVALS FOR THE PION '/
2 ' I J   TOTAL  EFF_T  EFFT    UP   EFF_U  EFFU '
3 '  DOWN  EFF_D  EFFD   NCH   EXC  SDEL_LO SDEL_HI ',
4 ' Ppi_IN Ppi_A Pd_A   RDEL  USRQ  RMRS')
C
DO I=1,NEXC
WRITE(6,652)
652 FORMAT(1H )
JDEL=NDEL(I)
DO J=1,JDEL
NCHLO=NCH(I,J)
NCHHI=NCH(I,J+1)-1
WRITE(6,655) I,J,CTOT(I,J),CEFT(I,J),EFFT(I,J),CTOU(I,J),
1 CEFU(I,J),EFFU(I,J),CTOD(I,J),CEFD(I,J),EFFD(I,J),
2 NCHLO,NCHHI,EXC(I),DEL(I,J),DEL(I,J+1),PPII(I,J),
3 PPIAV(I,J),PDAV(I,J),DELR(I,J),QEFF(I,J),RMRS(I,J)
ENDDO
ENDDO
655 FORMAT(1H ,I1,I2,F8.1,F7.1,F6.3,2F7.1,F6.3,2F7.1,F6.3,
1 I4,I3,F6.2,2F8.3,F8.2,F6.1,F6.0,F6.2,2F6.3)

C
C--------------------------------------------------------------------------
C
WRITE(6,670)
670 FORMAT('0 CROSS SECTIONS AND ANALYZING POWERS '/
1'    I    EXC    J   Ppi_AV     SIGO    dSIGO     SIGA ',
2 '   dSIGA     SIGU    dSIGU     SIGD    dSIGd   ',
3 '    Ano     dAno ')
C
C Cross section factor
```

```
DENOM=dWMRS*dWSASP*TARG_N*COMP_LIVE*(RMWOK/100.0)*(SMWOK/100.0)
C Calculate cross sections and analyzing powers
DO I=1,NEXC
FI=FFI(I) ! For error correction factor
WRITE(7,750) IRUN,EXC(I),NDEL(I)
750 FORMAT(' RUN, EXC, NDEL :',I4,F8.2,I5)
WRITE(6,652)
NDELJ=NDEL(I)
DO J=1,NDELJ
QQQ=DABS(PPII(I,J))*(1.0D-30)
FNCO=CTOT(I,J)
SIGO=0.0
dSIGO=0.0
   AO=DENOM*(PROT_UP+PROT_DN)*EFFT(I,J)*RMRS(I,J)*QQQ
IF(AO.EQ.0.0) GO TO 72
SIGO=FNCO/AO
dSIGO=DSQRT(FNCO)/AO
dSIGO=dSIGO*DSQRT(1.0+FI*FNCO)
72 FNCU=CTOU(I,J)
SIGU=0.0
dSIGU=0.0
   AU=DENOM*PROT_UP*EFFU(I,J)*RMRS(I,J)*QQQ
IF(AU.EQ.0.0) GO TO 74
SIGU=FNCU/AU
dSIGU=DSQRT(FNCU)/AU
dSIGU=dSIGU*DSQRT(1.0+FI*FNCU)
74 FNCD=CTOD(I,J)
SIGD=0.0
dSIGD=0.0
   AD=DENOM*PROT_DN*EFFD(I,J)*RMRS(I,J)*QQQ
IF(AD.EQ.0.0) GO TO 76
SIGD=FNCD/AD
dSIGD=DSQRT(FNCD)/AD
dSIGD=dSIGD*DSQRT(1.0+FI*FNCD)
76 SIGA=(PDN*SIGU+PUP*SIGD)/(PUP+PDN)
dSIGA=DSQRT((PDN*dSIGU)**2+(PUP*dSIGD)**2)/(PUP+PDN)
ANO=0.0
dANO=0.0
IF(SIGU.EQ.0.0.AND.SIGD.EQ.0.0) GO TO 78
```

```
ANO=-(SIGU-SIGD)/(PDN*SIGU+PUP*SIGD)
dANO=(PUP+PDN)*DSQRT((SIGD*dSIGU)**2+(SIGU*dSIGD)**2)/
1 (PDN*SIGU+PUP*SIGD)**2
78 CONTINUE
WRITE(6,680) I,EXC(I),J,PPIAV(I,J),SIGO,dSIGO,SIGA,dSIGA,
1 SIGU,dSIGU,SIGD,dSIGD,ANO,dANO
680 FORMAT(1H ,I4,F8.2,I4,F9.2,F10.3,F8.3,F10.3,F8.3,F10.3,F8.3,
1 F10.3,F8.3,F11.3,F8.3)
WRITE(7,680) I,EXC(I),J,PPIAV(I,J),SIGO,dSIGO,SIGA,dSIGA,
1 SIGU,dSIGU,SIGD,dSIGD,ANO,dANO
ENDDO
ENDDO
C
99 CONTINUE
END
```

Appendix E

DASS.TWO program

What follows is the TWOTRAN program, DASSB5.TWO, used for the data acquisition for experiment E634.

```
PROGRAM DASSB5
!
! Increase Max Event Size for RLAM, RSCAL  dah 21/8/94
! Re-arrange Scalers to be SASP-32, MRS-32, IBP-3x12  dah 20/8/94
! Addition of SASP,MRS angle readout in BEGINRUN.  Decoded values
!   stored after scaler data, and in SASPAngle, MRSAngle
! dah 3/3/94
! Program SASPB5 with addition of data from MRS, as in MRSB7.
! RSTART changed to explicitly disable LAMs from MRS ADC/TDCs
! dah 9 Jan 94
!   Setup for LAM to come from SASP when SASP-MRS coincidence.
! dah 19 Dec 93
!
! Changed from B=7 to B=5, to accomodate MRS in B=7  dah 14 Dec 93
! Have disabled RFE.  This clobbers the delay settings needed to
!  produce the pulse width defined by TRMIN and TRMAX.  WHY was it
! in here in the first place???            dah 26/11/93
!
! First try at TWOTRAN to run SASP (all by itself)!
! Adapted from MRS_NP.TWO, but with Lots of Changes
!
! I am assuming (for any of you who are paddling around in here) that
! the branch number is 7, Crate 7 is the main SASP crate (with all the
! ADC's / TDC's in it) and Crate 5 is the MRS crate (run with the
! "other" Crate controller - as we did in CSB), which contains
! (mostly) the Polarimeter scalers
```

```
!
! If not, it would be really nice to be able to just change the
! following lines
!
! PARAMETER BRANCH = 7
! PARAMETER CRMAIN = 7
! PARAMETER CRMRS = 5
!
! (but unfortunately, TWOTRAN doesn't recognize anything as useful
! as the PARAMETER statement)
!
! I am also assumng no LAM grader is present (just the plug on the
! back of the Crate controller), so all the old messing around with
! bits in the Jorway Model 75 is taken out
!
! As with standard MRS stuff, event type 1 is the Scaler event
! Event type 2 is the main data event
!
!************************************************************
ON(%BEGINRUN,%TYPE=1,%MAXSIZE=450) CALL RSTART
ON(%PAUSE,%TYPE=1,%MAXSIZE=450) CALL RPAUSE
ON(%CONTINUE,%TYPE=1,%MAXSIZE=450) CALL RCONTIN
ON(%B=5,%GLAM=12,%TYPE=2,%MAXSIZE=700) CALL RLAM
ON(%B=5,%GLAM=20,%TYPE=3,%MAXSIZE=350) CALL STUPID
!ON(%B=5,%GLAM=22,%TYPE=3,%MAXSIZE=350) CALL STUPID
ON(%B=5,%GLAM=9,%TYPE=4,%MAXSIZE=350) CALL STUPID
ON(%B=5,%GLAM=4,%TYPE=4,%MAXSIZE=350) CALL STUPID
ON(%PERIOD=50,%TYPE=1,%MAXSIZE=450) CALL RSCAL
!   ON(%PERIOD=300,%TYPE=1,%MAXSIZE=250) CALL RFE
ON(%ENDRUN, %TYPE=1,%MAXSIZE=400) CALL REND
END
!************************************************************
SUBROUTINE RSTART
INTEGER*4 MASK /16384/
INTEGER*4 L1 /1/
INTEGER*4 L2 /2/
INTEGER*4 L4 /4/
INTEGER*4 L60 /48/
INTEGER*4 L14 /12/
```

```
INTEGER*4 L200 /128/
INTEGER*4 L40000 /16384/
INTEGER*4 L42000 /17408/
Integer*4 LF00000/15728640/
Integer*4 InAngle,Outangle,SASPAngle,MRSAngle
LOGICAL SCALF
Common/angs/InAngle,Outangle
COMMON/CEV12/SCALF
! Generate inhibit on output register
CFSA (%B=7,%C=3,%N=21,%A=0,%F=20,%DATA=L14)
CFSA (%B=5,%C=4,%N=19,%A=0,%F=20,%DATA=L1)
! Raise Inhibit (just for safety)
CSSA (%B=7,%C=1,%N=30,%A=9,%F=26)              ! inhibit crate 1
CSSA (%B=7,%C=3,%N=30,%A=9,%F=26)              ! inhibit crate 3
CSSA (%B=5,%C=7,%N=30,%A=9,%F=26)              ! inhibit crate 7
CSSA (%B=5,%C=4,%N=30,%A=9,%F=26)              ! inhibit crate 4
CSSA (%B=5,%C=2,%N=30,%A=9,%F=26)              ! inhibit crate 5
! create clear in crates 2 and 7 to clear scalers
! We do this 5 times because we have observed ~30% failure rate
! to clear IBP scalers in crate 2
CSSA(%B=5,%C=7,%N=28,%A=9,%F=26)
CSSA(%B=5,%C=2,%N=28,%A=9,%F=26)
CSSA(%B=5,%C=7,%N=28,%A=9,%F=26)
CSSA(%B=5,%C=2,%N=28,%A=9,%F=26)
CSSA(%B=5,%C=7,%N=28,%A=9,%F=26)
CSSA(%B=5,%C=2,%N=28,%A=9,%F=26)
CSSA(%B=5,%C=7,%N=28,%A=9,%F=26)
CSSA(%B=5,%C=2,%N=28,%A=9,%F=26)
CSSA(%B=5,%C=7,%N=28,%A=9,%F=26)
CSSA(%B=5,%C=2,%N=28,%A=9,%F=26)
! Read the angle encoders
CFSA(%B=5,%C=4,%N=16,%A=0,%F=0,%DATA=InAngle)
CALL ANGLE_DECODE
SASPAngle = OutAngle
CFSA(%B=7,%C=1,%N=8,%A=0,%F=0,%DATA=InAngle)
InAngle = InAngle + LF00000 ! 'cause MRS gives but 5 digits, SASP 6
CALL ANGLE_DECODE
MRSAngle = OutAngle
! Disable TDC LAM
```

```
CSSA (%B=5,%C=7,%N=12,%A=0,%F=24)
! Enable Demands in Crate 7
CSSA (%B=5,%C=7,%N=30,%A=10,%F=26)
! Initialize TDC, ADC; enable TDC LAM
CSSA (%B=5,%C=7,%N=9,%A=0,%F=9)                ! clear TDC's
CSSA (%B=5,%C=7,%N=3,%A=0,%F=9)
CSSA (%B=5,%C=7,%N=2,%A=0,%F=9)                ! clear ADC's
CSSA (%B=5,%C=7,%N=3,%A=0,%F=9)
CSSA (%B=7,%C=3,%N=15,%A=0,%F=24)                !disable MRS LAMs
CSSA (%B=7,%C=3,%N=16,%A=0,%F=24)
 CSSA(%B=7,%C=3,%N=17,%A=0,%F=24)
 CSSA(%B=7,%C=3,%N=19,%A=0,%F=24)
CSSA (%B=7,%C=3,%N=15,%A=0,%F=9)                ! clear TDC's
CSSA (%B=7,%C=3,%N=16,%A=0,%F=9)
 CSSA(%B=7,%C=3,%N=17,%A=0,%F=9)
 CSSA(%B=7,%C=3,%N=19,%A=0,%F=9)
CSSA (%B=5,%C=7,%N=2,%A=0,%F=9)                ! clear ADC's
CSSA (%B=5,%C=7,%N=3,%A=0,%F=9)
! Initialize and set up LeCroy 4290 system
CSSA (%B=5,%C=4,%N=20,%A=0,%F=9)
CFSA (%B=5,%C=4,%N=20,%A=0,%F=16,%DATA=L40000)
CFSA (%B=5,%C=4,%N=20,%A=0,%F=16,%DATA=L42000)
CFSA (%B=5,%C=4,%N=19,%A=0,%F=20,%DATA=L4)
CSSA (%B=7,%C=3,%N=22,%A=0,%F=9)
CFSA (%B=7,%C=3,%N=22,%A=0,%F=16,%DATA=L40000)
CFSA (%B=7,%C=3,%N=22,%A=0,%F=16,%DATA=L42000)
CFSA (%B=7,%C=3,%N=21,%A=0,%F=20,%DATA=L200)
! Enable LAM
CSSA (%B=5,%C=7,%N=12,%A=0,%F=26)
! Send clear pulse on output register on B=5
CFSA (%B=5,%C=4,%N=19,%A=0,%F=20,%DATA=L2)
CFSA (%B=5,%C=4,%N=19,%A=0,%F=22,%DATA=L2)
! and on B=7
CFSA (%B=7,%C=3,%N=21,%A=0,%F=20,%DATA=L60)
CFSA (%B=7,%C=3,%N=21,%A=0,%F=22,%DATA=L60)
! Drop Inhibit
CSSA (%B=5,%C=7,%N=30,%A=9,%F=24)
CSSA (%B=5,%C=4,%N=30,%A=9,%F=24)
CSSA (%B=5,%C=2,%N=30,%A=9,%F=24)
```

```
CSSA (%B=7,%C=1,%N=30,%A=9,%F=24)
CSSA (%B=7,%C=3,%N=30,%A=9,%F=24)
! Send no inhibit on output registers
CFSA (%B=7,%C=3,%N=21,%A=0,%F=22,%DATA=L14)
CFSA (%B=5,%C=4,%N=19,%A=0,%F=22,%DATA=L1)
! Read scalers
SCALF = .TRUE.
CALL RSCAL
STORE SASPAngle ! tack the decoded angles on after the scalers
STORE MRSAngle
FLUSH
RETURN
END
!************************************************************
SUBROUTINE RPAUSE
INTEGER*4 L1 /1/
INTEGER*4 L14 /12/
! Generate inhibit on output registers
CFSA (%B=5,%C=4,%N=19,%A=0,%F=20,%DATA=L1)
CFSA (%B=7,%C=3,%N=21,%A=0,%F=20,%DATA=L14)
! Raise Inhibit
CSSA (%B=5,%C=7,%N=30,%A=9,%F=26)
CSSA (%B=5,%C=4,%N=30,%A=9,%F=26)
CSSA (%B=5,%C=2,%N=30,%A=9,%F=26)
CSSA (%B=7,%C=3,%N=30,%A=9,%F=26)
CSSA (%B=7,%C=1,%N=30,%A=9,%F=26)
! read scalers
CALL RSCAL
FLUSH
RETURN
END
!************************************************************
SUBROUTINE RCONTIN
INTEGER*4 L2 /2/
INTEGER*4 L1 /1/
INTEGER*4 L4 /4/
INTEGER*4 L14 /12/
INTEGER*4 L60 /48/
INTEGER*4 L200 /128/
```

```
INTEGER*4 L40000 /16384/
INTEGER*4 L42000 /17408/
! Disable TDC LAM
CSSA(%B=5,%C=7,%N=12,%A=0,%F=24)
! Clear TDC, ADC
CSSA(%B=5,%C=7,%N=2,%A=0,%F=9)
CSSA(%B=5,%C=7,%N=3,%A=0,%F=9)
CSSA(%B=5,%C=7,%N=9,%A=0,%F=9)
CSSA(%B=5,%C=7,%N=12,%A=0,%F=9)
CSSA(%B=7,%C=3,%N=15,%A=0,%F=9)
CSSA(%B=7,%C=3,%N=16,%A=0,%F=9)
CSSA(%B=7,%C=3,%N=17,%A=0,%F=9)
CSSA(%B=7,%C=3,%N=19,%A=0,%F=9)
CSSA(%B=7,%C=3,%N=22,%A=0,%F=9)
! Set up LeCroy 4290 system
CSSA (%B=5,%C=4,%N=20,%A=0,%F=9)
CFSA (%B=5,%C=4,%N=20,%A=0,%F=16,%DATA=L40000)
CFSA (%B=5,%C=4,%N=20,%A=0,%F=16,%DATA=L42000)
CFSA (%B=5,%C=4,%N=19,%A=0,%F=20,%DATA=L4)
CSSA (%B=7,%C=3,%N=22,%A=0,%F=9)
CFSA (%B=7,%C=3,%N=22,%A=0,%F=16,%DATA=L40000)
CFSA (%B=7,%C=3,%N=22,%A=0,%F=16,%DATA=L42000)
CFSA (%B=7,%C=3,%N=21,%A=0,%F=20,%DATA=L200)
! Enable TDC LAM
CSSA(%B=5,%C=7,%N=12,%A=0,%F=26)
! Send clear pulse on output register
CFSA (%B=5,%C=4,%N=19,%A=0,%F=20,%DATA=L2)
CFSA (%B=5,%C=4,%N=19,%A=0,%F=22,%DATA=L2)
! Drop Inhibit
CSSA (%B=5,%C=7,%N=30,%A=9,%F=24)
CSSA (%B=5,%C=4,%N=30,%A=9,%F=24)
CSSA (%B=5,%C=2,%N=30,%A=9,%F=24)
CSSA (%B=7,%C=1,%N=30,%A=9,%F=24)
CSSA (%B=7,%C=3,%N=30,%A=9,%F=24)
! Send no inhibit on output registers
CFSA (%B=5,%C=4,%N=19,%A=0,%F=22,%DATA=L1)
CFSA (%B=7,%C=3,%N=21,%A=0,%F=22,%DATA=L14)
! Read scalers
CALL RSCAL
```

```
RETURN
END
!************************************************************
SUBROUTINE RSCAL
INTEGER*4 I17440 /7968/
INTEGER*4 L1 /1/
! Flags to keep track of whether there are things other
! than scaler events happening.
! SCALF is set .FALSE. by scalers, .TRUE. by LAM events.
! If it is .FALSE. on entry to scaler events (indicating two
! successive scaler events), the buffer is flushed.
! This forces updating of scaler page.
LOGICAL SCALF
LOGICAL OLDSCF
COMMON /CEV12/ SCALF
!
OLDSCF = SCALF
SCALF = .FALSE.
! Set up scalers read
CFSA(%B=5,%C=7,%N=4,%A=0,%F=16,%DATA=I17440)
! Read C=7 32-channel scaler
CFQIGNORE(%B=5,%C=7,%N=4,%A=0,%F=2,%R=32)          ! read 32 scalers
! then read MRS scalers
CFSA(%B=7,%C=3,%N=14,%A=0,%F=16,%DATA=I17440)
! Read C=7 32-channel scaler
CFQIGNORE(%B=7,%C=3,%N=14,%A=0,%F=2,%R=32)          ! read 32 scalers
! Now read IBP scalers from Crate 5
CFSCAN(%B=5,%C=2,%N=8,%A=0,%F=0,%R=12)             ! read 12 IBP scalers
CFSCAN(%B=5,%C=2,%N=9,%A=0,%F=0,%R=12)             ! read 12 IBP scalers
CFSCAN(%B=5,%C=2,%N=10,%A=0,%F=0,%R=12)            ! read 12 IBP scalers
! Mark buffer to be analyzed regardless
MUSTPROCESS
IF (OLDSCF) GOTO 10
FLUSH
10 RETURN
END
!************************************************************
SUBROUTINE RLAM
INTEGER*4 L1 /1/
```

```
INTEGER*4 L2 /2/
INTEGER*4 L3 /3/
INTEGER*4 L4 /4/
INTEGER*4 L200 /128/
! This identifies various types of events (to allow for mixed
! MRS / SASP / DASS experiments later on
! Only IFSASP is used so far
INTEGER*2 IFMRS/1/
INTEGER*2 IFSASP/2/
INTEGER*2 IFDASS/3/
LOGICAL SCALF
COMMON /CEV12/ SCALF
SCALF = .TRUE.
!
STORE IFDASS
! MRS part of DASS event
!  Read DCR
CFSA(%B=7,%C=3,%N=18,%A=0,%F=2)
!  Read TDC
CSSCAN(%B=7,%C=3,%N=15,%A=0,%F=0,%R=8)
!  Read ADC
CSSCAN(%B=7,%C=3,%N=19,%A=0,%F=0,%R=12)
!  Read ADC
CSSCAN(%B=7,%C=3,%N=17,%A=0,%F=0,%R=3)
!  Read ADC
CSSCAN(%B=7,%C=3,%N=16,%A=0,%F=0,%R=3)
! Clear TDC, ADC's
 CSSA(%B=7,%C=3,%N=15,%A=0,%F=9)
 CSSA(%B=7,%C=3,%N=16,%A=0,%F=9)
 CSSA(%B=7,%C=3,%N=17,%A=0,%F=9)
 CSSA(%B=7,%C=3,%N=19,%A=0,%F=9)
! Drift chamber data out through 4299
CSQSTOP(%B=7,%C=3,%N=22,%A=1,%F=2,%R=110)
!
! clear 4299
CSSA (%B=7,%C=3,%N=22,%A=0,%F=11)
! end of MRS part

! SASP event
```

```
! Response to LAM from TDC in slot 12
! Disable 4299 clear
CFSA (%B=5,%C=4,%N=19,%A=0,%F=22,%DATA=L4)
! Read DCR (16 bits)
CSSA(%B=5,%C=4,%N=13,%A=0,%F=2)
! Read TDC's
CSSCAN(%B=5,%C=7,%N=9,%A=0,%F=0,%R=8)
CSSCAN(%B=5,%C=7,%N=12,%A=0,%F=0,%R=8)
! Read ADC's
CSSCAN(%B=5,%C=7,%N=2,%A=0,%F=0,%R=12)
CSSCAN(%B=5,%C=7,%N=3,%A=0,%F=0,%R=12)
! Clear TDC, ADC (I assume Clear on the Output register does this, so why
! waste the time)
 CSSA(%B=5,%C=7,%N=2,%A=0,%F=9)
 CSSA(%B=5,%C=7,%N=3,%A=0,%F=9)
 CSSA(%B=5,%C=7,%N=9,%A=0,%F=9)
 CSSA(%B=5,%C=7,%N=12,%A=0,%F=9)
! Send clear pulse on output register
CFSA (%B=5,%C=4,%N=19,%A=0,%F=20,%DATA=L2)
CFSA (%B=5,%C=4,%N=19,%A=0,%F=22,%DATA=L2)
!
! Drift chamber readout via 4299
CSQSTOP(%B=5,%C=4,%N=20,%A=1,%F=2,%R=110)
!
! enable O/P REG 4299 clear, and clear it
CFSA (%B=5,%C=4,%N=19,%A=0,%F=20,%DATA=L4)
CSSA (%B=5,%C=4,%N=20,%A=0,%F=11)
RETURN
END
!************************************************************
SUBROUTINE REND
INTEGER*4 L1 /1/
INTEGER*4 L14 /12/
INTEGER*4 LCH1 /2/
! Generate inhibit on output registers
CFSA (%B=5,%C=4,%N=19,%A=0,%F=20,%DATA=L1)
CFSA (%B=7,%C=3,%N=21,%A=0,%F=20,%DATA=L14)
! Disable LAM
CSSA (%B=5,%C=7,%N=12,%A=0,%F=24)
```

```
! Raise Inhibit
CSSA (%B=5,%C=7,%N=30,%A=9,%F=26)
CSSA (%B=5,%C=4,%N=30,%A=9,%F=26)
CSSA (%B=5,%C=2,%N=30,%A=9,%F=26)
CSSA (%B=7,%C=1,%N=30,%A=9,%F=26)
CSSA (%B=7,%C=3,%N=30,%A=9,%F=26)
! Read final scaler values
CALL RSCAL
! Clear TDC, ADC, 4290
CSSA (%B=5,%C=7,%N=2,%A=0,%F=9)
CSSA (%B=5,%C=7,%N=3,%A=0,%F=9)
CSSA (%B=5,%C=7,%N=9,%A=0,%F=9)
CSSA (%B=5,%C=7,%N=12,%A=0,%F=9)
CSSA (%B=5,%C=4,%N=20,%A=0,%F=9)
CSSA (%B=7,%C=3,%N=15,%A=0,%F=9)
CSSA (%B=7,%C=3,%N=16,%A=0,%F=9)
CSSA (%B=7,%C=3,%N=17,%A=0,%F=9)
CSSA (%B=7,%C=3,%N=19,%A=0,%F=9)
CSSA (%B=7,%C=3,%N=22,%A=0,%F=9)
RETURN
END
SUBROUTINE STUPID
RETURN
END
!
! SUBROUTINE RFE
! CSSA (%B=5,%C=7,%N=8,%A=7,%F=16,%DATA=0)
! CSSA (%B=5,%C=7,%N=8,%A=8,%F=16,%DATA=0)
! CSSA (%B=5,%C=7,%N=8,%A=9,%F=16,%DATA=0)
! CSSA (%B=5,%C=7,%N=8,%A=10,%F=16,%DATA=0)
! RETURN
! END
!
SUBROUTINE ANGLE_DECODE
Integer*4 InAngle, OutAngle,tmp,scr
Common/angs/InAngle,OutAngle
! Accept complementary BCD, return decimal value
scr=InAngle
OutAngle=0
```

```
Do 20 j=1,5 ! 5 digits
 tmp = scr/16
 tmp = scr - 16*tmp
 tmp = 15 - tmp
 Do 10 k=1,j
  tmp = 10*tmp
10 Continue
 OutAngle = OutAngle + tmp/10
 scr = scr/16
20 continue
Return
End
```

Appendix F

USRQ Subroutine

The user routine USRQ, given below, was used to calculate the MRS and SASP focal plane acceptance and the SASP pion survival efficiency during off-line analysis.

```
SUBROUTINE USRQ(EFFVECTOR,BMRS,RDEL,BSASP,SDEL)
C Subroutine USRQ.FOR, for calculating MRS focal plane acceptance,
C SASP focal plane acceptance, and the SASP pion survival efficiency.
C W.R. Falk, May 5, 1995
C NOTE  Select appropriate orientation of FPP: M=1 (Correct), M=2 (Wrong)
C
C INPUT: BMRS,RDEL,BSASP,SDEL
C
C OUTPUT: EFFVECTOR(0)=R_ACC,The MRS focal plane acceptance
C EFFVECTOR(1)=S_ACC,The SASP focal plane acceptance
C EFFVECTOR(2)=SURVIV The SASP pion survival fraction
C EFFVECTOR(3)=R_ACC*S_ACC*SURVIV
C
REAL*4 EFFVECTOR(0:3),BMRS,RDEL,BSASP,SDEL
C
C  1. Parameters for MRS ACCEPTANCE vs. RDEL for the correct orientation of
C FPP cage. The Central Ray @ 16475 is assumed for the RDEL calc's.
C
DATA R1A,R2A,R3A,R4A,R5A,R6A/1.0005,1.84332E-03,-1.96837E-03,
1        -1.77419E-07,-9.35692E-05,1.99692E-06/
C
C  2. Parameters for MRS ACCEPTANCE vs. RDEL for the wrong orientation of
C FPP cage. The Central Ray @ 16475 is assumed for the RDEL calc's.
C
DATA R1B,R2B,R3B,R4B,R5B,R6B/1.0112,-3.14531E-03,-1.54384E-02,
1         3.00655E-03,-7.62206E-05,-1.56994E-05/
```

```
C
C  3. Parameters characterizing the SASP effective pion length.
C
DATA AA,AB,AC,AD/906.60,-1.3081,3.85717E-03,-3.64865E-06/
DATA BA,BB,BC,BD/-1.6247,2.59342E-02,-3.79387E-05,1.62509E-08/
DATA CA,CB,CC,CD/0.18867,-1.32423E-03,4.58248E-06,-5.42283E-09/
DATA DA,DB,DC,DD/9.48187E-03,-4.89838E-05,1.10364E-07,
1  -8.97919E-11/
DATA EA,EB,EC,ED/-1.75380E-03,1.20465E-05,-4.27421E-08,
1  4.77286E-11/
DATA FA,FB,FC,FD/5.12961E-05,-4.01958E-07,1.45585E-09,
1 -1.62380E-12/
C ---------------------------------------------------------------------
C
C MRS Acceptance
C PMC is the MRS central momentum
    PMC=80.357*BMRS ! MRS central momentum (MeV/c)
X=RDEL
R_ACC=0.0
C Select appropriate orientation of FPP: M=1 (Correct), M=2 (Wrong)
M=2
GO TO (12,14),M
12 IF(RDEL.LT.-8.5.OR.RDEL.GT.8.5) GO TO 16
R_ACC = R1A + R2A*X + R3A*X**2 + R4A*X**3 + R5A*X**4 + R6A*X**5
GO TO 16
14 IF(RDEL.LT.-5.5.OR.RDEL.GT.9.0) GO TO 16
R_ACC = R1B + R2B*X + R3B*X**2 + R4B*X**3 + R5B*X**4 + R6B*X**5
16 CONTINUE
C ---------------------------------------------------------------------
C
C SASP Acceptance {File: [FALK.DASS.SASP]SASP_ACC.}
C Fit parameters for the SASP acceptance using pp->dpi+ data and
C my pion survival correction, May 8, 1995
S_ACC=0.0
C  IF(SDEL.LT.-16.0.OR.SDEL.GT.20.0) GO TO 25
X=SDEL
        S_ACC = 1.0025 -4.83442E-03*X- 7.24290E-04*X**2
1 + 3.06517E-05*X**3  -7.17974E-06*X**4 + 2.32954E-07*X**5
25 CONTINUE
```

```
C ------------------------------------------------------------------
C
C Parameterization of the SASP effective pion length.
C PSC is the SASP central momentum
PSC=50.311*BSASP ! SASP central momentum (MeV/c)
A = AA + AB*PSC + AC*PSC**2 + AD*PSC**3
B = BA + BB*PSC + BC*PSC**2 + BD*PSC**3
C = CA + CB*PSC + CC*PSC**2 + CD*PSC**3
D = DA + DB*PSC + DC*PSC**2 + DD*PSC**3
E = EA + EB*PSC + EC*PSC**2 + ED*PSC**3
F = FA + FB*PSC + FC*PSC**2 + FD*PSC**3
C
SURVIV=0.0
IF(SDEL.LT.-16.0.OR.SDEL.GT.20.0) GO TO 35
EFF_L=A+B*SDEL+C*SDEL**2+D*SDEL**3+E*SDEL**4+F*SDEL**5
C
TAU_C=780.4 ! Pion decay length (cm)
PS=PSC*(1.0+SDEL/100.0) ! Pion momentum
SURVIV=EXP((-139.57*EFF_L)/(TAU_C*PS)) ! Pion survival fraction
35 CONTINUE
C ------------------------------------------------------------------
C
RSEFF=R_ACC*S_ACC*SURVIV !Composite efficiency
EFFVECTOR(0)=R_ACC ! The MRS focal plane acceptance
EFFVECTOR(1)=S_ACC ! The SASP focal plane acceptance
EFFVECTOR(2)=SURVIV ! The SASP pion survival fraction
EFFVECTOR(3)=RSEFF ! The composite efficiency
C
RETURN
END
C ------------------------------------------------------------------
```

Appendix G

E634 NOVA OPSEQ

The NOVA OPSEQ used for E634 off-line analysis follows.

```
IF ($EVENTTYPE==1)THEN
  EVAL RATES
  OUTPUT $RAW
  INCR HBEAM BY I_NA
  IF (IPOLUP>0)THEN
    INCR HPOLUP
  ENDIF
  IF (IPOLDW>0)THEN
    INCR HPOLDW
  ENDIF
  INCR HACCUPL BY IACCUPL
  INCR HACCUPR BY IACCUPR
  GOTO $END_OPSEQ
ENDIF
IF ($EVENTTYPE==2)THEN
  OUTPUT $RAW
  IF (DELCUT)THEN
    INCR HDPB
    IF (MTESTCNT)THEN
    ENDIF
    INCR HMPID
    IF (MMWOK)THEN
      INCR HMPID_OK
    ENDIF
    IF (MMWOK1)THEN
    ENDIF
    IF (MXOYO)THEN
```

```
  INCR HMXF1
  INCR HMX1YO
ENDIF
IF (MPID_DEUT)THEN
  INCR HMDIAG
  INCR HMTIME
  INCR HMPOS
  INCR HMXOYO
  INCR HMCH
  IF (MEFFXY)THEN
  ENDIF
  IF (MEFFXO)THEN
  ENDIF
  IF (MEFFYO)THEN
  ENDIF
  IF (MEFFXU)THEN
  ENDIF
  IF (MEFFX1)THEN
  ENDIF
  IF (MEFFU1)THEN
  ENDIF
  IF (MEFFX2)THEN
  ENDIF
  IF (MEFFU2)THEN
  ENDIF
  IF (MMWOK2)THEN
  ENDIF
  IF (MMWOK3)THEN
    INCR HMPHT
    INCR HMXI
    INCR HMYI
    INCR HMTH_TGT
    INCR HMPH_TGT
    INCR HMTH_VDC
    INCR HMPH_VDC
    IF (MXFCALC)THEN
      IF (MXOYO)THEN
        INCR HMXFYO
        IF (MTHTCUT)THEN
```

```
                IF (MPHTCUT)THEN
                  IF (MXICUT)THEN
                    IF (MYICUT)THEN
                      INCR HMXF2
                      EVAL MTGTVECTOR
                      EVAL MVDCVECTOR
                      EVAL RXFKC
                      INCR HMXFKC
                      IF (MOPT_COND)THEN
                      IF (MOPTIMIZE==1|MOPTIMIZE==11)THEN
                      EVAL MRUNSUMS
                      INCR HMXFKOPT
                      ENDIF
                      IF (MOPTIMIZE==2)THEN
                      EVAL MNEWCOEFS
                      ENDIF
                      ENDIF
                    ENDIF
                  ENDIF
                ENDIF
              ENDIF
            ENDIF
          ENDIF
        ENDIF
      ENDIF
    ENDIF
  ENDIF
ENDIF
INCR HSPID
INCR HSPID_RF
IF (LPD0)THEN
  INCR HSTRFPD0
ENDIF
IF (LPD1)THEN
  INCR HSTRFPD1
ENDIF
IF (LPD2)THEN
  INCR HSTRFPD2
ENDIF
IF (LPD3)THEN
  INCR HSTRFPD3
ENDIF
```

```
IF (LPD4)THEN
  INCR HSTRFPD4
ENDIF
IF (LMWOK)THEN
  INCR HSTRF_OK
ENDIF
IF (LPID_PION)THEN
  EVAL SRMATRIX
  EVAL SXFVECTOR
  INCR HSTHPH
  INCR HMADC
  INCR HSADC
  INCR HSTDC
  INCR HSDIAG
  INCR HSTIME
  INCR HSPOS
  INCR HSANGLE
  INCR HSXFXI
  INCR HSCH
  IF (LEFFXU)THEN
  ENDIF
  IF (LEFFX1)THEN
  ENDIF
  IF (LEFFU1)THEN
  ENDIF
  IF (LEFFX2)THEN
  ENDIF
  IF (LEFFU2)THEN
  ENDIF
  IF (LMWOK1)THEN
    INCR HLTMRS_ALL
    IF (MPIDBAD)THEN
      INCR HLTMRS_BAD
    ENDIF
    INCR HSYI
    INCR HSXI
    INCR HSTH_TGT
    INCR HSPH_TGT
    INCR HSTH_VDC
```

```
      INCR HSPH_VDC
      INCR HSXKPH
      INCR HSXFYI
      INCR HSTHX
      INCR HSX2ES
      INCR HSX1ES
      INCR HSXFA
      IF (LXFCALC)THEN
        INCR HSXFYO
        INCR HSXFTHX
        IF (LTHTCUT)THEN
          IF (LPHTCUT)THEN
            IF (LYICUT)THEN
              INCR HSXF
              EVAL LTGTVECTOR
              EVAL LVDCVECTOR
              EVAL SXFKC
              INCR HSXFKC
              IF (LOPT_COND)THEN
                IF (LOPTIMIZE==1|LOPTIMIZE==11)THEN
                  EVAL LRUNSUMS
                  INCR HSXFKOPT
                ENDIF
                IF (LOPTIMIZE==2)THEN
                  EVAL LNEWCOEFS
                ENDIF
              ENDIF
            ENDIF
          ENDIF
        ENDIF
        INCR HSXF_WIDE
      ENDIF
    ENDIF
  ENDIF
  IF (MMWOK4)THEN
  ENDIF
  IF (MEANTCUT)THEN
    EVAL EFFVECTOR
    IF (RSEFF~=0.00)THEN
```

```
IF (MEVENT_OK1)THEN
  IF (MX011)THEN
  ENDIF
  IF (MX012)THEN
  ENDIF
  IF (MX013)THEN
  ENDIF
  IF (MY011)THEN
  ENDIF
  IF (MY012)THEN
  ENDIF
  IF (MY013)THEN
  ENDIF
  IF (MX0Y01)THEN
  ENDIF
  IF (MX0Y02)THEN
  ENDIF
  IF (MX0Y03)THEN
  ENDIF
ENDIF
IF (LEVENT_OK1)THEN
  IF (LTHTCUT1)THEN
  ENDIF
  IF (LTHTCUT2)THEN
  ENDIF
  IF (LTHTCUT3)THEN
  ENDIF
  IF (LPHTCUT1)THEN
  ENDIF
  IF (LPHTCUT2)THEN
  ENDIF
  IF (LPHTCUT3)THEN
  ENDIF
  IF (LANGCUT1)THEN
  ENDIF
  IF (LANGCUT2)THEN
  ENDIF
  IF (LANGCUT3)THEN
  ENDIF
```

```
ENDIF
IF (MEVENT_OK)THEN
  IF (LEVENT_OK)THEN
    INCR HX1CORR
    INCR HMX1SX1
    INCR HMXFSXF
    INCR HLTMRS
    INCR HDRMASS
    INCR HSDEL
    INCR HSTH_DRMASS
    INCR HSPH_DRMASS
    INCR HRTH_DRMASS
    INCR HRPH_DRMASS
    INCR HSPID_RFC
    IF (LTMRS_P)THEN
      INCR HDRMDEL_T
      INCR HDRMDEL_N
      INCR HDRMDEL_NC
      INCR HDRMDEL_NE BY RSEFF
      INCR HDRMDEL_NEC BY RSEFF
      INCR HSDELRACC BY R_ACC
      INCR HSDELSACC BY S_ACC
      INCR HSDELSURV BY SURVIV
      INCR HDRMASS_P
      IF (SPIN_UP)THEN
        INCR HDRMDEL_U
        INCR HDRMDEL_UC
        INCR HDRMDEL_UE BY RSEFF
        INCR HDRMDEL_UEC BY RSEFF
        INCR HDRMASS_PU
      ENDIF
      IF (SPIN_DOWN)THEN
        INCR HDRMDEL_D
        INCR HDRMDEL_DC
        INCR HDRMDEL_DE BY RSEFF
        INCR HDRMDEL_DEC BY RSEFF
        INCR HDRMASS_PD
      ENDIF
    ENDIF
```

```
                    IF (LTMRS_R)THEN
                      INCR HDRMDEL_R
                      INCR HDRMDEL_N BY   -1.000000
                      INCR HDRMDEL_NE BY NEG_RSEFF
                      INCR HSDELRACC BY NEG_R_ACC
                      INCR HSDELSACC BY NEG_S_ACC
                      INCR HSDELSURV BY NEG_SURVIV
                      INCR HDRMASS_R
                      IF (SPIN_UP)THEN
                        INCR HDRMDEL_U BY   -1.000000
                        INCR HDRMDEL_UE BY NEG_RSEFF
                        INCR HDRMASS_RU
                      ENDIF
                      IF (SPIN_DOWN)THEN
                        INCR HDRMDEL_D BY   -1.000000
                        INCR HDRMDEL_DE BY NEG_RSEFF
                        INCR HDRMASS_RD
                      ENDIF
                    ENDIF
                  ENDIF
                ENDIF
              ENDIF
            ENDIF
          ENDIF
        ENDIF
      ENDIF
    ENDIF
EOF
```